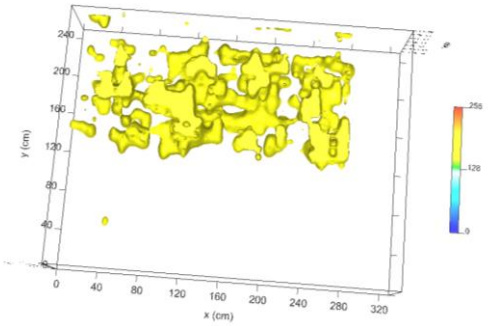

GEOPHYSICAL SURVEYS AT THE MONASTERY OF ST JOHN IN MUSTAIR (Swiss)

The Director

Dott.ssa Costanza Miliani

Costanza Miliani
17.11.2022 12:12:22 GMT+01:00

The Scientific Manager

Dott. Giovanni Leucci

LEUCCI GIOVANN
2022.11.16 11:48:25
CN=LEUCCI GIOVANNI
C=IT
2.5.4.4=LEUCCI
2.5.4.42=GIOVANNI
Dirigente di Ricerca
RSA/2048 bits

SEPTEMBER 2022

Sede secondaria di Lecce c/o Campus Universitario Ecotekne
Prov.le Lecce-Monteroni / 73100 Lecce
Tel. +39 0832422200 Fax. +39 0832422225

INDEX

Sede di Napoli
Via Cardinale Guglielmo Sanfelice, 8 / 80134 Napoli
Email segreteria.ispc@ispc.cnr.it – segreteria.direzione@ispc.cnr.it

INTRODUCTION

With reference to the "Diagnostics for Conservation at Müstair Monastery" project (DIACOMM, mol_1) with Dr. Patrick Cassitti in charge (IPERION HS 2nd call for access to MOLAB of 01/02/2021 closed on 30/06/2021 and with notification for access to the user of 10/09/2021) are reported by followed the results obtained from the geophysical survey.

To study the state the state of conservation of the fresco inside the monastery of San Giovanni in Mustair, geophysical surveys with ground-penetrating radar (GPR) were undertaken in September 2022. The surveyed area is shown in Fig. 1.

The GPR data weed using the Sir 3000 georadar system (GSSI) with the 2GHz, and 900MHz antennae along grids with parallel profiles set 0.1 m apart for the 2GHz and 0.25m apart for 900MHz.

Data were acquired by the Laboratory of Geophysics of the Institute of Heritage Science (National Research Council) team. The team was composed by Dr Vincenzo Di Fiore (ISPC Napoli), Dr Ivan Ferrari (ISPC Lecce), Dr Daniela Tarallo (ISPC Napoli), and Dr Michele Punzo (ISPC Napoli). The measurements were carried out on the 13 and 14 September 2022.

Ground-penetrating Radar: BACKGROUND THEORY

GPR surveys success is mainly dependent on soil and sediment mineralogy, clay content, ground moisture, depth of burial, surface topography, and vegetation (Conyers 2004; Leucci, 2007; Leucci, 2015; Leucci, 2019). It is not a geophysical method that can be immediately applied to any geographic or archaeological setting. However, with thoughtful modifications in acquisition and data processing methodology, GPR can adapt to many different site conditions. Most GPR practitioners have assumed that the method would only be successful in areas where soils and underlying sediment are dry (Annan and Davis 1978). Although radar wave penetration, and the

ability to reflect energy to the surface, are often enhanced in a dry environment, recent work has demonstrated that dryness is not necessarily a prerequisite for GPR surveys and even very wet environments are suitable, as long as the medium is not electrically conductive (Conyers 2004). The GPR method involves the transmission of high-frequency electromagnetic radio (radar) pulses into the earth and measuring the time elapsed between transmission, the reflection of a buried discontinuity and reception back at a surface radar antenna. A pulse of radar energy is generated on a dipole transmitting antenna placed on, or near, the ground surface. The resulting wave of electromagnetic energy propagates downward into the ground, where some energy can be reflected back to the surface at discontinuities (Fig. 2).

Sede di Napoli
Via Cardinale Guglielmo Sanfelice, 8 / 80134 Napoli
Email segreteria.ispc@ispc.cnr.it – segreteria.direzione@ispc.cnr.it

The discontinuities where reflections occur are usually created by changes in electrical properties of the sediment or soil, lithologic changes, differences in bulk density at stratigraphic interfaces and, most crucial, water content variations. Reflection can also occur at interfaces between anomalous archaeological features and the surrounding soil or sediment. Void spaces in the ground, encountered in burials, tombs, or tunnels, will also generate significant radar reflections due to a considerable change in radar wave velocity. The depth to which radar energy can penetrate and the amount of definition expected in the subsurface are partially controlled by the frequency of the radar energy transmitted. Radar energy frequency controls both the wavelength of the propagating wave and the amount of weakening, or attenuation, of the waves in the ground. Standard GPR antennas used in archaeology propagate radar energy that varies in band width from about 10 megahertz (MHz) to 2500 MHz. Antennas usually come in standard frequencies. Each antenna has one centre frequency but produces radar energy that ranges around that centre by about two octaves (one half and two times the centre frequency). The most efficient method in subsurface GPR mapping is to establish a grid across a survey area before acquiring data. Usually, rectangular grids are set with one meter or less transect spacing. Rectangular grids produce data that are easier to process and interpret. Other grid acquisition patterns may be necessary because of surface topography or other obstructions. Data from non-rectilinear surveys is just as valuable as those acquired in rectangular shaped grids. However, more field time may be necessary for surveying, and reflection data must be manipulated differently during computer processing and interpretation for reflection amplitude analysis. The two-way travel time and the amplitude and wavelength of the reflected radar waves derived from the pulses are amplified, processed and recorded for immediate viewing and later post-acquisition processing and display. During field data acquisition, radar transmission is repeated many times a second as the antennas are pulled along the ground surface in transects. The distance along each line is recorded to place all reflections within a surveyed grid accurately. In this fashion, two-dimensional profiles, which approximate vertical “slices” through the earth, are created along each grid line.

Radar energy becomes both dispersed and attenuated as it radiates into the ground. When portions of the originally transmitted signal are reflected back toward the surface, they will suffer additional attenuation by the material they pass before finally being recorded at the surface. Therefore, to be detected as reflections, important subsurface interfaces must have sufficient electrical contrast at their boundary and must be located at a shallow enough depth where sufficient radar energy is still available for reflection. As radar energy is propagated to increasing depths, the signal becomes weaker as it spreads out over more surface area and absorbed by the ground, making it less available

Sede di Napoli
Via Cardinale Guglielmo Sanfelice, 8 / 80134 Napoli
Email segreteria.ispc@ispc.cnr.it – segreteria.direzione@ispc.cnr.it

for reflection. The maximum depth of resolution for every site will vary with the geologic conditions and the equipment being used. Post-acquisition data filtering and other data amplification techniques (termed range-gaining) can sometimes be applied to reflection data after acquisition, enhancing some very low amplitude reflections to make them more visible. Many ground-penetrating radar novices envision the propagating radar pattern as a narrow “pencil” shaped beam focused directly down from the antenna. GPR waves radiated from standard commercial antennas radiate energy into the ground in an elliptical cone with the apex

of the cone at the centre of the transmitting antenna (Conyers 2004; Leucci, 2015, Giannino and Leucci, 2021). This elliptical cone of transmission occurs because the electrical field produced by the antenna is generated parallel to its long axis and is therefore usually radiating into the ground perpendicular to the direction of antenna movement along the ground surface. The radiation pattern is generated from a horizontal electric dipole antenna to which elements are sometimes added that effectively reduce upward radiation, called shields. Sometimes the only shielding mechanism is a radar-absorbing surface placed above the antenna to neutralize upward radiating energy. Because of cost and portability considerations (size and weight), the use of more complex radar antennas that might be able to focus energy more efficiently into the ground in a more narrow beam has to date, been limited in archaeology. Some antennas, especially those in the low-frequency range from 10 to 100 MHz, are often not shielded and radiate radar energy in all directions. Using unshielded antennas can generate reflections from a nearby person pulling the radar antenna or other objects nearby, such as trees or buildings. Discrimination of individual targets, especially those of interest in the subsurface, can be difficult if these types of antennas are used. However, if the unwanted reflections generated from unshielded antennas can be identified, they can be easily filtered out later. Suppose reflections are recorded from randomly located trees, surface obstructions, or people moving about randomly near the antenna. In that case, they are more difficult to discriminate from important subsurface reflections and interpretation of the data is much more difficult. One of the most important variables in GPR surveys is the selection of antennas with the correct operating frequency for the depth necessary and the resolution of the features of interest (Conyers 2004a). In most cases, proper antenna frequency selection can make the difference between success and failure in a GPR survey and must be planned for in advance. The greater the necessary depth of investigation, the lower the antenna frequency should be used (Leucci, 2008). But lower frequency antennas are much larger, heavier and more difficult to transport to and within the field than high-frequency antennas. For instance, a 100 MHz antenna is about 2 meters long. It is difficult to transport to and from the field but must usually be moved along transect lines using some form of wheeled vehicle or sledge. In

Sede di Napoli
Via Cardinale Guglielmo Sanfelice, 8 / 80134 Napoli
Email segreteria.ispc@ispc.cnr.it – segreteria.direzione@ispc.cnr.it

contrast, antennas greater than 400 MHz are usually 50 centimetres or smaller in maximum dimension, weigh very little, and easily fit into a suitcase. Low-frequency antennas (10–120 MHz) generate long wave-length radar energy that can penetrate up to 50 meters in certain conditions but only resolve extensive subsurface features. In pure ice, antennas of this frequency have been known to transmit radar energy many kilometres. In contrast, the maximum depth of penetration of a 900 MHz antenna is about one meter or less in typical soils, but its generated reflections can resolve features down to a few centimetres in dimension (Conyers 2004; Leucci, 2008). A trade-off, therefore, exists between depth of penetration and subsurface resolution. The depth of penetration and the subsurface resolution is highly variable, depending on site-specific factors such as overburden composition, porosity, and retained moisture. If large amounts of electrically-conductive clay are present, then attenuation of the radar energy with depth will occur very rapidly, irrespective of radar energy frequency. Attenuation can also occur if sediment or soils are saturated with salty water, especially sea water. The ability to resolve buried features are mostly determined by the frequency and, therefore, the wavelengths of the radar energy being transmitted into the ground. The wavelength necessary for resolution varies depending on whether a three-dimensional object or an undulating surface is investigated. For GPR to resolve three-dimensional objects, reflections from at least two surfaces, usually a top and bottom interface, must be distinct. However, the resolution of a single buried planar surface needs only one distinct reflection, and therefore wavelength is not as important in its resolution. Radar energy reflected off a buried subsurface interface that slopes away from a surface transmitting antenna will be reflected away from the receiving antenna and lost. This sloping interface would therefore go unnoticed in reflection profiles. A buried surface with this orientation would only be visible if a different traverse were located where the same buried interface is sloping toward the surface antennas. This is why it is important always to acquire lines of reflection data within a closely spaced surface grid and sometimes in transects perpendicular to each other. Some features in the subsurface may be described as “point targets”, while others are more similar to planar surfaces. Planar surfaces can be stratigraphic and soil horizons or large flat archaeological features such as floors. Point targets are features such as walls, tunnels, voids, artefacts or any other non-planar object. Depending on a planar surface’s thickness, reflectivity, orientation and depth of burial, it is potentially visible with any frequency data, constrained only by the conditions discussed above. Point sources, however, often have a little surface area with which to reflect radar energy and therefore are usually difficult to identify and map. They are sometimes indistinguishable from the surrounding material, often visible only as small reflection hyperbolas visible on one profile within a grid. In most geological and archaeological settings, the materials through which radar waves pass

Sede di Napoli
Via Cardinale Guglielmo Sanfelice, 8 / 80134 Napoli
Email segreteria.ispc@ispc.cnr.it – segreteria.direzione@ispc.cnr.it

may contain many small discontinuities that reflect energy, which can only be described as clutter (if they are not the survey's target). The clutter resolution is dependent on the wavelength of the radar energy being propagated. Suppose both the features to be resolved and the discontinuities producing the clutter are on the order of one wavelength in size. In that case, the reflection profiles will appear to contain only clutter, and there can be no discrimination between the two. Clutter can also be produced by large discontinuities, such as cobbles and boulders, but only when a lower frequency antenna that produces a long wavelength is used. In all cases, if not a large planar surface, the features to be resolved should be much larger than the clutter and greater than one wavelength of the propagating energy in dimension (Conyers 2004). The raw reflection data collected by GPR is nothing more than a collection of many individual traces along two-dimensional transects within a grid. Each reflection trace contains a series of waves that vary in amplitude depending on the amount and intensity of energy reflection at buried interfaces. When these traces are plotted sequentially in standard two-dimensional profiles, specific amplitudes within individual traces containing important reflection information are sometimes difficult to visualize and interpret. Rarely is the standard interpretation of GPR data, which consists of viewing each profile and then mapping important reflections and other anomalies sufficient, especially when the buried features and stratigraphy are complex. In areas where buried materials are difficult to discern, different processing and interpretation methods must be used, one of which is amplitude analysis. In the past, when GPR reflection data were collected that had no discernable reflections or recognizable anomalies of any sort, the survey has usually declared a failure and little if any interpretation was conducted. With the advent of more powerful computers and sophisticated software programs that can manipulate large sets of digital data, important subsurface information in the form of amplitude changes within the reflected waves has been extracted from these types of GPR data (Conyers 2004). An analysis of the spatial distribution of the amplitudes of reflected waves is important because it is an indicator of subsurface changes in lithology and other physical properties. The higher the contrasting velocity at a buried interface, the greater the reflected wave amplitude. Suppose amplitude changes can be related to important buried features and stratigraphy. In that case, the location of higher or lower amplitudes at specific depths can be used to reconstruct the subsurface in three dimensions. Areas of low amplitude waves indicate uniform matrix material or soils, while those of high amplitude denote areas of high subsurface contrast such as buried archaeological features, voids or important stratigraphic changes. To be correctly interpreted, amplitude differences must be analyzed in discrete slices that examine only the strength of reflections within specific depths in the ground. Each slice consists of the spatial distribution of all reflected wave amplitudes at various depths, which are indicative of these

Sede di Napoli
Via Cardinale Guglielmo Sanfelice, 8 / 80134 Napoli
Email segreteria.ispc@ispc.cnr.it – segreteria.direzione@ispc.cnr.it

changes in sediments, soils and buried materials. Amplitude slices need not be constructed horizontally or even in equal time intervals. They can vary in thickness and orientation, depending on questions (Conyers and Goodman, 1997). Surface topography and the subsurface orientation of features and stratigraphy of a site may sometimes necessitate the construction of slices that are neither uniform in thickness nor horizontal. To compute horizontal amplitude slices, the computer compares amplitude variations within traces recorded within a defined time window (that can become depth windows if velocities are known). When this is done, both positive and negative amplitudes of reflections are compared to the norm of all amplitudes within that window. No differentiation is usually made between positive or negative amplitudes in these analyses; only the magnitude of amplitude deviation from the norm. Low amplitude variations within any one slice denote little subsurface reflection and therefore indicate the presence of fairly homogeneous material. High amplitudes indicate significant subsurface discontinuities, in many cases detecting the presence of buried features. An abrupt change between an area of low and high amplitude can be very significant and may indicate the presence of a major buried interface between two media. Degrees of amplitude variation in each time slice can be assigned arbitrary colours or shades of grey along a nominal scale. Usually, there are no specific amplitude units assigned to these colour or tonal changes.

Using three-dimensional GPR reflection data, buried features can be rendered into isosurface images, meaning that the interfaces producing the reflections are placed in a three-dimensional picture, and a pattern or colour is assigned to specific amplitudes for them to be visible (Conyers 2004; Goodman et al. 2004; Leckebusch 2003). Typical amplitudes (usually the highest ones) in programs that produce these images can be patterned or coloured while others are made transparent. To simulate sun rays, computer-generated light sources can then be used to shade and shadow the rendered features to enhance them. The elements can be rotated and shaded until the desired image results.

GPR data processing

One of the significant advantages of the GPR method is that the raw data is acquired in a manner that allows it to be easily viewed in real-time using a computer screen. Often very little processing is required for an initial interpretation of the data, with most of the effort directed towards data visualization. On the other hand, it may be necessary to perform sophisticated data processing depending on the application and target of interest. Many practitioners find that techniques common to seismic reflection, such as migration, can be applied. The outcome of processing is a cross-section of the subsurface EM properties, displayed in terms of the two-way travel time, i.e. the time taken for a wave to move from the transmitter to a reflector and return to the receiver. The amount of processing undertaken can range from basic, which allows rapid data output, to the more time-

Sede di Napoli
Via Cardinale Guglielmo Sanfelice, 8 / 80134 Napoli
Email segreteria.ispc@ispc.cnr.it – segreteria.direzione@ispc.cnr.it

consuming application of algorithms designed for use on the seismic dataset (Ylmaz, 1987), which produce high-quality work (Conyers and Goodman, 1997). The processing sequence usually developed for GPR raw data is following done.

Zero-time adjusts (static shift) – The airwave is the first waveform to arrive at the receiver during a GPR survey. There is a delay in the arrival time of the first break of the air wave on the radar section due to the length of the cable connecting the antennae and the control unit. Therefore need to associate zero-time with zero-depth, so any time offset due to instrument recording must be removed before interpretation of the radar image.

Background removal filter (subtract average trace to remove banding) - Background noise is a repetitive signal created by slight ringing in the antennae, which produces a coherent banding effect, parallel to the surface wave, across the section (Conyers and Goodman,1997). The filter is a simple arithmetic process that sums all the amplitudes of reflections recorded simultaneously along with a profile divided by the number of traces summed; the resulting composite digital wave, which is an average of all background noise, is then subtracted from the data set. In this process, care must be taken not to remove actual linear events in the profile. The time window where the filter operates must be specified so that the filter is not applied until after the surface wave.

Horizontal (distance) stretch to get constant trace separation (horizontal normalization) – This correction needs to remove non-constant motion effects along with the profile. Data are collected continuously and will not be represented correctly in the image if steps are not taken to correct the horizontal data coverage variable.

Gain – Gain is used to compensate for amplitude variations in the GPR image; early signal arrival times have greater amplitude than later because these early signals have not travelled as far. The loss of signal amplitude is related to geometric spreading and intrinsic attenuation. Various time-variable gain functions may be applied to equalize the amplitudes of the recorded signals. The most commonly used is an automatic gain control (AGC), a time-varying gain that runs a window of chosen length along each trace, point by point, finding the average amplitude over the length of the window about each topic. A gain function is then applied such that the average at each point is made constant along the trace.

Topographic corrections – Surveyed elevation data apply topography to the GPR survey profiles. Firstly trace windowing is used to remove all artefacts in the survey that arrived before the time zero arrivals. The elevation recorded along the GPR line is then entered into the data processing package. The time zero arrivals are hung from the topographic profile by applying a time shift to each trace.

Frequency filtering - Although GPR data are collected with source and receiver antennae of specified

Sede di Napoli
Via Cardinale Guglielmo Sanfelice, 8 / 80134 Napoli
Email segreteria.ispc@ispc.cnr.it – segreteria.direzione@ispc.cnr.it

dominant frequency, the recorded signals include a band of frequencies around the dominant frequency component. Frequency filtering removes unwanted high and/or low frequencies to produce a more interpretable GPR image. Highpass filtering maintains the high frequencies in the signal but removes the low-frequency components. Low-pass filtering does just the opposite, eliminating high frequencies and retaining the low-frequency components. A combination of these two effects can be achieved with a band-pass filter, where the filter retains all frequencies in the pass band but removes the high and low frequencies outside of the pass band.

Deconvolution - When the time-domain GPR pulse propagates in the subsurface, convolution is the physical process that describes how the propagating wavelet interacts with the earth filter (the reflection and transmission response of the subsurface). Deconvolution is an inverse filtering operation that attempts to remove the effects of the source wavelet better to interpret GPR profiles as images of the earth structure. Deconvolution operators can degrade GPR images when the source signature is not known. Deconvolution operators are designed to assume that the propagating source wavelet is a minimum phase (i.e., most of its energy is associated with early times in the wavelet). This assumption is not necessarily valid for GPR signals. With GPR, the ground becomes part of the antennae, and the source pulse can vary from trace to trace and is not necessarily the minimum phase. All filtering operations borrowed from seismic data processing must be applied with care as some of the underlying assumptions for elastic waves generated at the earth's surface are not valid or are different for electromagnetic waves. For more, see Ylmaz (1987)

Migration - Migration is a processing technique that attempts to correct that energy in the GPR profile image is not necessarily correctly associated with depths below the 2-D survey line. As with deconvolution, migration can be seen as an inverse processing step that attempts to correct the geometry of the subsurface in the GPR image concerning the survey geometry. For example, a subsurface scattering point in a GPR image is a hyperbolic-shaped feature. Migration would associate all the energy in the wavelets making up the hyperbolic feature with the point of diffraction, and imaging the actual earth structure (the heterogeneity represented by the point diffractor) would be imaged more clearly. Migration operators require an excellent subsurface EM wave velocity estimate to apply the correct adjustments to the GPR image. For more, see Ylmaz (1987).

F-K filter - Fourier transforms techniques, or f-k filtering, i.e. using filters designed and applied in the frequency-wavenumber (or f-k) domain (Yilmaz, 1987). It is well known that a dipping line in the x-t domain maps to a line passing through the origin and with an orientation normal to the original line in the f-k amplitude spectrum. In other words, a line of constant apparent velocity corresponds to a line of constant slope in the f-k domain. In particular, horizontal lines map to the vertical direction along

Sede di Napoli
Via Cardinale Guglielmo Sanfelice, 8 / 80134 Napoli
Email segreteria.ispc@ispc.cnr.it – segreteria.direzione@ispc.cnr.it

the f-axis. Dipping events that overlap in the x-t domain can be separated in the f-k domain by their dips. This allows the elimination of certain types of unwanted energy from the data, representing linear coherent noise. Regardless of their location, lines with the same dip (parallel lines) map to the same radial line in the f-k amplitude spectrum, so that f-k filters could be effective for removing at the same time all undesired lines with the same slope, but impractical if one wants to remove only some of them instead of the whole family. Fan filters are generally used for dip filtering. In these cases, the amplitude spectrum of the input is multiplied by a suitable function, the amplitude response of the filter consisting of ones in a fan-shaped zone and zeros elsewhere, to obtain the amplitude spectrum of the output, whereas the phase spectrum is left unchanged. Finally, the filtered signal is received by a twodimensional inverse Fourier transform.

The Wavelet Transform is possible to decompose the radar signal into different scales where signal and certain noises may be effectively separated/isolated (multiresolution analysis). Subsequent noise muting is easily achieved in the Wavelet Transform (WT) domain operating only on the scales where the offending noise appears.

Time-slice analysis – An analysis of the spatial distribution of reflected wave amplitudes is essential because it indicates potentially meaningful subsurface changes in lithology or other physical properties of materials in the ground. If amplitude changes can be related to the presence of important buried features, the location of those changes can be used to reconstruct the subsurface in three dimensions. Areas of low-amplitude waves usually indicate uniform matrix material or soils. At the same time, those of high amplitude denote areas of high subsurface contrast such as buried archaeological features, voids, or significant stratigraphic changes. To be interpreted, amplitude differences must be analyzed in slices that examine only changes within specified depths in the ground. Each amplitude slice consists of the spatial distribution of all reflected wave amplitudes, which are indicative of these changes in sediments, soils, and buried materials. Amplitude slices need not be constructed horizontally or even in equal depth intervals. They can vary in thickness and orientation, depending on the questions. To produce horizontal amplitude slice maps, the computer compares amplitude variations within traces recorded within a defined time window. For instance, if data were recorded to a maximum of 30 nanoseconds in the ground, six slices of 5 nanoseconds in thickness would be analyzed, and the spatial distribution of amplitudes in each slice would be produced. When this is done, both positive and negative amplitudes of reflections are compared to the norm of all amplitudes within that window. No differentiation is usually made between positive or negative amplitudes in these analyses; only the magnitude of amplitude deviation from the norm is expressed. An abrupt change between an area of low and high amplitude can be very significant and

Sede di Napoli
Via Cardinale Guglielmo Sanfelice, 8 / 80134 Napoli
Email segreteria.ispc@ispc.cnr.it – segreteria.direzione@ispc.cnr.it

may indicate the presence of an important buried interface between two media. Degrees of amplitude variation in each slice can be assigned arbitrary colours or shades of grey along a nominal scale. Usually, there are no specific amplitude units assigned to these colour or tonal changes. Slices produced in thicknesses based on radar travel time can readily be converted to depth slices if the velocity of energy movement through the material (or its RDP) is calculated. This is the preferred format for most archaeological applications. Several computer programs can estimate the velocity of radar travel times from individual reflection profiles; alternatively, direct measurements can be made in the field if open excavations are present (Conyers and Lucius 1996).

Time-depth conversion – The EM-wave velocity can be estimated from GPR data in several ways (Conyers and Goodman 1997; Huisman et al. 2003; Leucci 2019, Leucci 2020); the conventional methods involve common depth-point (CDP) and wide-angle reflection and refraction (WARR) data sets. Both methods require two antennae in separate units and relatively long acquisition times. In the first case, both antennae are simultaneously moved apart on either side of the midpoint of the profile. In the second case, the position of one antenna is fixed while the other is moved along the profile direction. The EM-wave velocity can be more quickly and easily determined from the reflection profiles acquired in continuous mode, using the characteristic hyperbolic shape of reflection from a point source (Fruhwirth et al. 1996). This is a very common method of velocity estimation, and it is based on the phenomenon that a small object reflects EM waves in almost every direction.

Sede di Napoli
Via Cardinale Guglielmo Sanfelice, 8 / 80134 Napoli
Email segreteria.ispc@ispc.cnr.it – segreteria.direzione@ispc.cnr.it

GPR DATA ANALYSIS: The 900 MHz antenna

The surveyed zone was divided into three main areas, the lower pane, the middle pane and the upper pane (Fig. 1). The location of GPR profiles is shows in the Fig. 1.

The lower pane: On the lower pane 10 GPR profiles were acquired. GPR-slice software (gpr-survey.com) was used to process the 2D radar sections. To eliminate a small noise component and make it easy to interpret GPR data, the following processing sequence was applied:

1) Zero-time adjust (static shift) to associate zero-time with zero-depth;
2) Background removal;
3) Frequency filtering to remove high-frequency noise;
4) Migration, to correct the shape and dimension of reflection events related to the anomalies present in the surveyed structure.

The processed GPR profiles acquired in area CC are shown in Figs. 3 and 4.

The reflection event evidenced by a dashed yellow rectangular (labelled B) is probably related to the presence of different materials insert into the frescoes. The thickness seems to be about 70cm (see the yellow dashed line).

The A's reflection events are related to probable void spaces. Here is possible to note a change in the polarity of the electromagnetic wave. It was found at about 45cm in depth. The dimensions are about 2-3cm.

The reflection events labelled F at a depth of about 30-45cm are related to the probable presence of fractures in the wall.

Lower panel 3D Visualization: A way of obtaining visually useful maps for understanding the plan distribution of reflection amplitudes within specific time intervals is the creation of horizontal time slices. These are maps on which the reflection amplitudes have been projected at a specified time (or depth) with a selected time interval (Conyers, 2006). In a graphic method developed by Goodman et al. (2006), termed 'overlay analysis', the strongest and weakest reflectors at a depth of each slice are assigned specific colours. This technique allows the linkage of anomalies buried at different depths. This represents an improvement in imaging because subtle features indistinguishable on radargrams can be seen and interpreted more easily. The present report uses the time-slice technique to display the amplitude variations within consecutive time windows of width Δt=0.5 ns. Time (or depth) slices can be seen as a virtual excavation that places the interest anomalies at their depth.

The time slices show the amplitude using a range defined by blue as zero and red as the maximum

Sede di Napoli
Via Cardinale Guglielmo Sanfelice, 8 / 80134 Napoli
Email segreteria.ispc@ispc.cnr.it – segreteria.direzione@ispc.cnr.it

value. Figs. 5 and 6 show the depth slices from 0.0 m to 70 cm in depth.

In the slices ranging from 3.8cm to 15cm depth (Fig. 5), relatively high-amplitude alignments (labelled B) are visible. These correspond to the anomalies labelled B in the 2D radargram. The dashed dark lines highlight a high-amplitude anomaly (labelled F) in the time slices (Figs. 5 and 6) ranging from 45cm to 70cm depth. This corresponds to the probable fractures. The time slices ranging from 41cm to 56cm (Fig. 5) depth show another high amplitude anomaly (labelled A) probably related to void space.

Fig 7 shows the more significant depth slices overlapped with the planimetry of the wall. It is possible to see the position of the high amplitude anomalies B and F.

Moreover, the highest amplitudes were rendered into an isosurface (Conyers and Goodman, 1997; Conyers, 2004, 2012; Leucci, 2019; Leucci, 2020; Giannino and Leucci, 2021). Three-dimensional amplitude isosurface rendering displays amplitudes of equal value in the GPR study volume. Shading is usually used to illuminate these surfaces, giving the appearance of real archaeological structures. In this case, threshold calibration is a delicate task to obtain valuable results. Fig. 8 shows the isosurfaces amplitude visualization.

Middle pane

On the middle pane, 14 GPR profiles were acquired (Fig. 1). The GPR data were processed similarly used for the lower pane. The profiles acquired in the middle pane are shown in Fig. 1.

The processed GPR profiles are shown in Figs. 9,…, 12.

The reflection event evidenced by a dashed yellow line represents the end of the wall and therefore has a thickness of about 70cm.

The F's reflection events, evidenced by a dashed red line, are related to probable fractures.

The reflection events labelled D at a depth of about 13cm are related to a probable small crack.

Some reflection events labelled V at depths of 19 cm and 45cm, respectively, are probably related to void spaces.

Middle pane: 3D visualization: In this case, the time-slice technique has been used to display the amplitude variations within consecutive time windows of width Δt=0.5 ns.

Fig. 13 shows the depth slices from 0.0cm to 60cm in depth.

In the slices ranging from 0cm to 16cm depth (Fig. 13), relatively high-amplitude alignments (labelled D) are visible. These could be related to a small crack. The dashed dark lines highlight a high-amplitude anomaly (labelled F) in the time slices (Fig. 13) ranging from 15cm to 24cm depth; the high-amplitude anomaly (labelled V) corresponds to void spaces.

Sede di Napoli
Via Cardinale Guglielmo Sanfelice, 8 / 80134 Napoli
Email segreteria.ispc@ispc.cnr.it – segreteria.direzione@ispc.cnr.it

Fig 14 shows the more significant depth slices overlapped with the planimetry of the wall. It is possible to see the position of the high amplitude anomalies F and D.

Fig. 15 show the isosurface visualization. Here is possible to see the position of the anomalous zones well.

Upper pane

On the upper pane 12 GPR profiles were acquired. Also, in this case, the GPR data profiles were processed in 2D using GPR-slice software with the above describes processing steps. The acquired profiles are shown in Fig. 1.

The processed GPR profiles acquired on the upper pane are shown in Figs. 16,…, 18.

The reflection event evidenced by a dashed yellow rectangle (labelled R) is probably related to the reinforcement. Its depth ranges from about 7cm to 23cm.

The reflection events labelled V is related to the probably void spaces.

The reflection events labelled F at a depth of about 50cm are related to a fracture. The reflection events evidenced by a dashed yellow line is the end of the wall.

Upper pane: 3D visualization: Also, in this case, the depth slices analysis shows the distribution of the anomalies zone in the three dimensions (Fig. 19).

In the slices ranging from 7.8cm to 23cm depth (Fig. 19), relatively high-amplitude alignments (labelled R) are visible. These could be related to a structure of reinforcement. In the time slices ranging from 27cm to 30cm depth, a high-amplitude anomaly (labelled V) is visible. This corresponds to a probable void space. The deeper time slice show other high amplitude alignments (F). They could be correlated to fractures.

Fig 20 shows the more significant depth slices overlapped with the planimetry of the investigated wall. It is possible to see the position of the high amplitude anomalies R and F.

Fig. 21 shows the isosurface visualization. Here is possible to see the position of the anomalous zones well. In this case, the anomalies labelled R and F are well evidenced.

The 2 GHz GPR data analysis

Sede di Napoli
Via Cardinale Guglielmo Sanfelice, 8 / 80134 Napoli
Email segreteria.ispc@ispc.cnr.it – segreteria.direzione@ispc.cnr.it

The surveyed zone, lower, middle and upper pane are shown in Fig. 22.

The high-frequency survey was undertaken to obtain detailed information relating to the frescoes. In this way, information was obtained regarding the thickness of the plaster and the zones of severance.

Lower pane

On the lower pane, 29 GPR profiles were acquired (Fig. 22).

The GPR data profiles were processed in 2D using GPR-slice software (gpr-survey.com). To eliminate a small noise component and make it easy to interpret GPR data, the following processing sequence was applied:

1) Zero-time adjust (static shift), to associate zero-time with zero-depth;
2) Background removal;
3) Frequency filtering to remove high-frequency noise;
4) Migration, to correct the shape and dimension of reflection events related to the structure present in the subsoil.

The processed GPR profiles acquired on the lower pane are shown in Figs. 23,…, 27.

The reflection event evidenced by dashed yellow lines is probably related to the two layers of plaster. they seem to have a thickness of about 4cm.

The reflection events labelled D is related to probable severance.

The reflection events labelled I are related to a probable reinforcement with a different material than the frescoes. The reflection events labelled F is seems to be due to a fracture.

The reflection event evidenced by a dashed red line is the end of the wall.

Lower pane: 3D visualization: The time-slice technique has been used to display the amplitude variations within consecutive time windows of width Δt=0.5 ns.

Fig. 28 shows the depth slices from 0cm to 56cm in depth.

In the slices, relatively high-amplitude alignments (labelled D) are visible. These could be related to severance. Also, anomaly I is visible on the first slices and related to a probable reinforcement with a different material than the frescoes. The anomaly F at a depth of about 22cm could be related to fractures

Fig 29 shows the more significant depth slices overlapped with the planimetry of the wall. It is possible to see the position of the high amplitude anomalies D, I and F.

Fig. 30 show the iso-surface visualization. Here is possible to see the spatial position of the anomalies D, I, and F.

Sede di Napoli
Via Cardinale Guglielmo Sanfelice, 8 / 80134 Napoli
Email segreteria.ispc@ispc.cnr.it – segreteria.direzione@ispc.cnr.it

Middle pane

On the middle pane 24 GPR profiles were acquired (Fig. 22).

The GPR data profiles were processed in 2D using the above described processing steps.

The processed GPR profiles acquired in on the middle pane are shown in Figs. 311,…, 36.

The reflection event evidenced by a dashed yellow rectangular (labelled E) is probably related to the high deteriorated area.

The reflection event evidenced by dashed yellow lines is probably related to the two layers of plaster. they seem to have a thickness of about 4cm.

The reflection event evidenced by a dashed red line is the end of the wall.

Middle pane: 3D visualization: Also, in this case, the time-slice technique has been used to display the amplitude variations within consecutive time windows of width Δt=0.6 ns.

Fig. 37 shows the depth slices from 0cm to 70cm in depth.

In the slice between 0cm and 4cm, relatively high-amplitude alignments (labelled D) are visible. These could be related to the phenomena of severance. They have evidenced thanks to the particular analysis performed to build the time slices. The deeper slices evidence the highly deteriorated zone.

Fig 38 shows the more significant depth slices overlapped with the planimetry of the wall. It is possible to see the position of the high amplitude anomalies D.

Fig. 39 show the iso-surface visualization. Here is possible to see the spatial position of anomalies D.

Upper pane

On the upper pane 34 GPR profiles were acquired (Fig. 22).

The GPR data profiles were processed using the above described steps.

The processed GPR profiles are shown in Figs. 40,…, 45.

The reflection event evidenced by a dashed yellow rectangular (labelled R) is probably related to the reinforcement.

The reflection events labelled F is related to the presence of fractured zones.

The reflection events labelled V at a depth of about 37cm are related to probable voids.

The reflection event evidenced by dashed yellow lines is probably related to the two layers of plaster. they seem to have a thickness of about 4cm.

The reflection event evidenced by a dashed red line is the end of the wall.

Sede di Napoli
Via Cardinale Guglielmo Sanfelice, 8 / 80134 Napoli
Email segreteria.ispc@ispc.cnr.it – segreteria.direzione@ispc.cnr.it

Upper pane: 3D visualization: The time-slice technique has been used to display the amplitude variations within consecutive time windows of width Δt=0.6 ns.

Fig. 46 shows the depth slices from 0cm to 60.7cm in depth.

In the slices, relatively high-amplitude alignments (labelled R) are visible. These could be related to probable reinforcement. They are at a depth between 4cm and 32m. At depths between 0cm and 4cm, anomaly D represents a probable severance. At depths between 32cm and 37 cm is possible to see the anomalies labelled F related to the presence of fractures.

Fig 47 shows the more significant depth slices overlapped with the planimetry of the wall. It is possible to see the position of the high amplitude anomalies R and D.

Fig. 48 show the iso-surface visualization. Here is possible to see the spatial position of anomaly R.

CONCLUSIONS

GPR results are encouraging. They evidenced the potentiality of the GPR method in the context of the frescoes of the San Giovanni Monastery. The data allowed evidence of the degree of conservation of the frescoes and the wall (Fig. 49).

There are two probably layers of plaster of variable thickness from 3cm to 4 cm. In some areas, a probable severance was found. GPR survey highlighted probable fractures in the wall formed by irregular ashlars. There is an area (R) in which there seems to be a reinforcement with a thickness of about 20cm.

REFERENCES

Annan, A.P. and Davis, J.L., 1978, Methodology for Radar Transillumination Experiments: Report of

Sede di Napoli
Via Cardinale Guglielmo Sanfelice, 8 / 80134 Napoli
Email segreteria.ispc@ispc.cnr.it – segreteria.direzione@ispc.cnr.it

Activities, Geological Survey of Canada, Paper, 78-1B, p. 107-110.

Annan A.P., Scaife J.E. and Giamou P. 1990. Mapping buried barrels with magnetics and ground penetrating radar. 60th SEG Meeting, San Francisco, USA, Expanded Abstracts, 422–423

Conyers, Lawrence B., 2004, Moisture and soil differences as related to the spatial accuracy of amplitude maps at two archaeological test sites. Proceedings of the Tenth International Conference on Ground Penetrating Radar, Delft, The Netherlands, June 21–24, 2004.

Conyers, Lawrence B. and Dean Goodman, 1997, Ground-penetrating Radar: An Introduction for Archaeologists. AltaMira Press, Walnut Creek, California.

Conyers LB. 2006. Innovative ground-penetrating radar methods for archaeological mapping. Archaeological Prospection 13(2): 139–141.

Conyers LB (2012) Interpreting ground-penetrating radar for archaeology. Left Coast Press, Walnut Creek

Davis J.L. and Annan A.P. 1989. GPR for high resolution mapping of soil and rock stratigraphy. Geophysical Prospecting 37, 531–551.

Fruhwirth R.K., Schmoller R. and Oberaigner E.R. 1996. Some aspects of the estimation of electromagnetic wave velocities. Proceedings of the 6th International Conference on Ground Penetrating Radar, Tohoku University, Sendai, Japan, pp. 135–138.

Gaffney, Chris and John Gater, 2003, Revealing the Buried Past: Geophysics for Archaeologists. Tempus, Stroud, Gloucestershire.

Giannino F. and Leucci G., 2021. Electromagnetic Methods in Geophysics: Applications in GeoRadar, FDEM, TDEM, and AEM. Wiley, pp 352, ISBN: 978-1-119-77098-5

Goodman, Dean and Piro, Salvatore, Nishimura, Yasushi, Patterson, Helen and Vince Gaffney, 2004, Discovery of a 1st century AD Roman amphitheatre and other structures at the Forum Novum by GPR. Journal of Environmental and Engineering Geophysics 9: 35–42.

Goodman D. 2013. GPR Slice Version 7.0 Manual. http://www.gpr-survey.com (accessed June 2013).

Goodman D, Piro S. 2013. GPR Remote Sensing in Archaeology. Geotechnologies and the Environment Series, Vol. 9, Springer-Verlag: Berlin; 233 pp.

Goodman D, Steinberg J, Damiata B, Nishimure Y, Schneider K, Hiromichi H, Hisashi N. 2006. GPR overlay analysis for archaeological prospection. Proceedings of the 11th International Conference on Ground Penetrating Radar, Columbus, Ohio; CD-rom.

Grandjean G., Gourry J.C. and Bitri A. 2000. Evaluation of GPR techniques for civil-engineering applications: study on a test site. Journal of Applied Geophysics 45, 141–156.

Grasmueck M. 1996. 3-D ground-penetrating radar applied to fracture imaging in gneiss. Geophysics

Sede di Napoli
Via Cardinale Guglielmo Sanfelice, 8 / 80134 Napoli
Email segreteria.ispc@ispc.cnr.it – segreteria.direzione@ispc.cnr.it

61, 1050–1064. Greaves R.J., Lesmes D.P., Lee J.M. and Toksöz N. 1996. Velocity variations and water content estimated from multi-offset, ground-penetrating radar. Geophysics 61, 683–695.

Huisman J.A., Hubbard S.S., Redman J.D. and Annan A.P. 2003. Measuring soil water content with ground penetrating radar: A review. Vadose Zone Journal 2, 476–491.

Leckebusch, J., 2003, Ground-penetrating radar: A modern three-dimensional prospection method. Archaeological Prospection 10: 213–240.

Leucci G., 2008. ground penetrating radar:the electromagnetic signal attenuation and maximum penetration depth, Scholarly Research Exchange: Volume 2008 • Article ID 926091 • doi:10.3814/2008/926091;

Leucci G., 2015, Geofisica Applicata all'Archeologia e ai Beni Monumentali. Dario Flaccovio Editore, Palermo, pp. 368. ISBN: 9788857905068

Leucci G., 2019, Nondestructive Testing for Archaeology and Cultural Heritage: A practical guide and new perspective. Springer editore pp 217, ISBN 978-3-030-01898-6

Leucci G., 2020, Advances in Geophysical Methods Applied to Forensic Investigations: New Developments in Acquisition and Data Analysis Methodologies. Springer editore, pp 200, ISBN 978-3-030-46241-3

Mellet J.S. 1995. Ground penetrating radar applications in engineering, environmental management, and geology. Journal of Applied Geophysics 33, 157–166.

Miller, M.L., Freeland, R.S., and Koppenjan, S.K., 2002. Searching for Concealed Human Remains using GPR Imaging of Decomposition, Ninth International Conference on Ground Penetrating Radar, Santa Barbara, California, USA, April 30-May 2, pp. 539- 544.

Ylmaz O., Seismic Data Processing, in: E.B. Neitzel (Ed.), Seismic Data Processing, Society of Exploration Geophysicists, Tulsa USA, 1987.

Sede di Napoli
Via Cardinale Guglielmo Sanfelice, 8 / 80134 Napoli
Email segreteria.ispc@ispc.cnr.it – segreteria.direzione@ispc.cnr.it

FIGURES

Sede di Napoli
Via Cardinale Guglielmo Sanfelice, 8 / 80134 Napoli
Email segreteria.ispc@ispc.cnr.it – segreteria.direzione@ispc.cnr.it

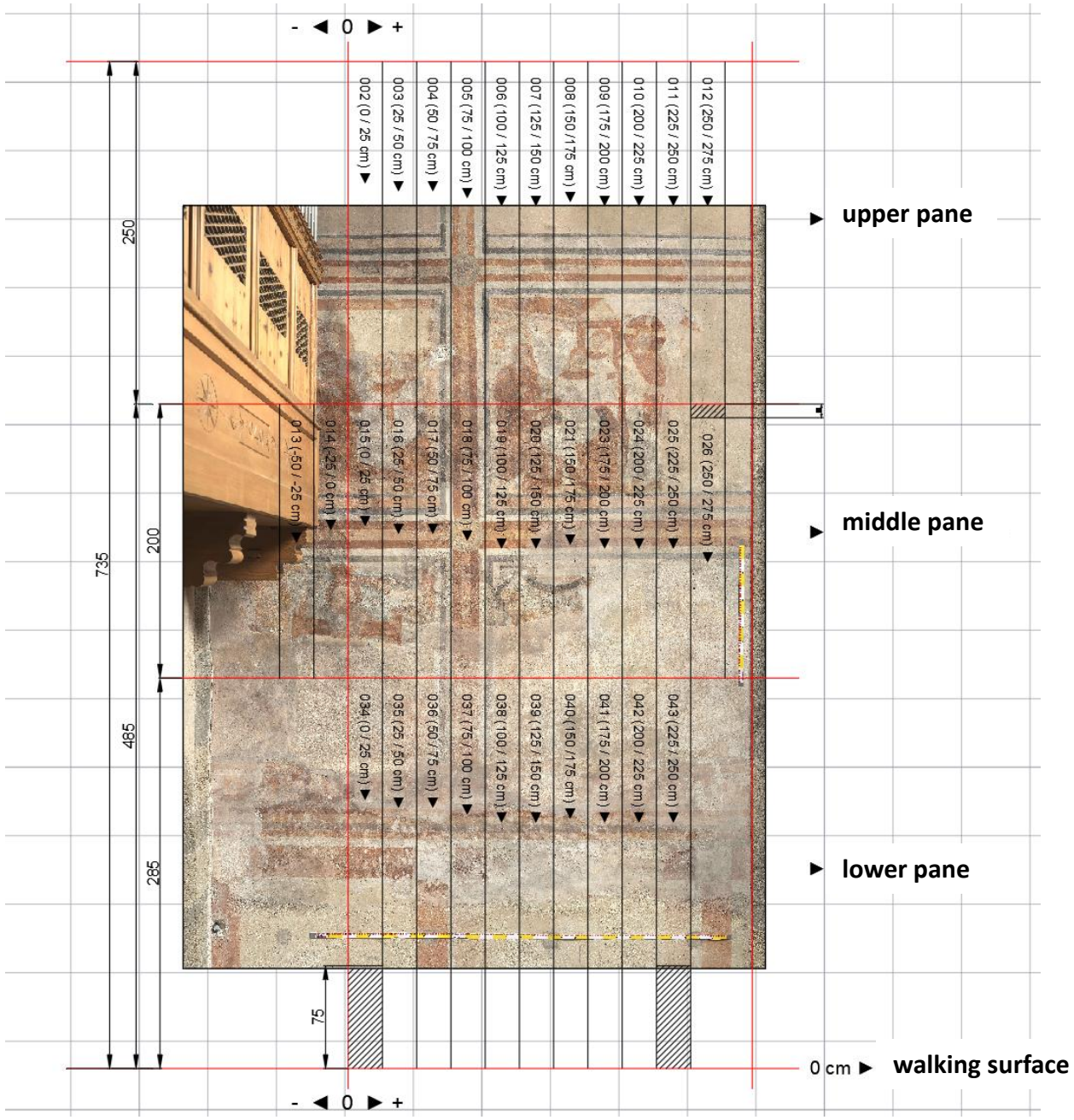

Fig. 1: 900MHz: location of radar profiles

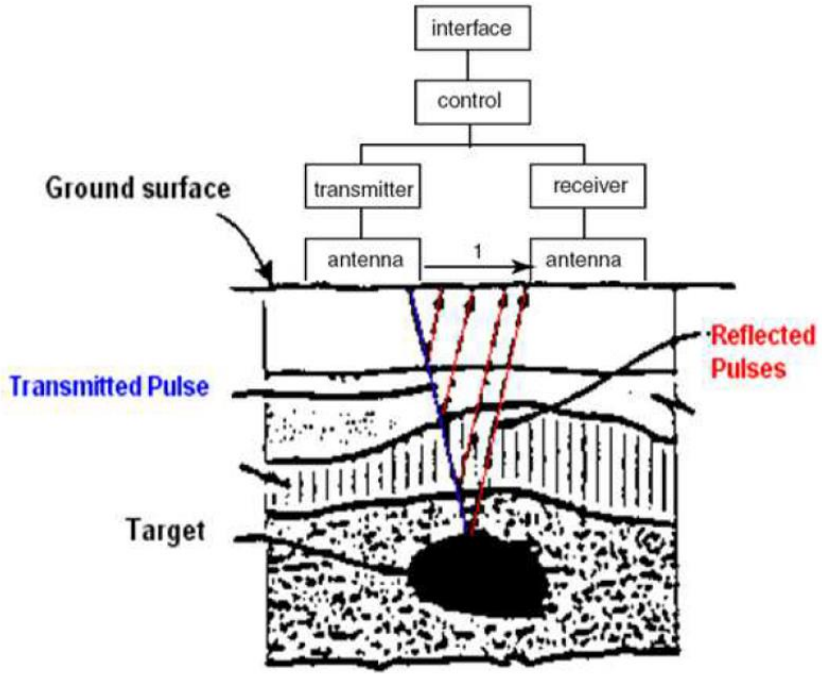

Fig. 2. A block diagram of a GPR system. The interface module enables the user to enter the system parameters and displays and records the data. The control unit generates the timing signals so that all components operate in unison. This unit also does some preliminary data processing. The pulse travel paths in order of arrival are direct air wave, direct ground wave, and reflections.

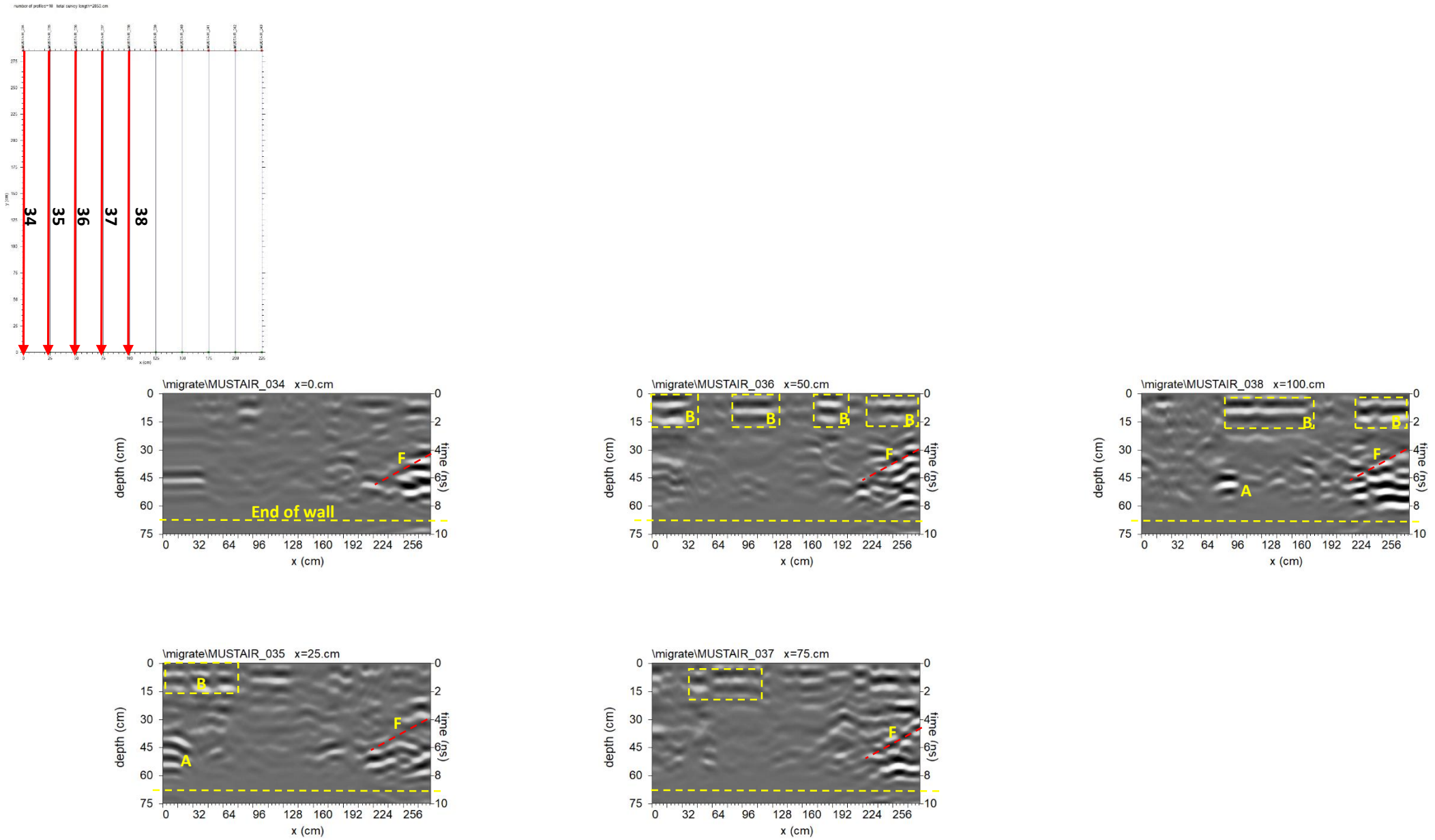

Fig. 3: 900MHz: lower pane: processed radar sections related to the profiles 34,…, 38; dashed yellow line indicates the end of the wall; A: probable void spaces; B: different material; F: fractures

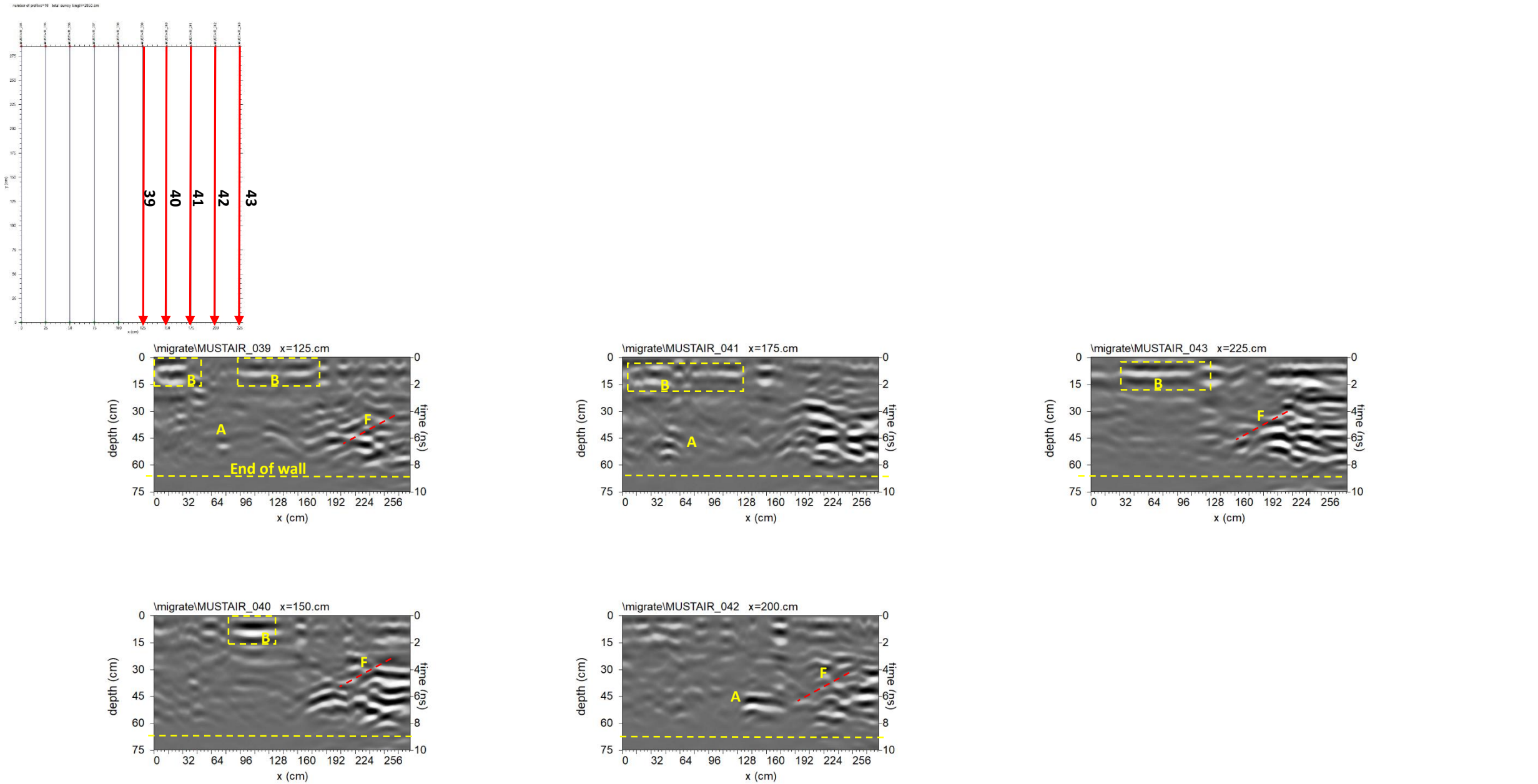

Fig. 4: 900MHz; lower pane: processed radar sections related to the profiles 39,…, 43; dashed yellow line indicates the end of the wall; A: probable void spaces; B: different material; F: fractures

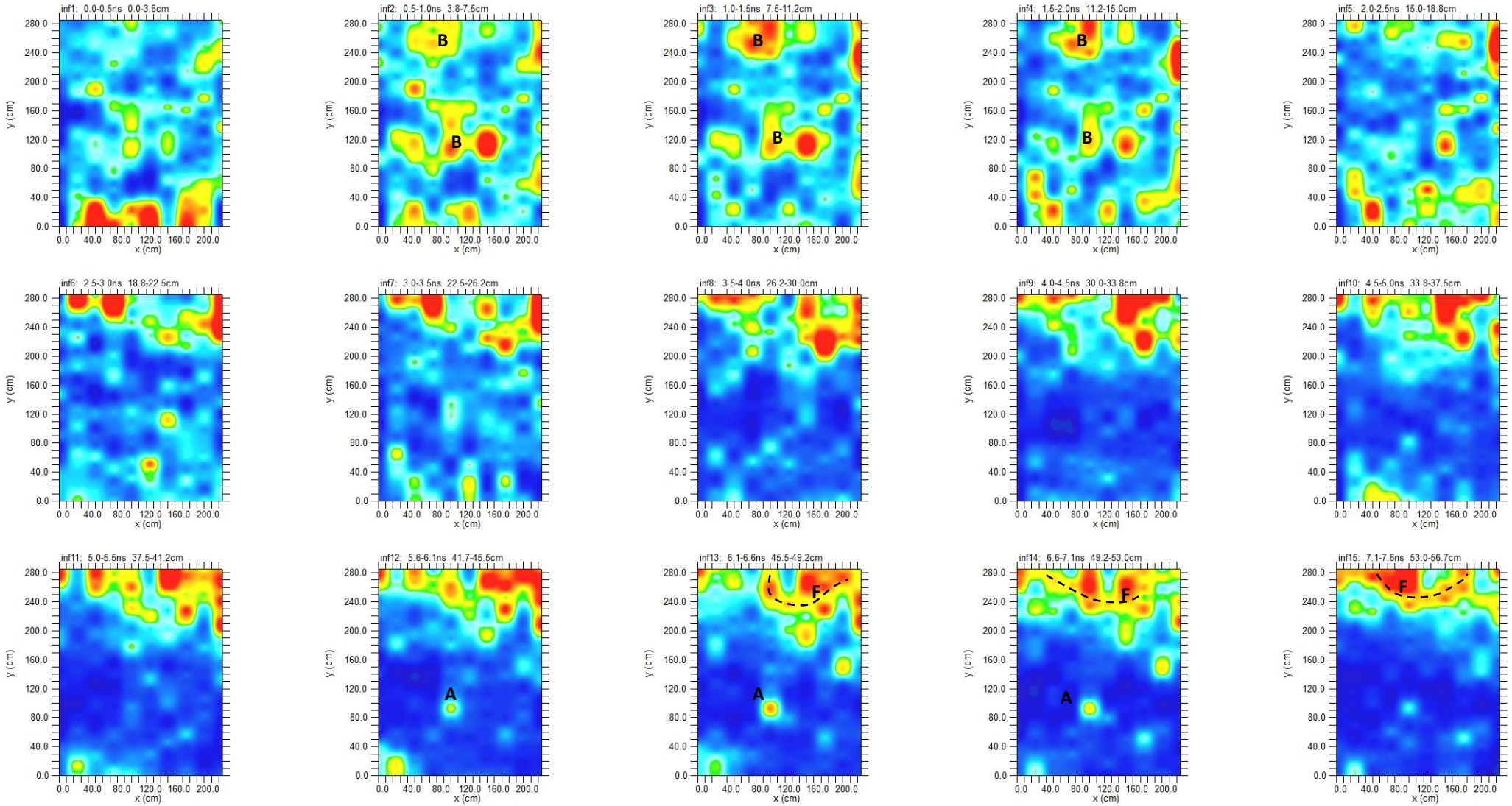

Fig. 5: 900MHz; lower pane: depth slices; dashed yellow line indicates the end of the wall;
A: probable void space; B: different material; F: fractures

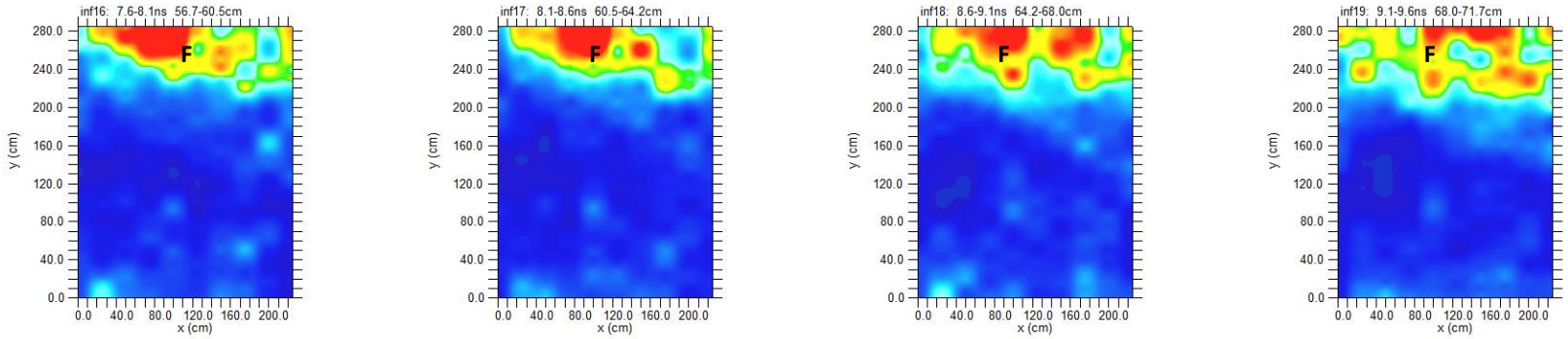

Fig. 6: 900MHz; lower pane: depth slices; F: fractures

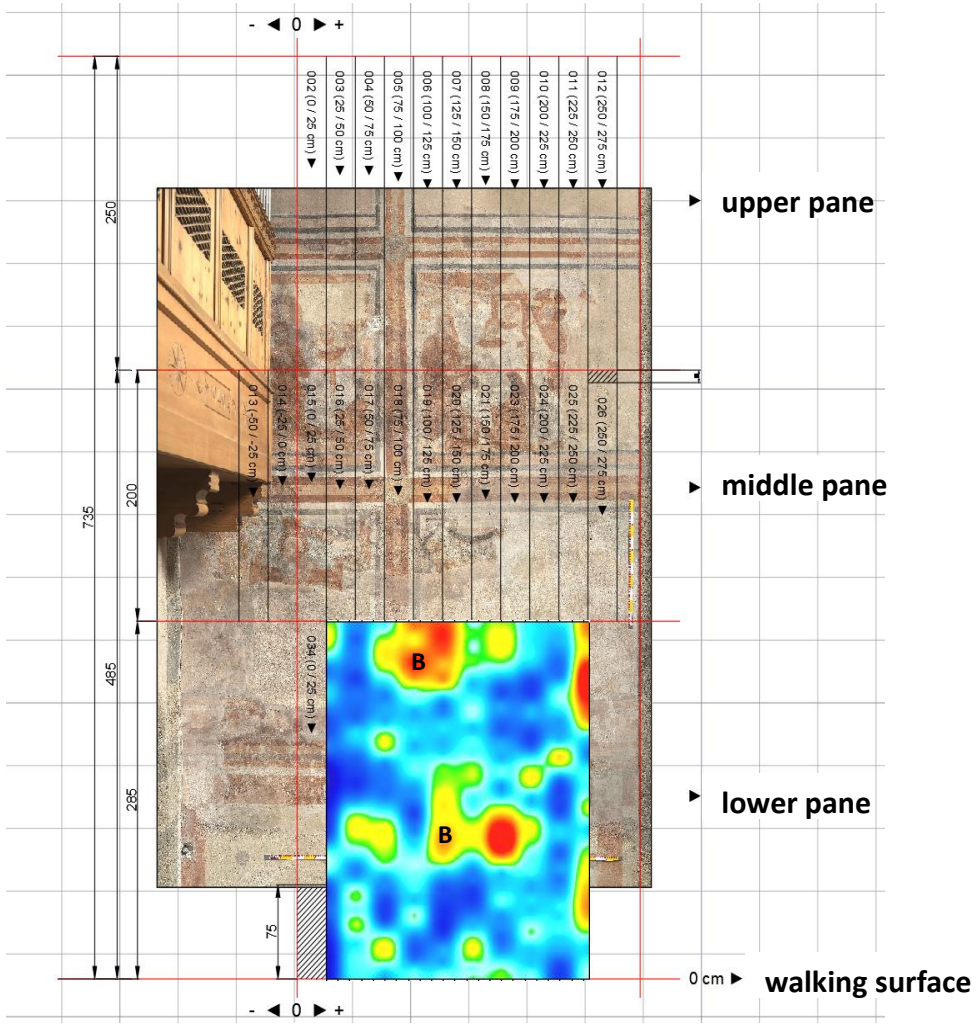

7.5-11.2cm

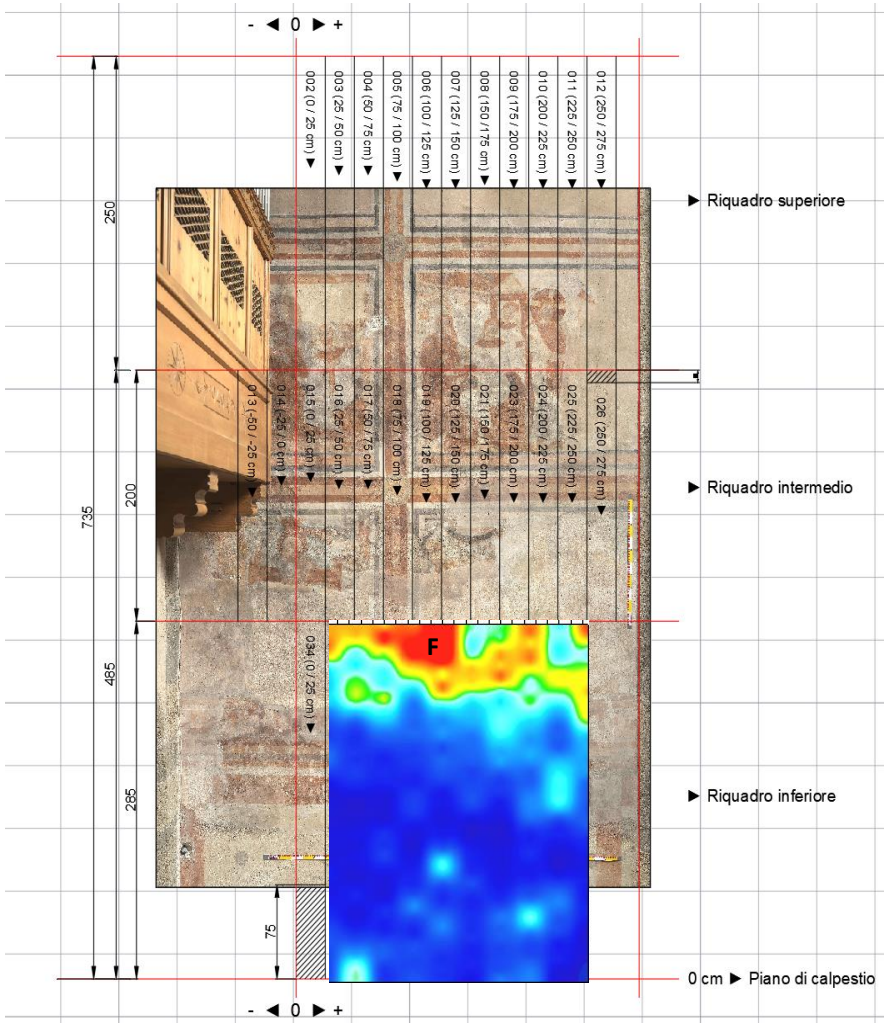

53-56.7cm

Fig. 7: 900MHz; lower pane: depth slices overlapped with the photo of the frescoes

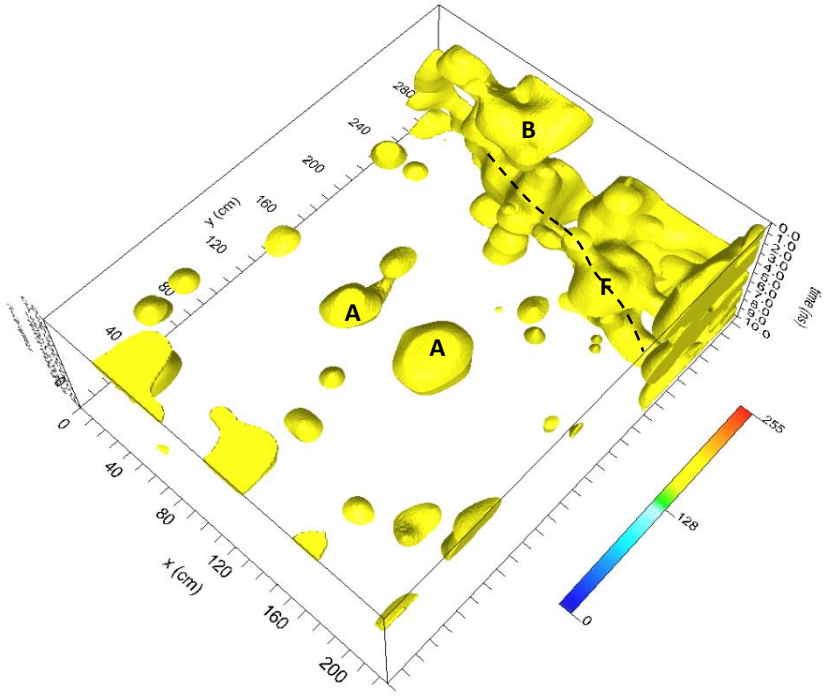

Fig. 8: 900MHz; lower pane: isosurfaces

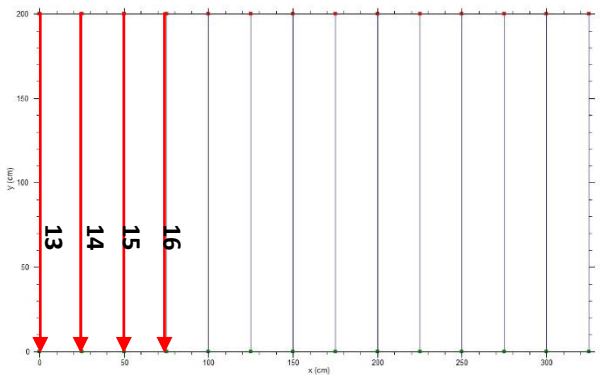

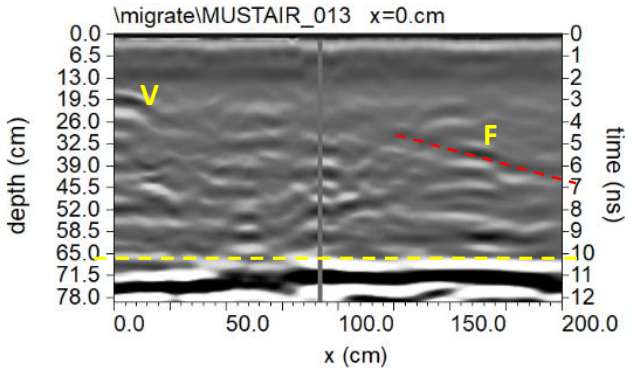

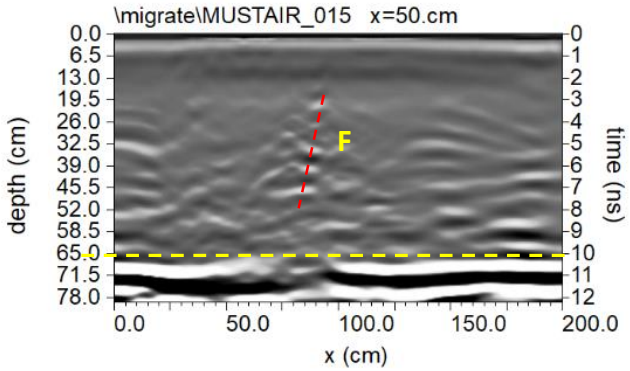

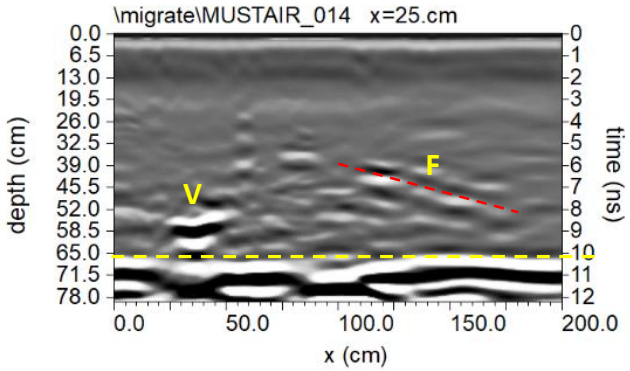

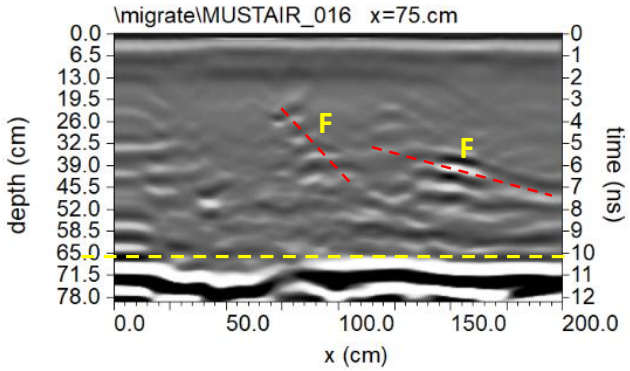

Fig. 9: 900MHz; middle pane: processed radar sections related to the profiles 13,…, 16; dashed yellow line indicates the end of the wall; V: probable void; F: fractures

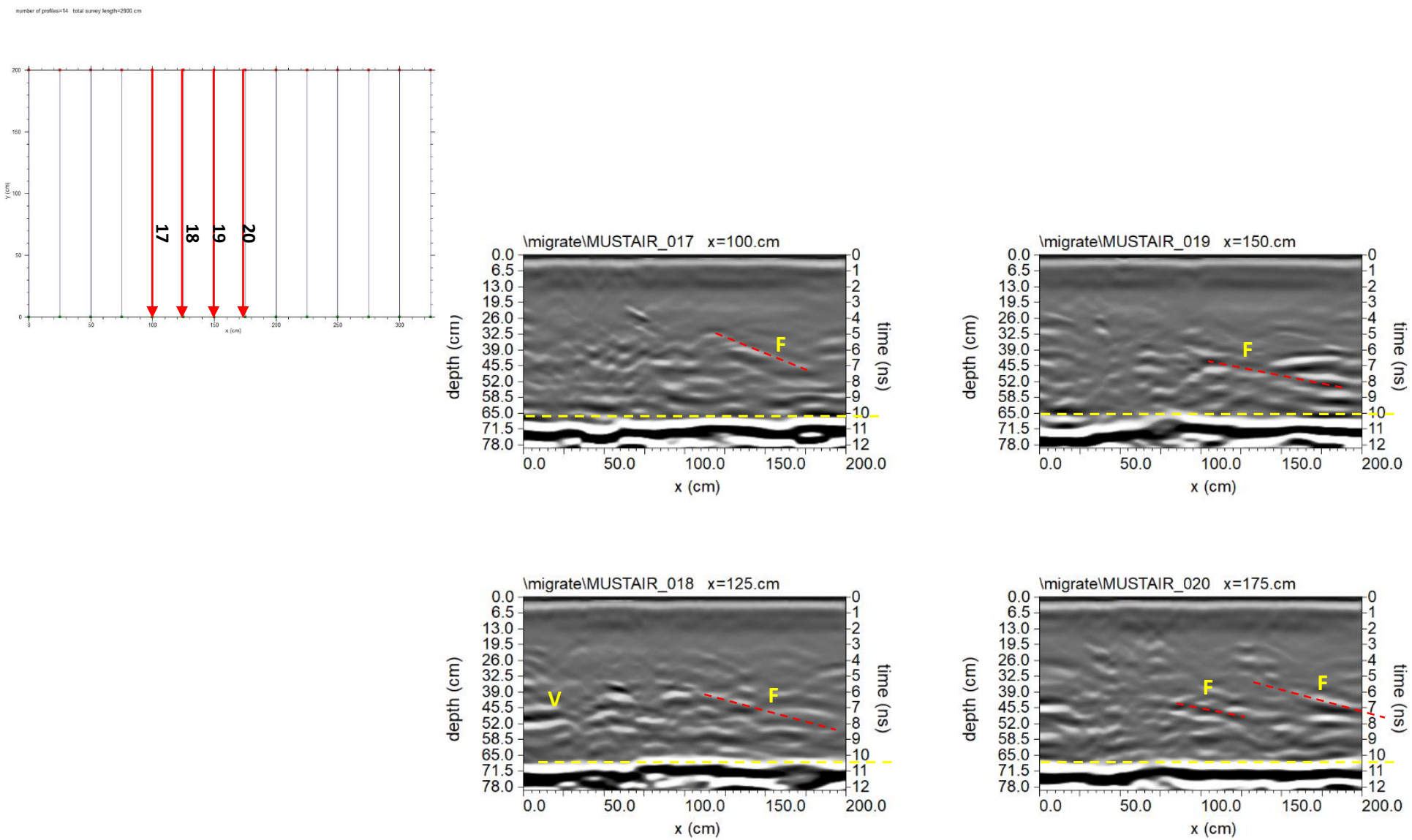

Fig. 10: 900MHz; middle pane: processed radar sections related to the profiles 17,…, 20; dashed yellow line indicates the end of the wall; V: probable void; F: fractures

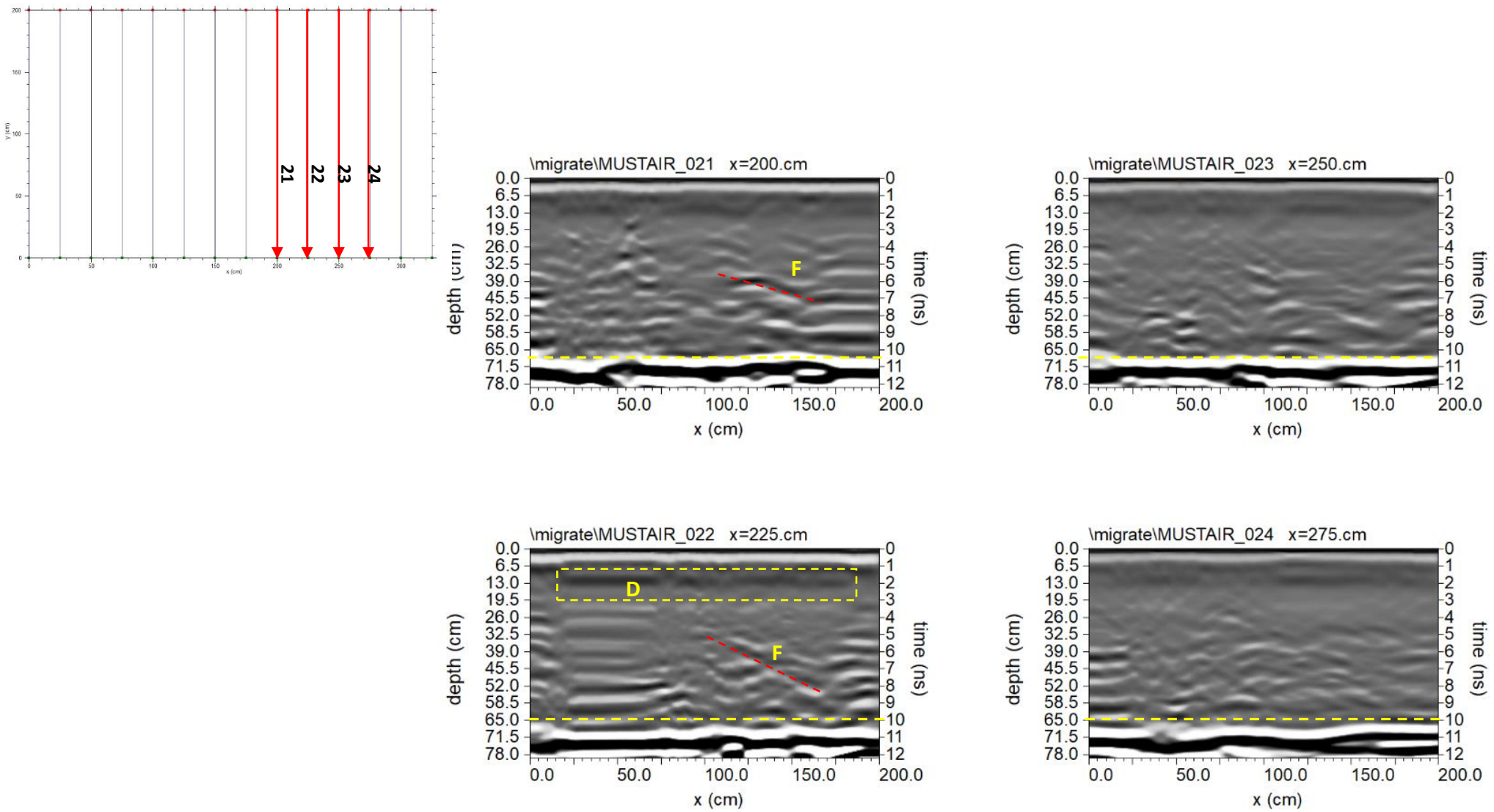

Fig. 11: 900MHz; middle pane: processed radar sections related to the profiles 21,…, 24; dashed yellow line indicates the end of the wall; D: probable small crack; F: fractures

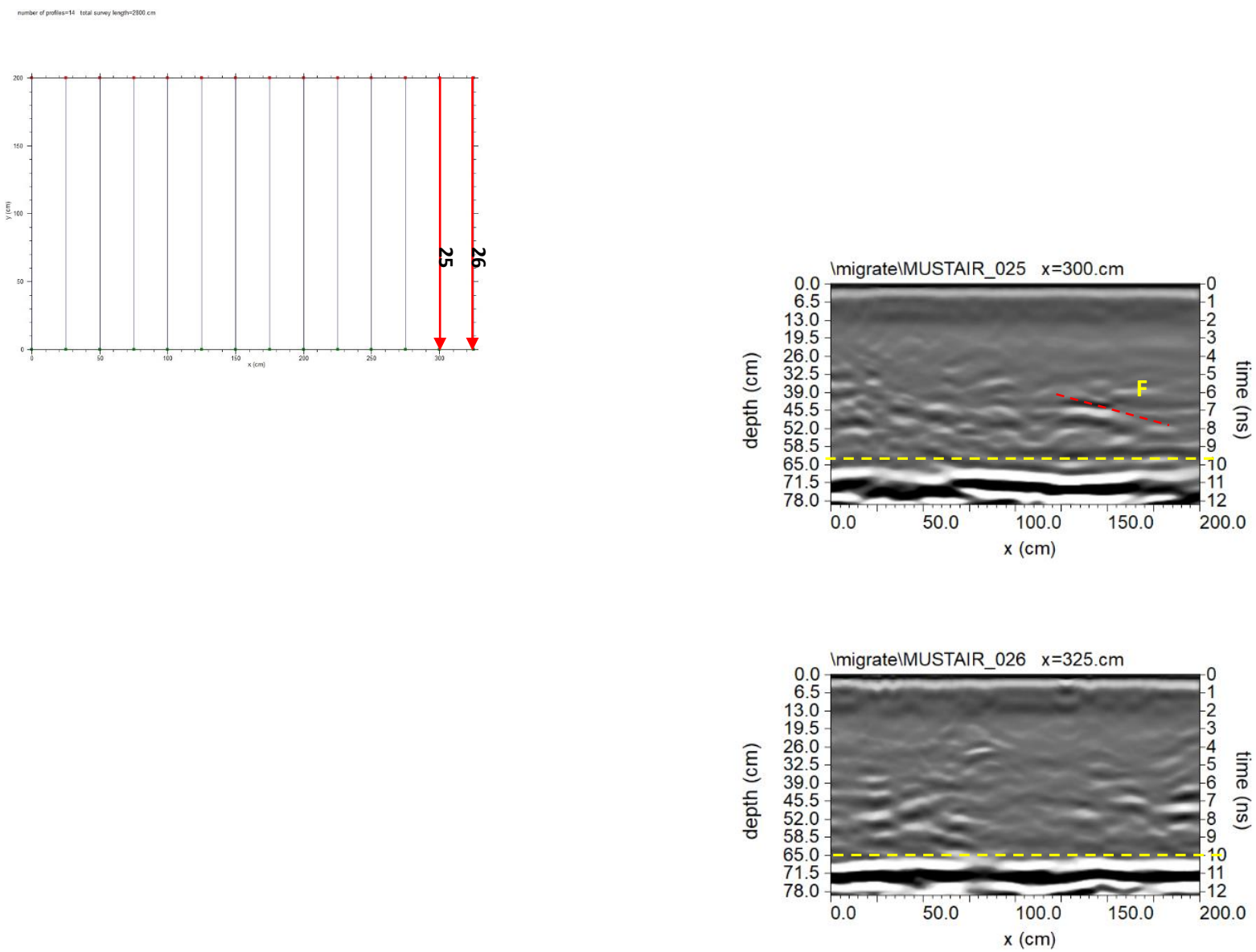

Fig. 12: 900MHz; middle pane: processed radar sections related to the profiles 25 and 26; dashed yellow line indicates the end of the wall; F: fractures

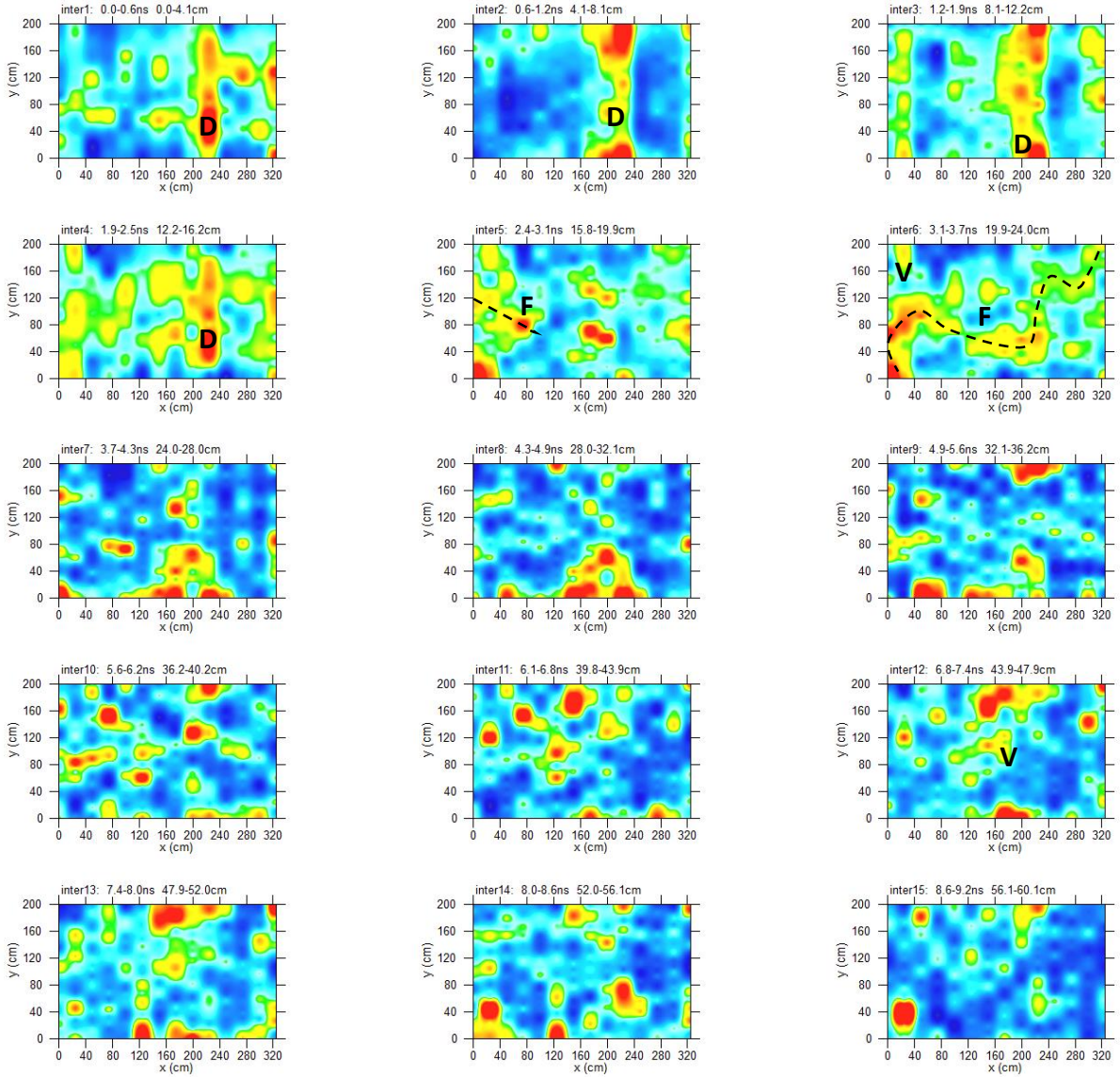

Fig. 13: 900MHz; middle pane:depth slices; D: probable small crack; F: fractures; V: probable void spaces

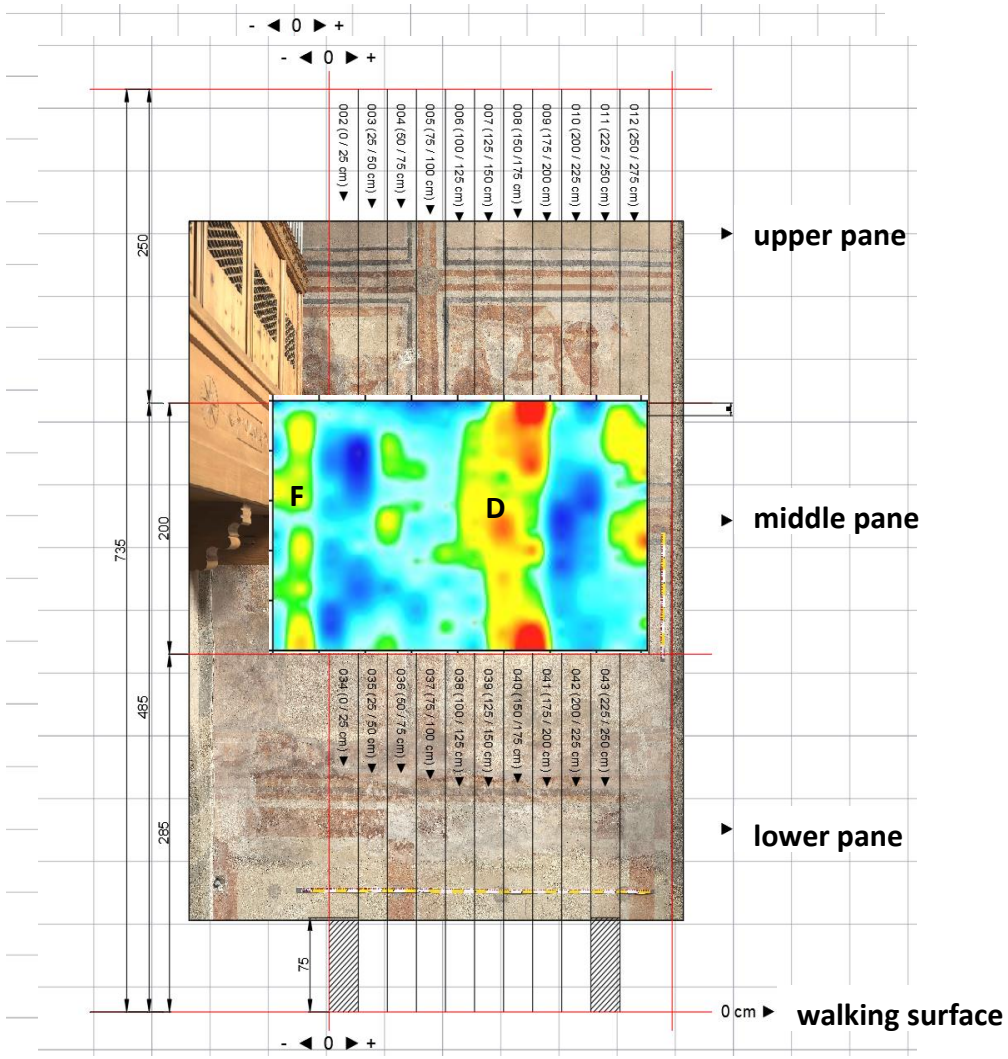

8.1-12.0cm

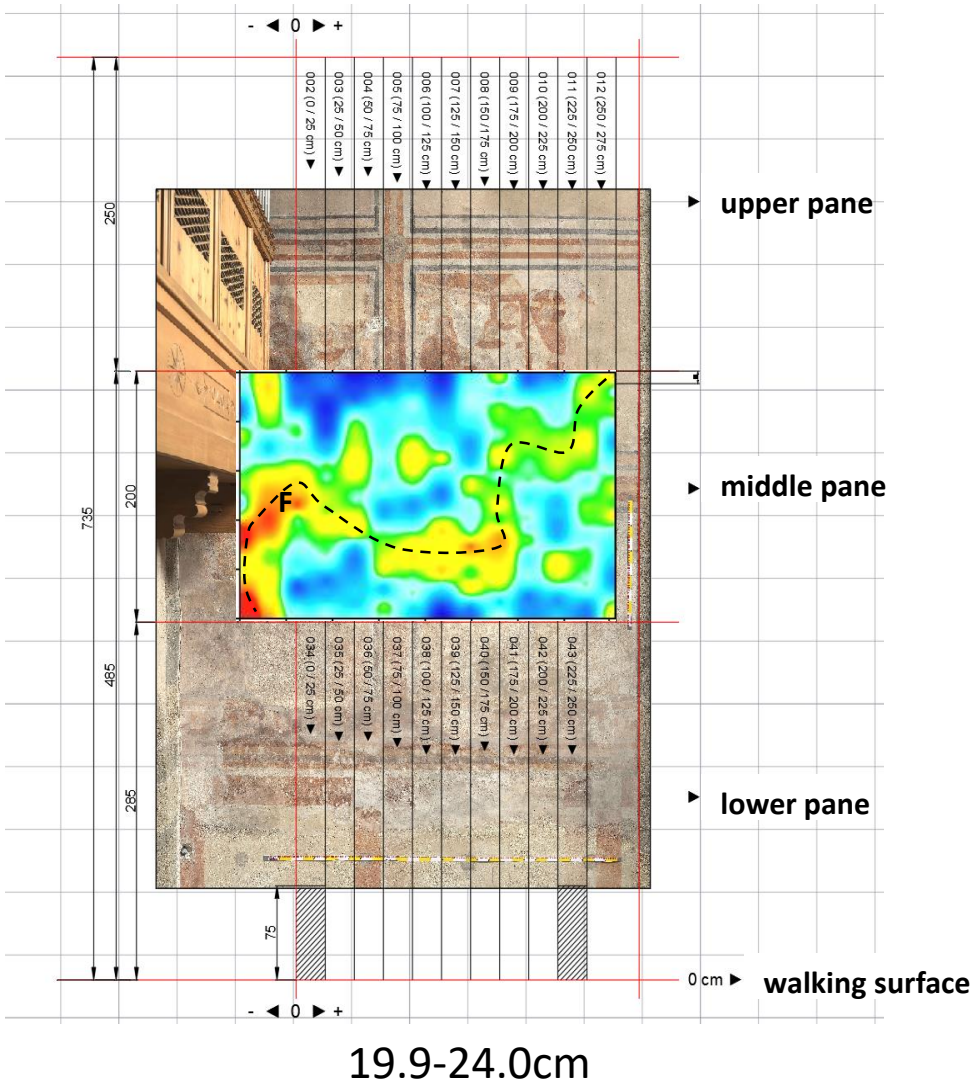

19.9-24.0cm

Fig. 14: 900MHz; middle pane: depth slices overlapped with the photo of the frescoes

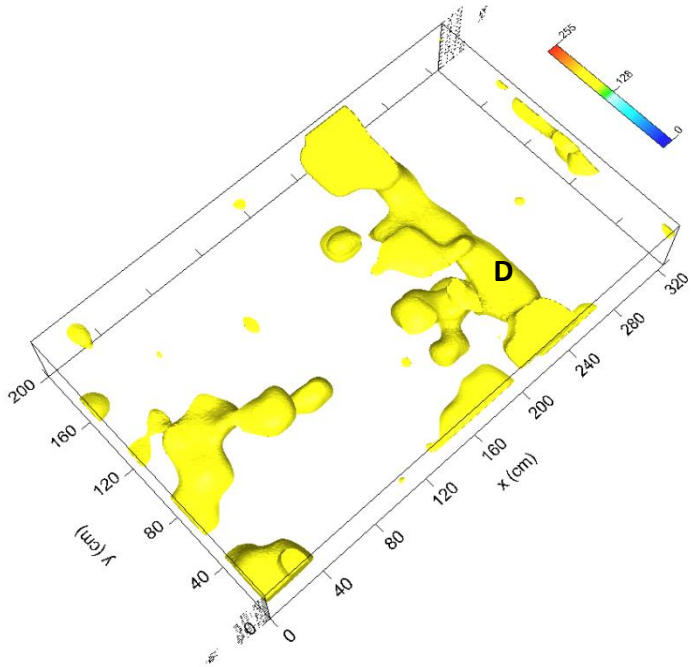

6.5-12.0cm

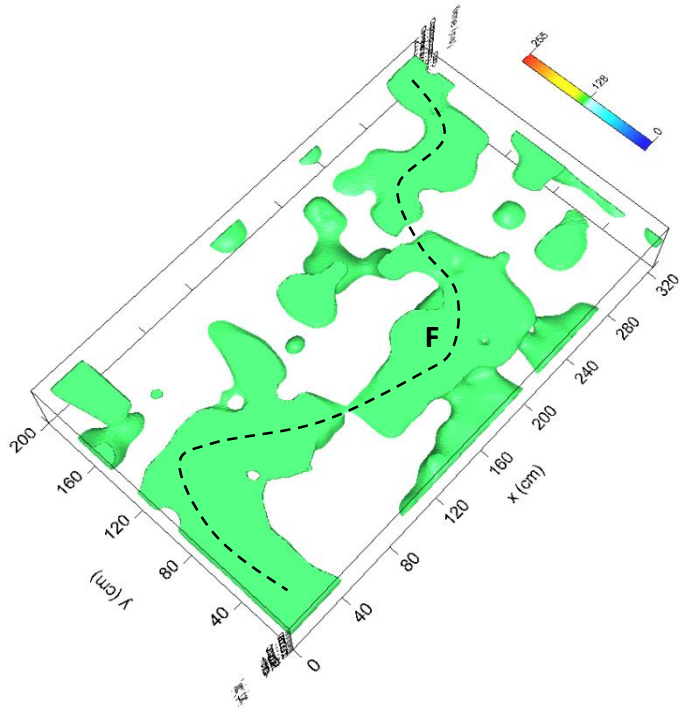

19.9-24.0cm

Fig. 15: 900MHz; middle pane: isosurfaces

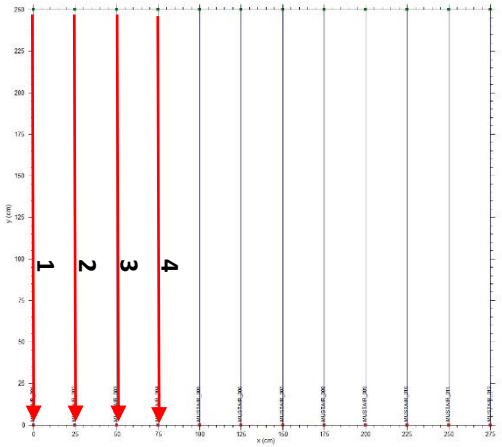

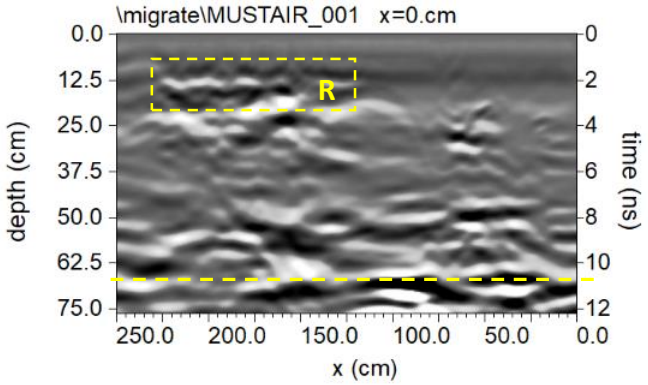

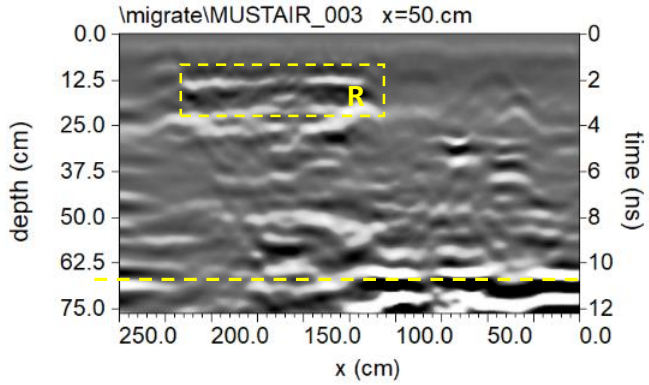

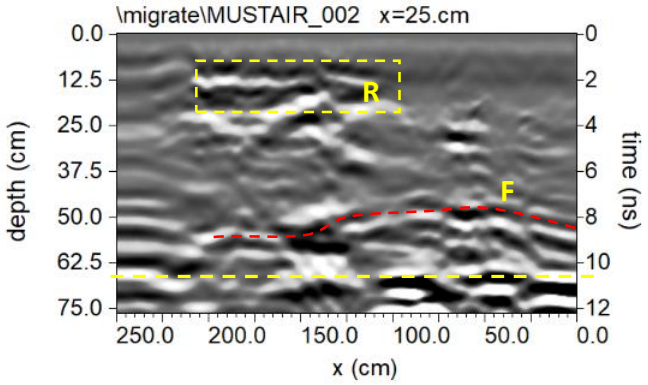

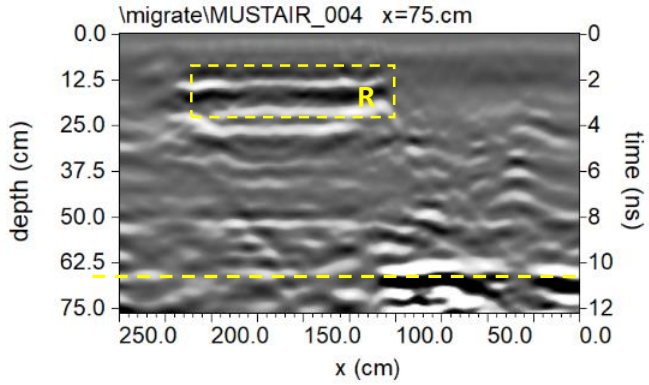

Fig. 16: 900MHz; upper pane: processed radar sections related to the profiles 1,…, 4; dashed yellow line indicates the end of the wall; R: probable reinforcement; F: fractures

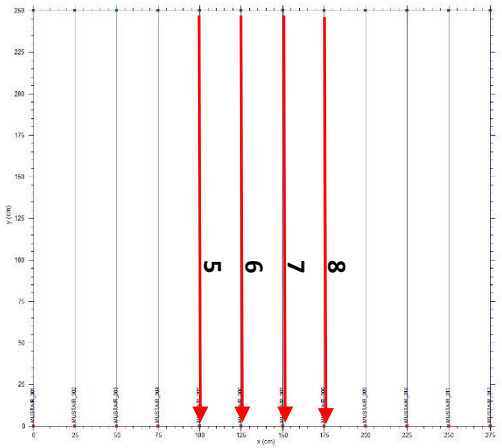

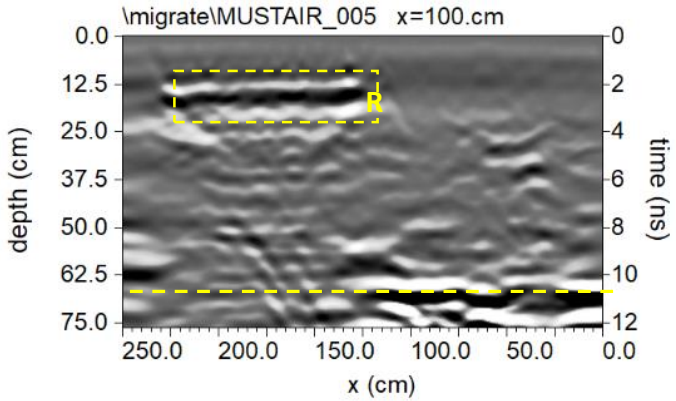

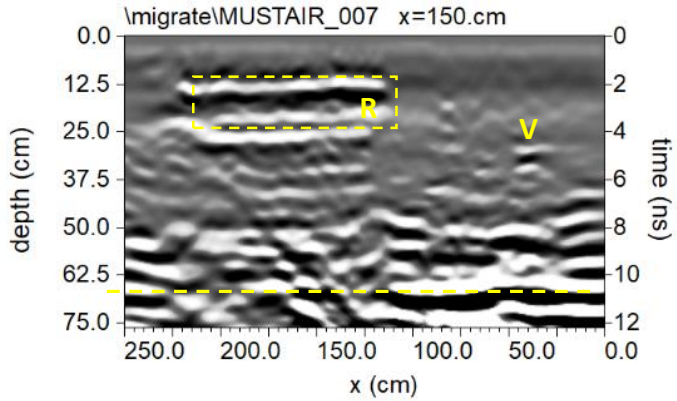

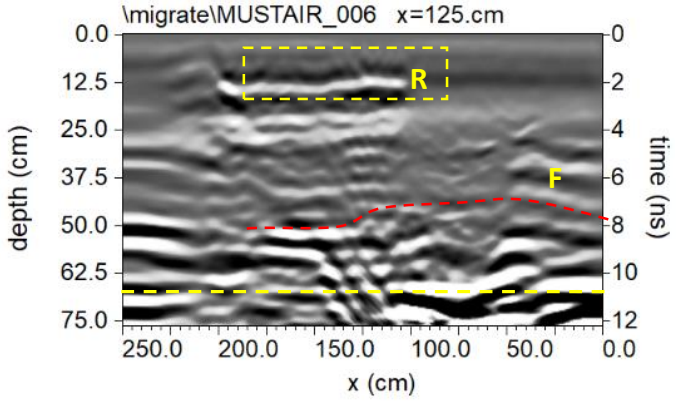

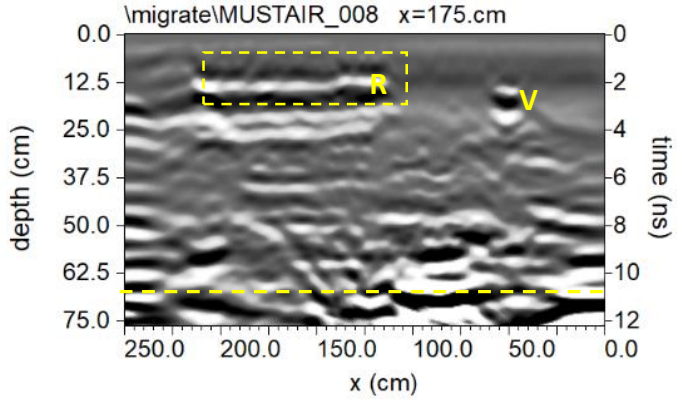

Fig. 17: 900MHz; upper pane: processed radar sections related to the profiles 5,…, 8; dashed yellow line indicates the end of the wall; R: probable reinforcement; F: fractures; V: probable void

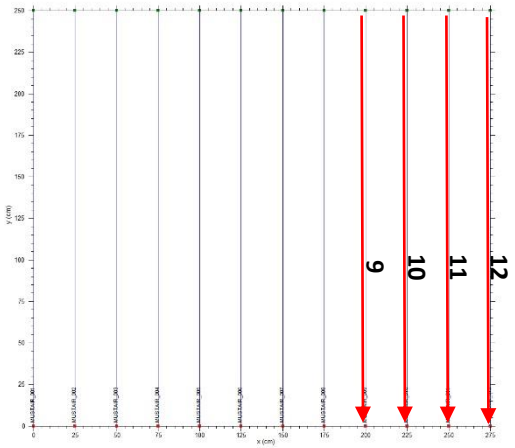

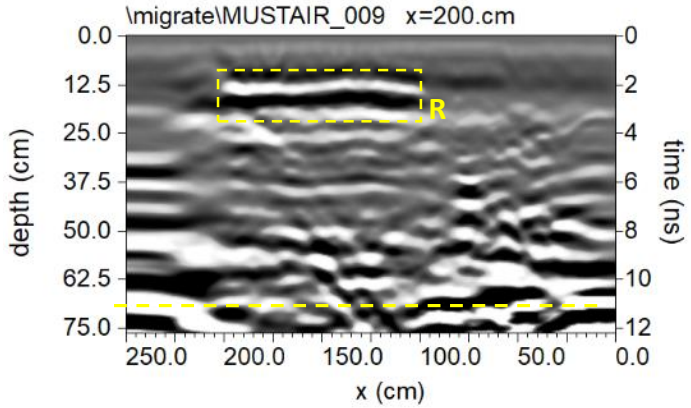

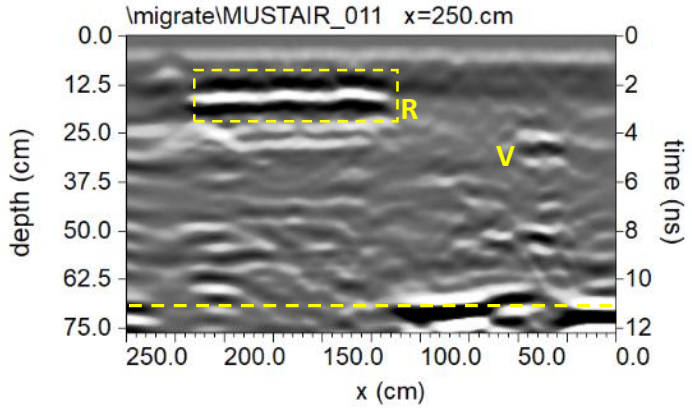

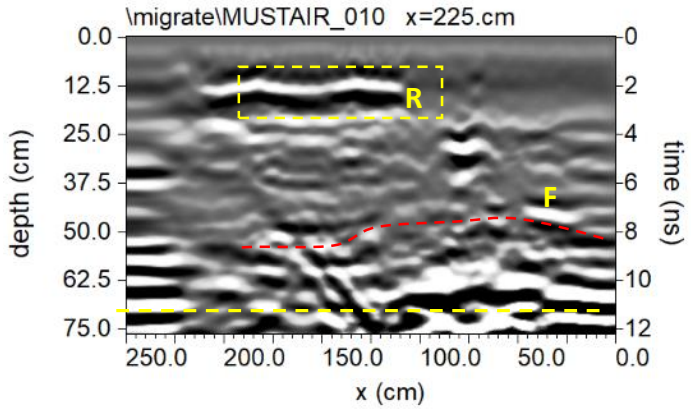

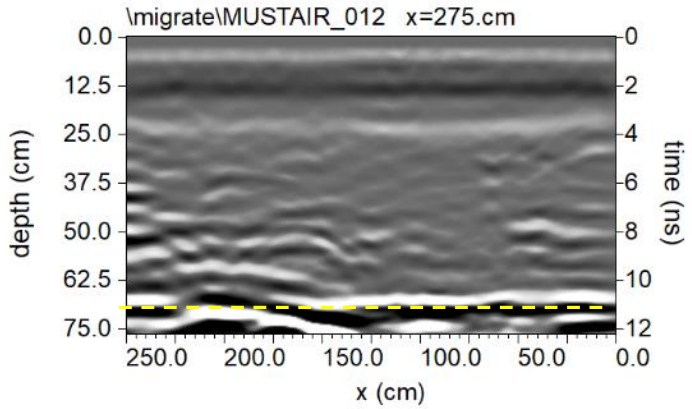

Fig. 18: 900MHz; upper pane: processed radar sections related to the profiles 9,…, 12; dashed yellow line indicates the end of the wall; R: probable reinforcement; F: fractures; V: probable void

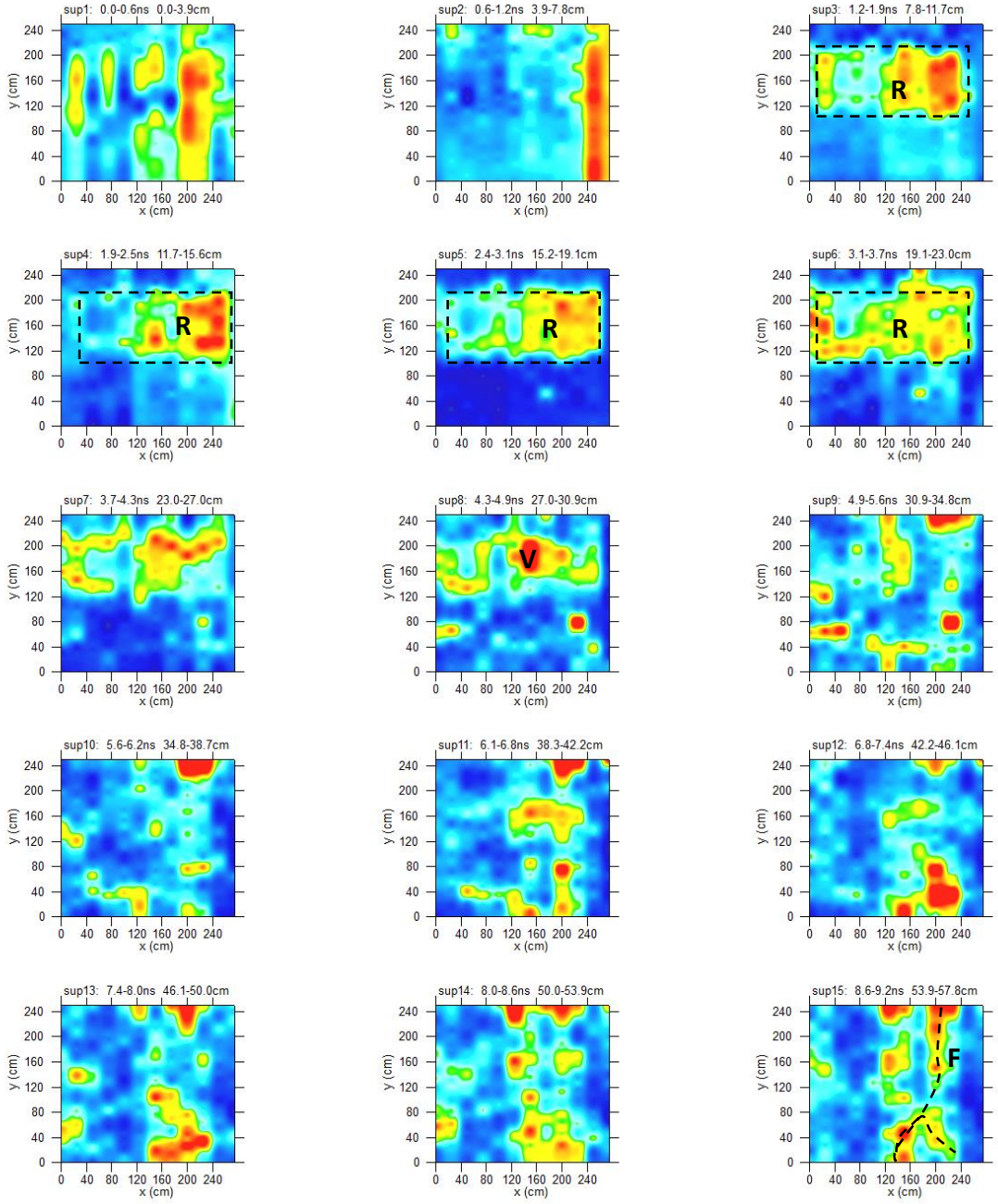

Fig. 19: 900MHz; upper pane: depth slices; R: probable reinforcement; F: fractures; V: probable void

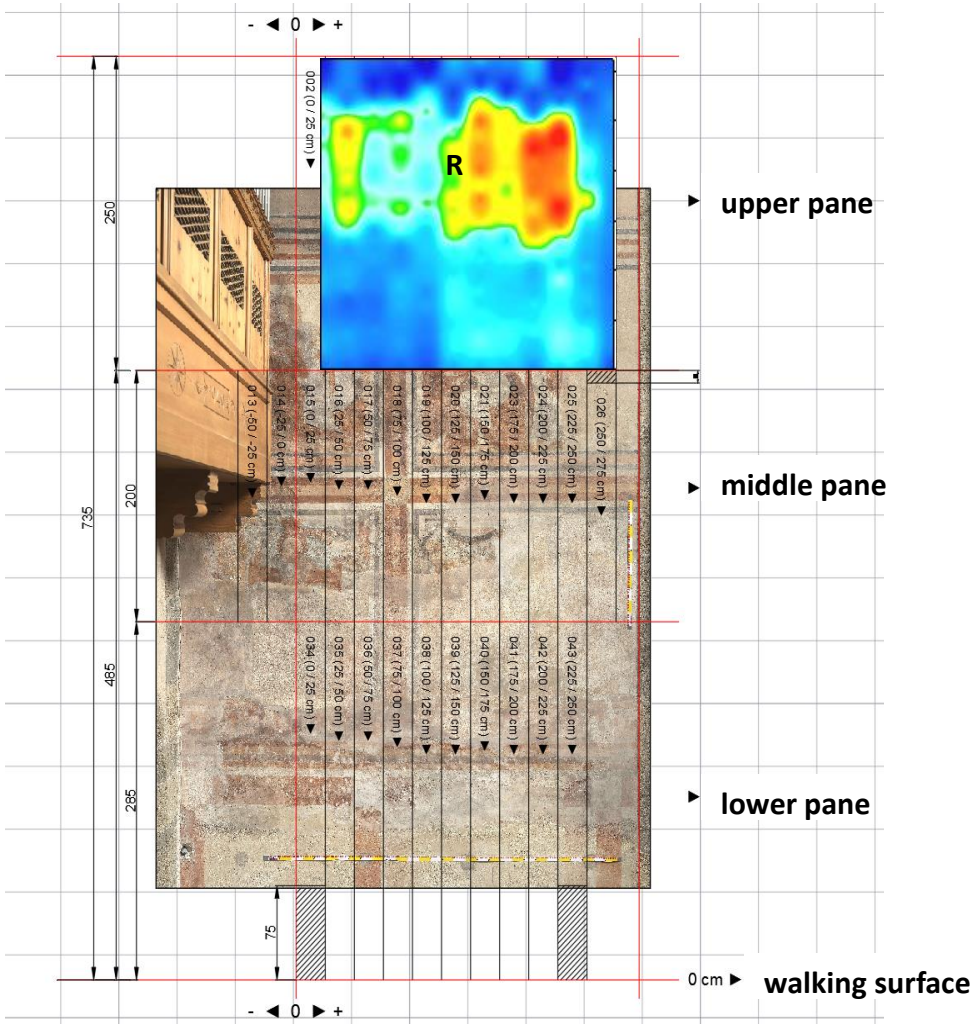

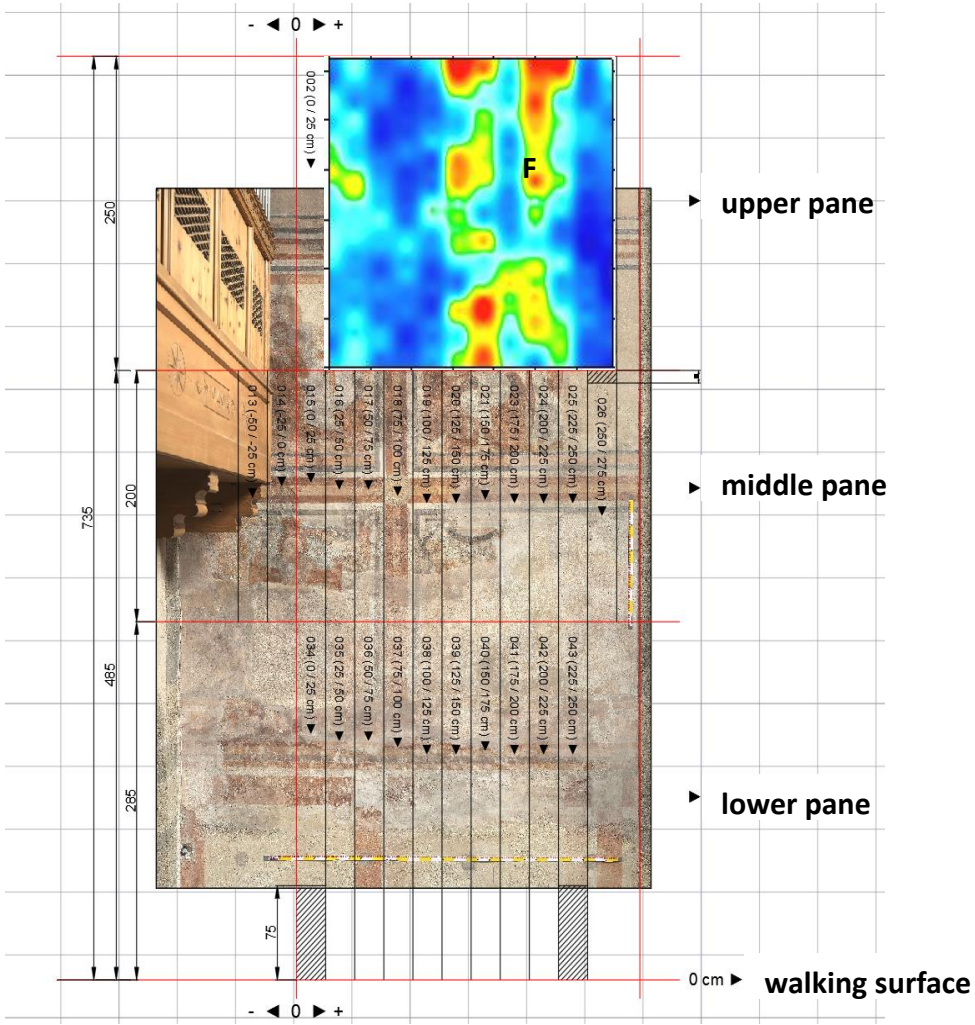

Fig. 20: 900MHz; upper pane: depth slices overlapped with the photo of the frescoes

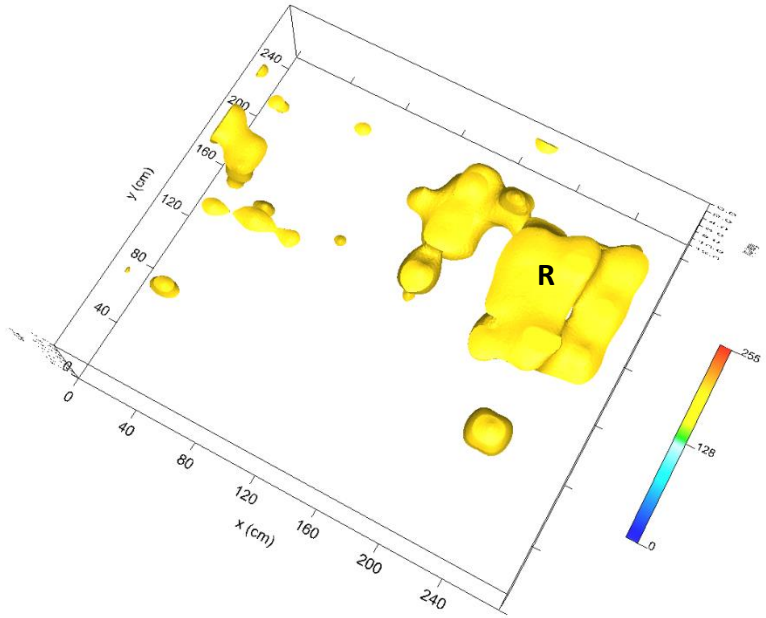

7.8-11.7cm

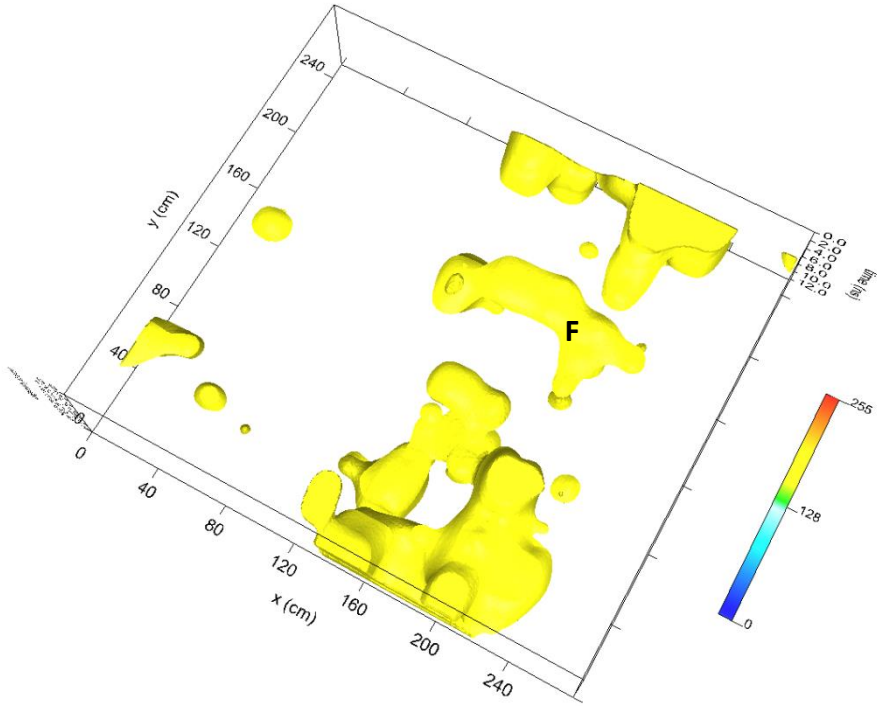

53.9-57.8cm

Fig. 21: 900MHz; upper pane: isosurfaces

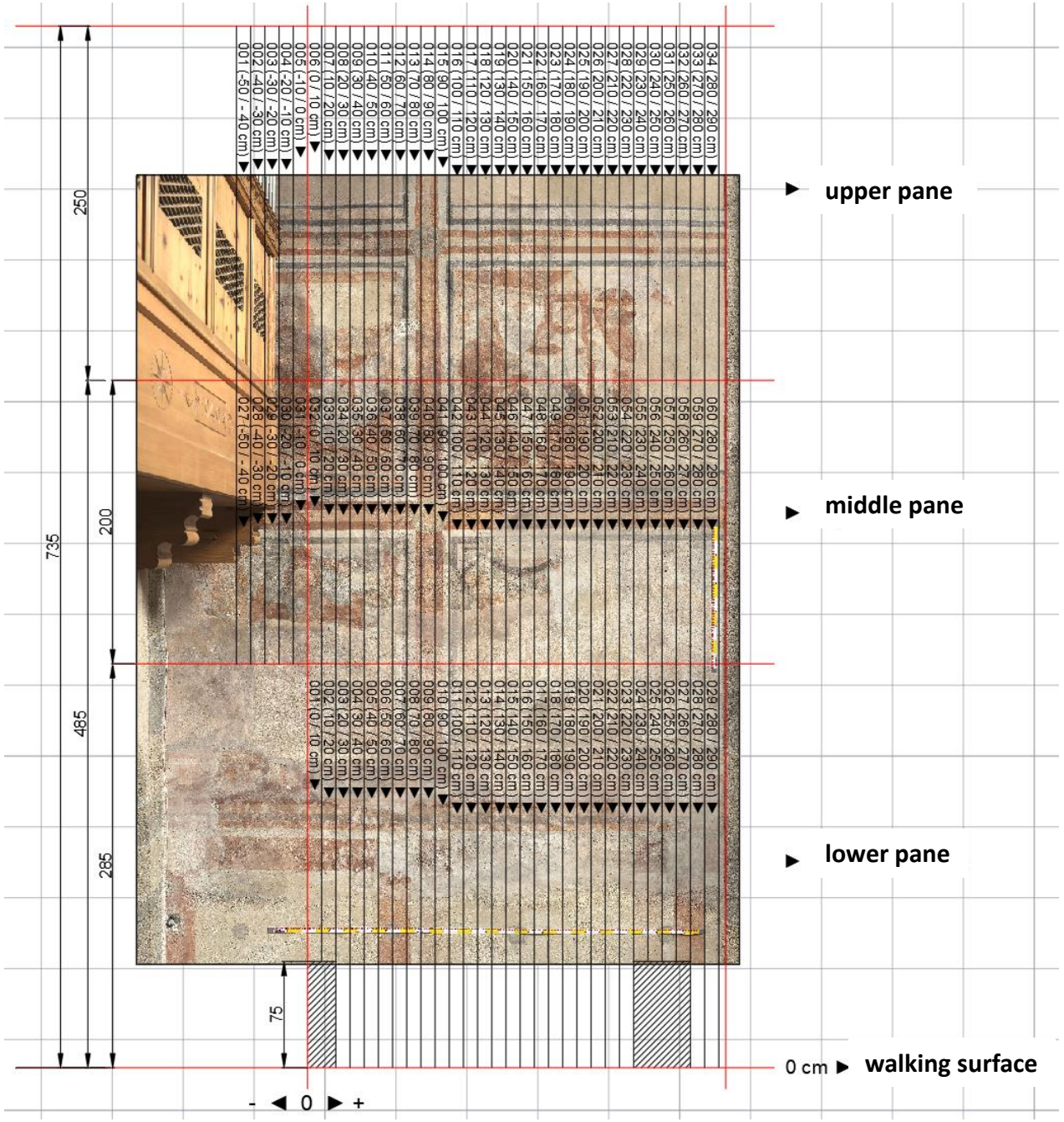

Fig. 22: 2GHz: location of radar profiles

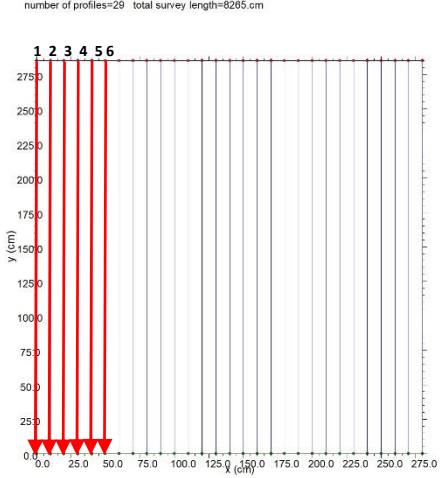

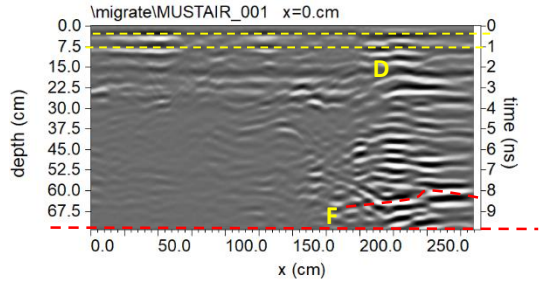

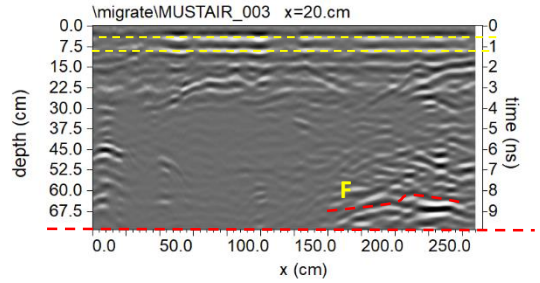

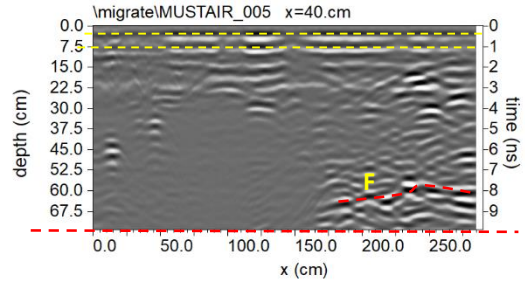

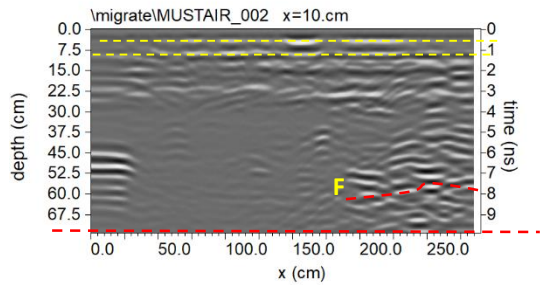

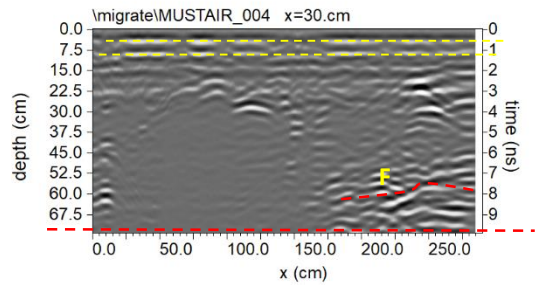

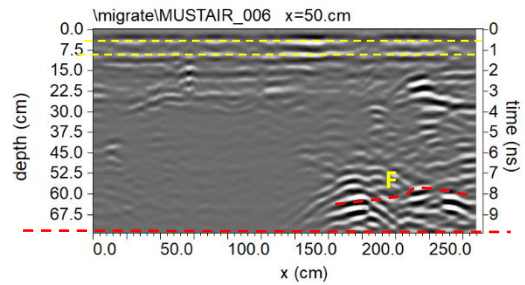

Fig. 23: 2GHz: lower pane: processed radar sections related to the profiles 1,…, 6; dashed red line indicates the end of the wall; dashed yellow lines indicates two layers of plaster; D: probable severance; F: fractures

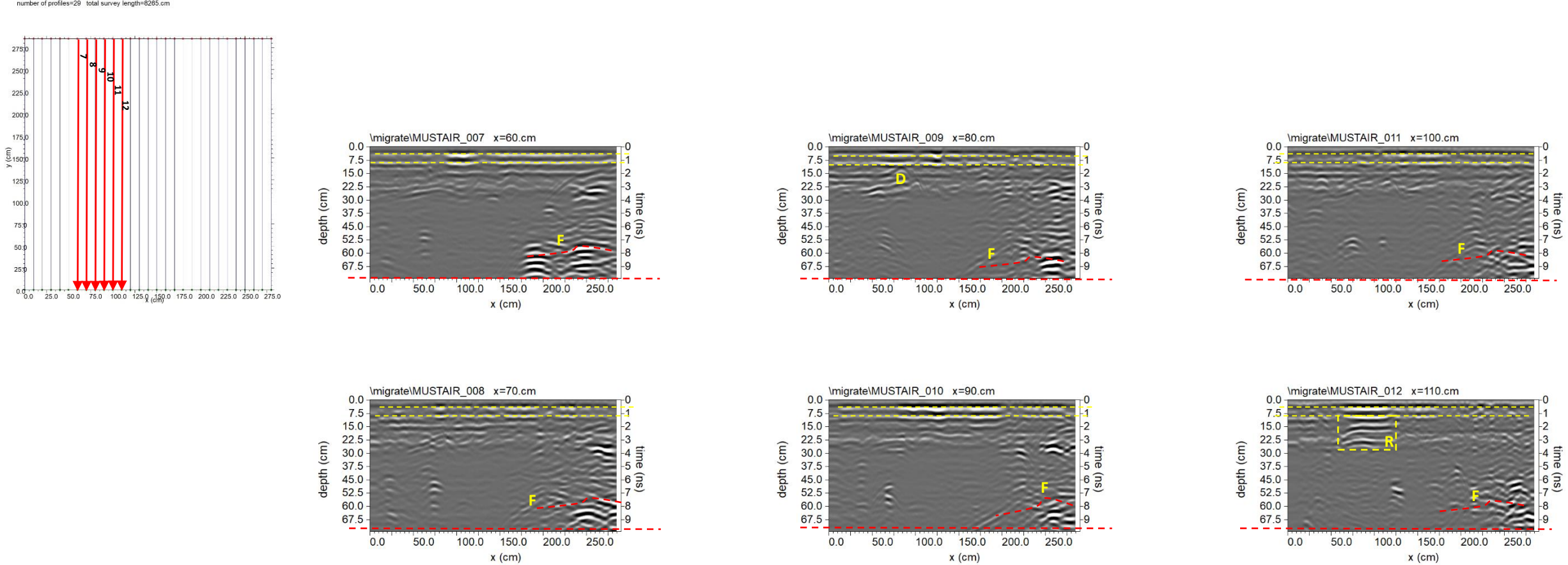

Fig. 24: 2GHz: lower pane: processed radar sections related to the profiles 7,…, 12; dashed red line indicates the end of the wall; dashed yellow lines indicates two layers of plaster; D: probable severance; F: fractures; R: probable reinforcement

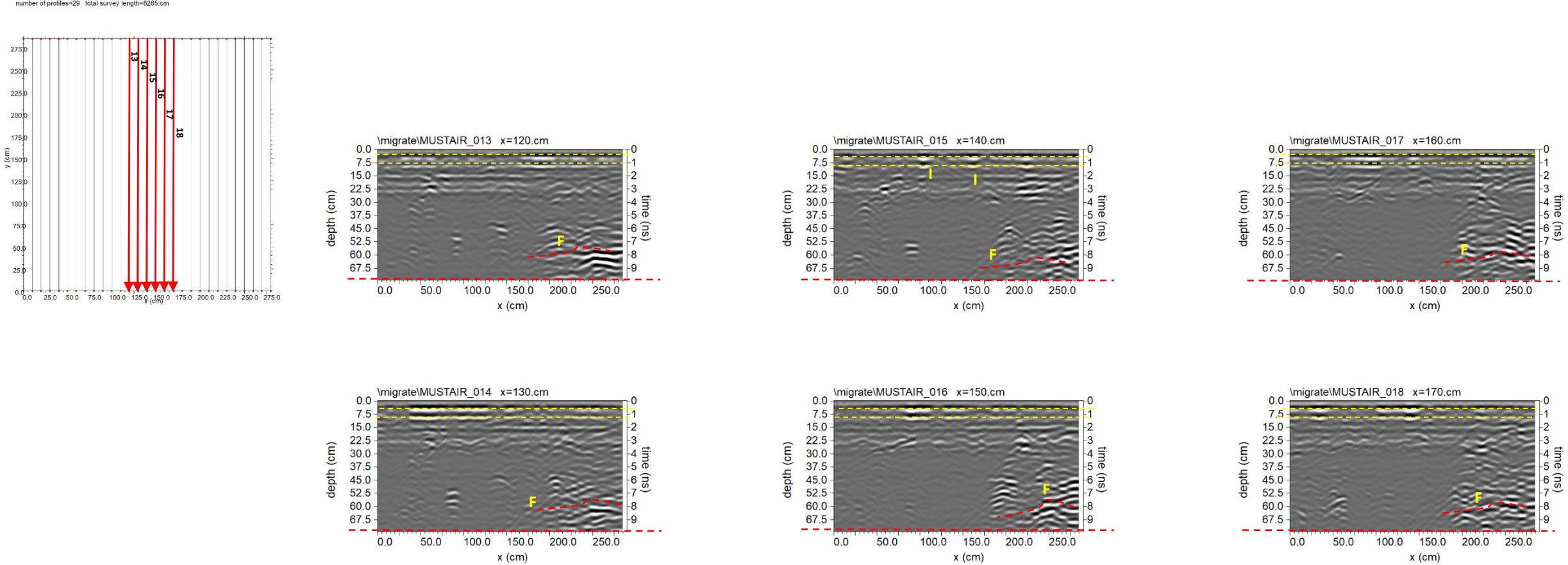

Fig. 25: 2GHz: lower pane: processed radar sections related to the profiles 13,…, 18; dashed red line indicates the end of the wall; dashed yellow lines indicates two layers of plaster; F: fractures; I: probable reinforcement

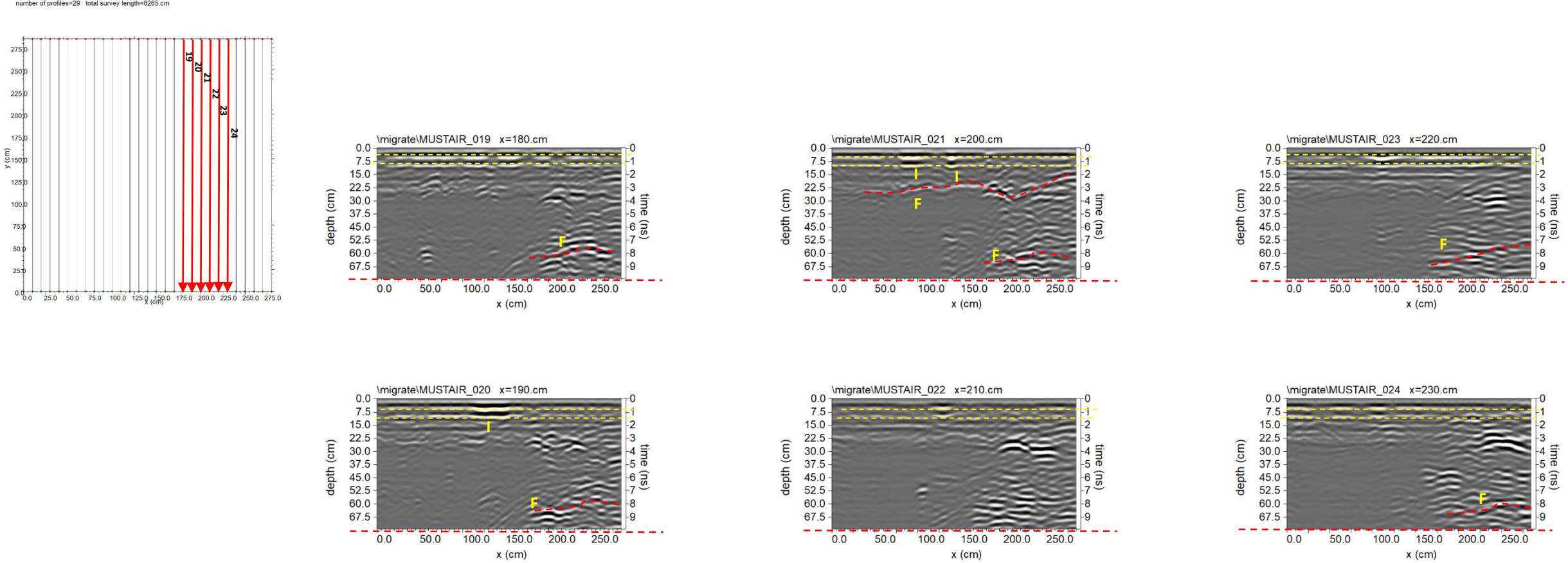

Fig. 26: 2GHz: lower pane: processed radar sections related to the profiles 19,…, 24; dashed red line indicates the end of the wall; dashed yellow lines indicates two layers of plaster; F: fractures; I: probable reinforcement

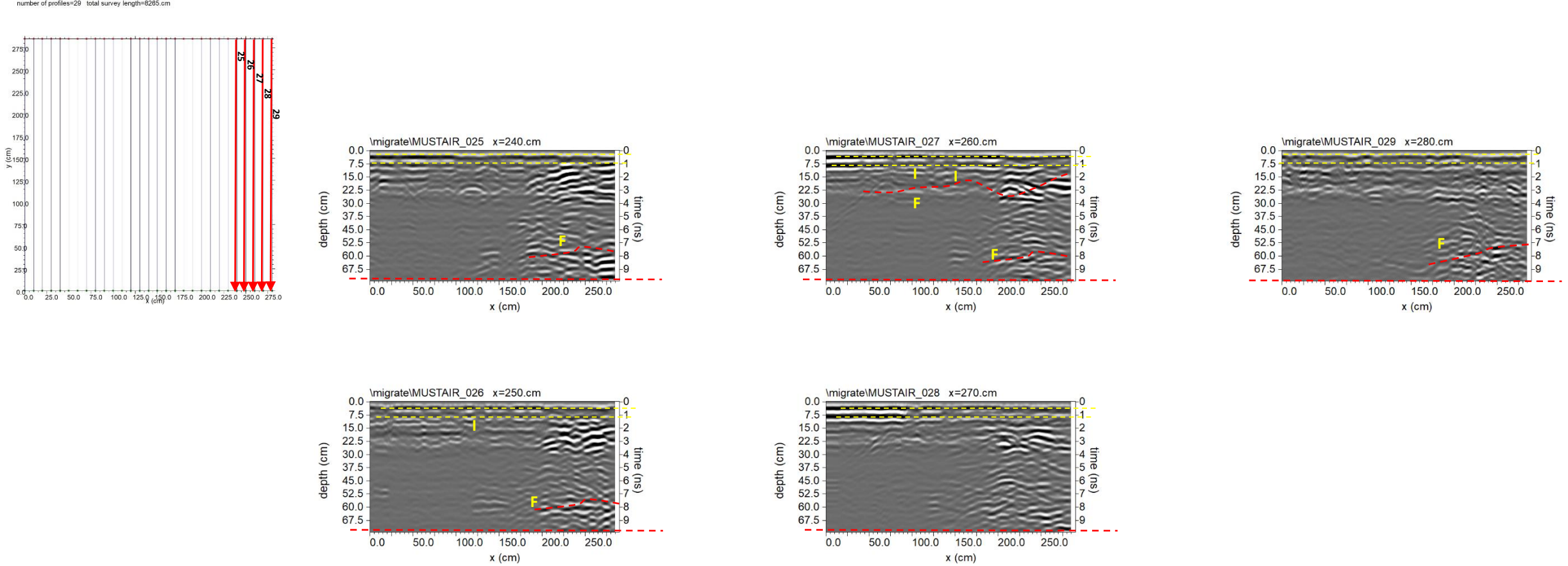

Fig. 27: 2GHz: lower pane: processed radar sections related to the profiles 25,…, 28; dashed red line indicates the end of the wall; dashed yellow lines indicates two layers of plaster; F: fractures; I: probable reinforcement

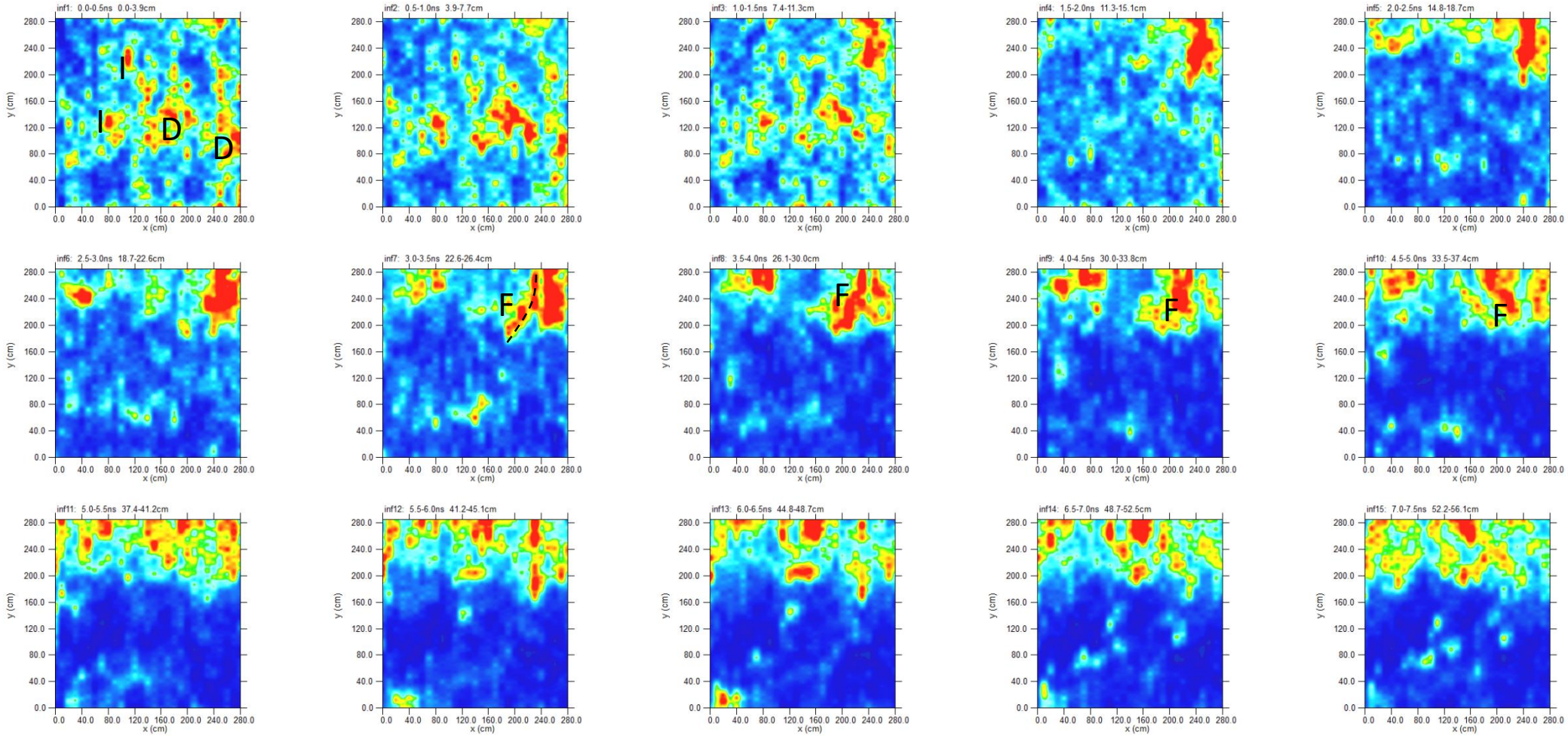

Fig. 28: 2GHz; lower pane: depth slices; D: probable severance; F: fractures; I: probable reinforcement

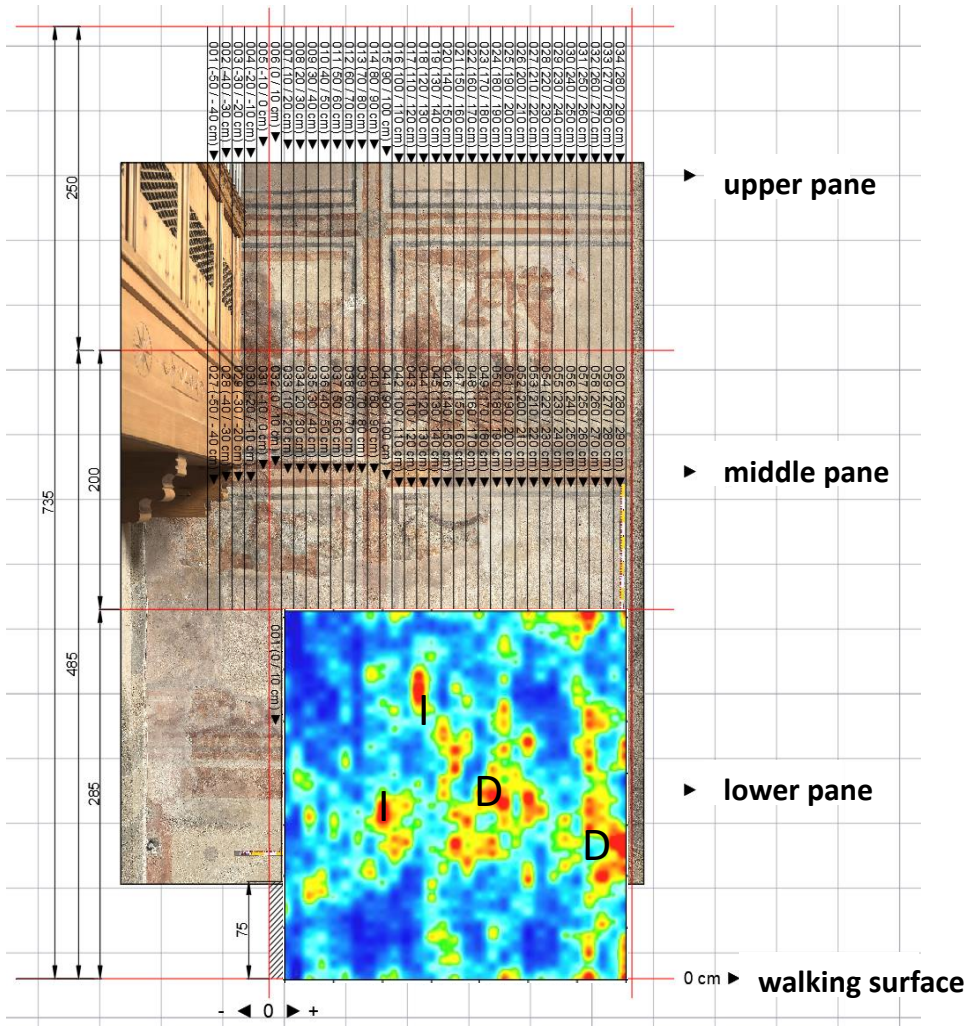

0-4cm

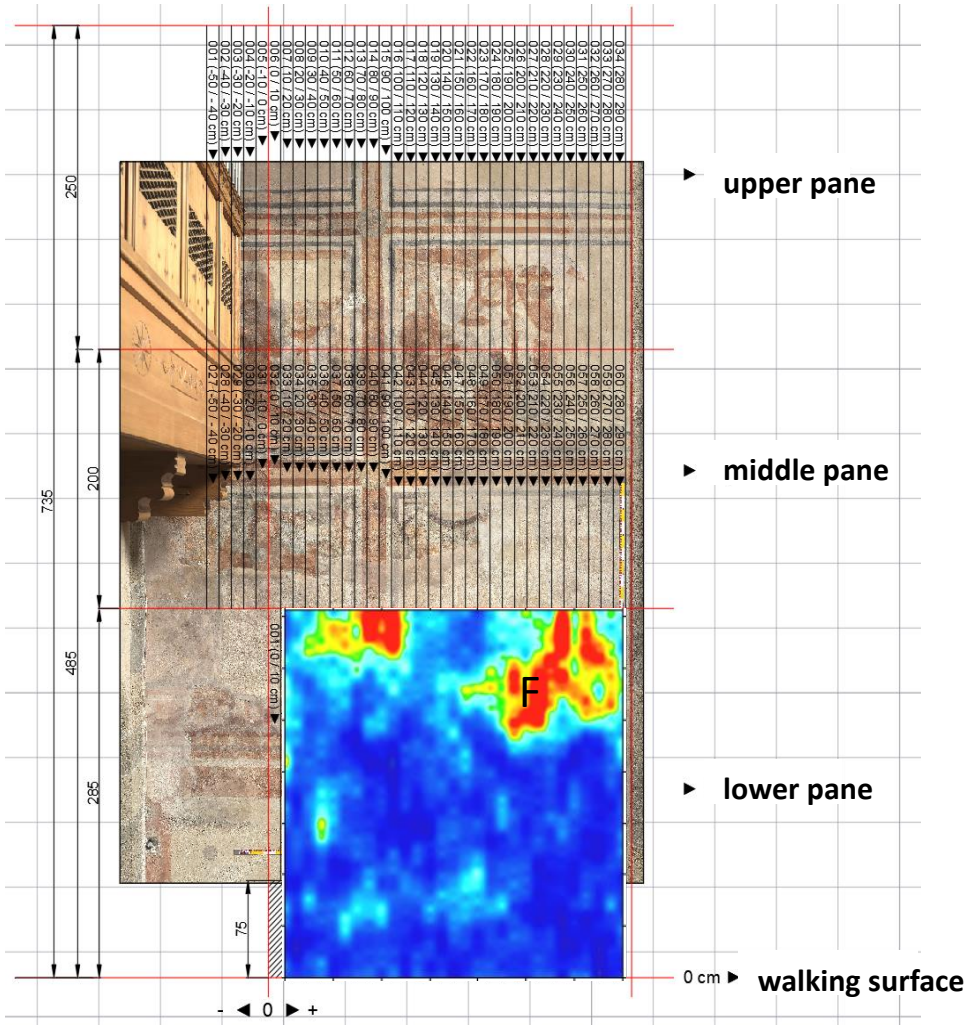

26-30cm

Fig. 29: 2GHz; lower pane : depth slices overlapped with the photo of the frescoes

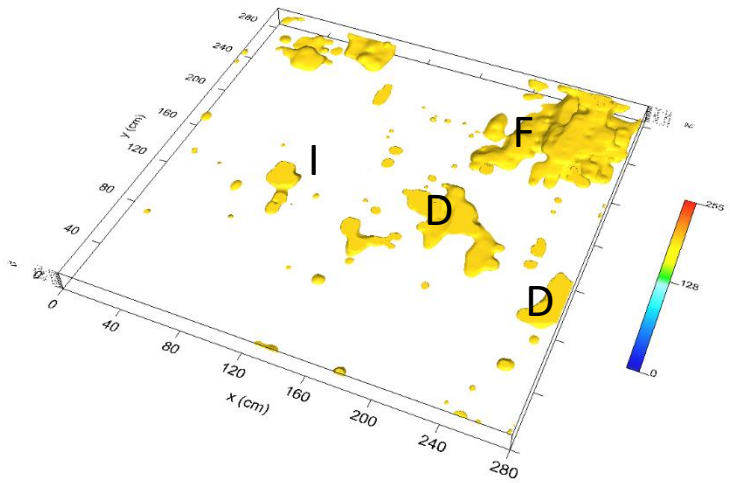

0-30cm

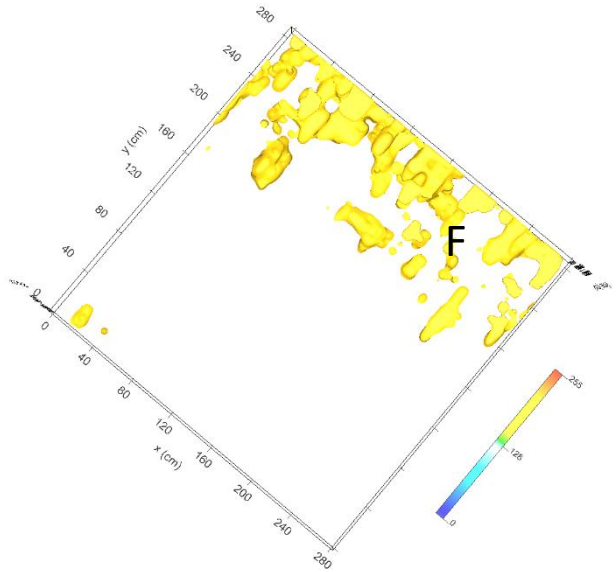

30-70cm

Fig. 30: 2GHz; lower pane: isosurfaces; D: probable severance; F: fractures; I: probable reinforcement

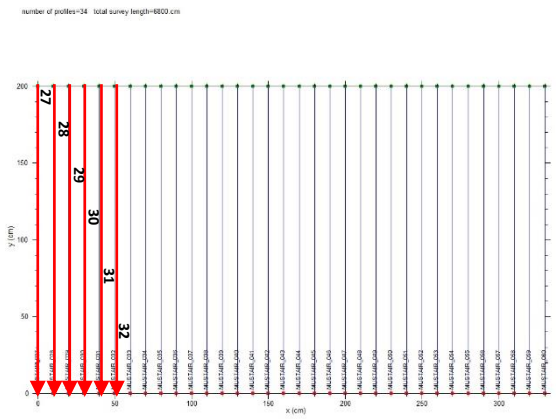

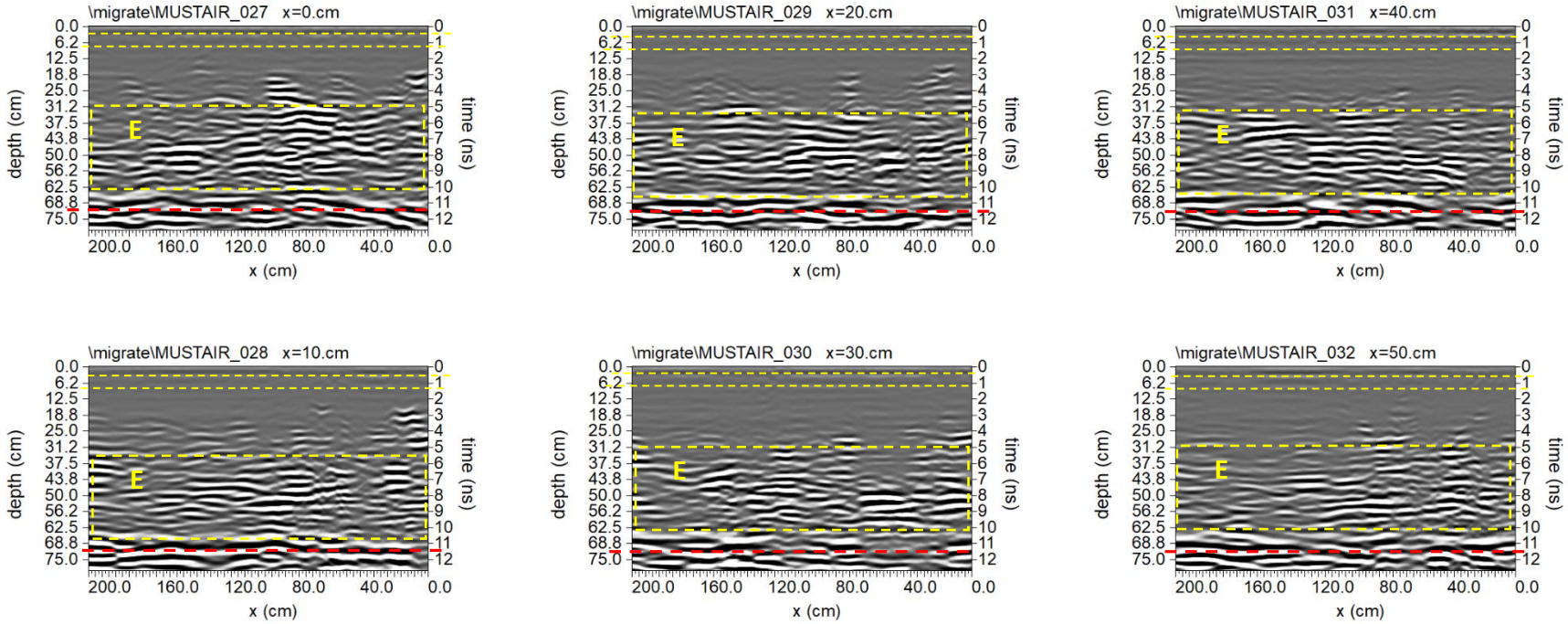

Fig. 31: 2GHz: middle pane: processed radar sections related to the profiles 27,…, 32; dashed red line indicates the end of the wall; dashed yellow lines indicates two layers of plaster; E: very deteriorated area;

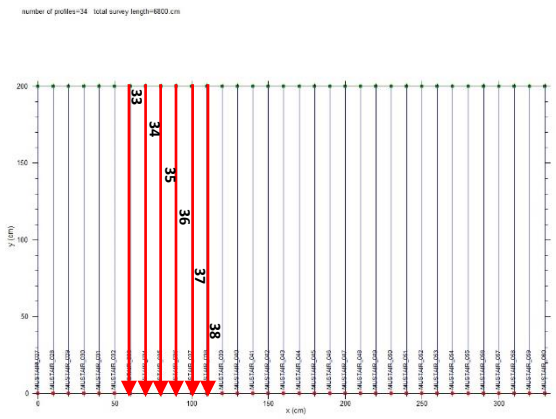

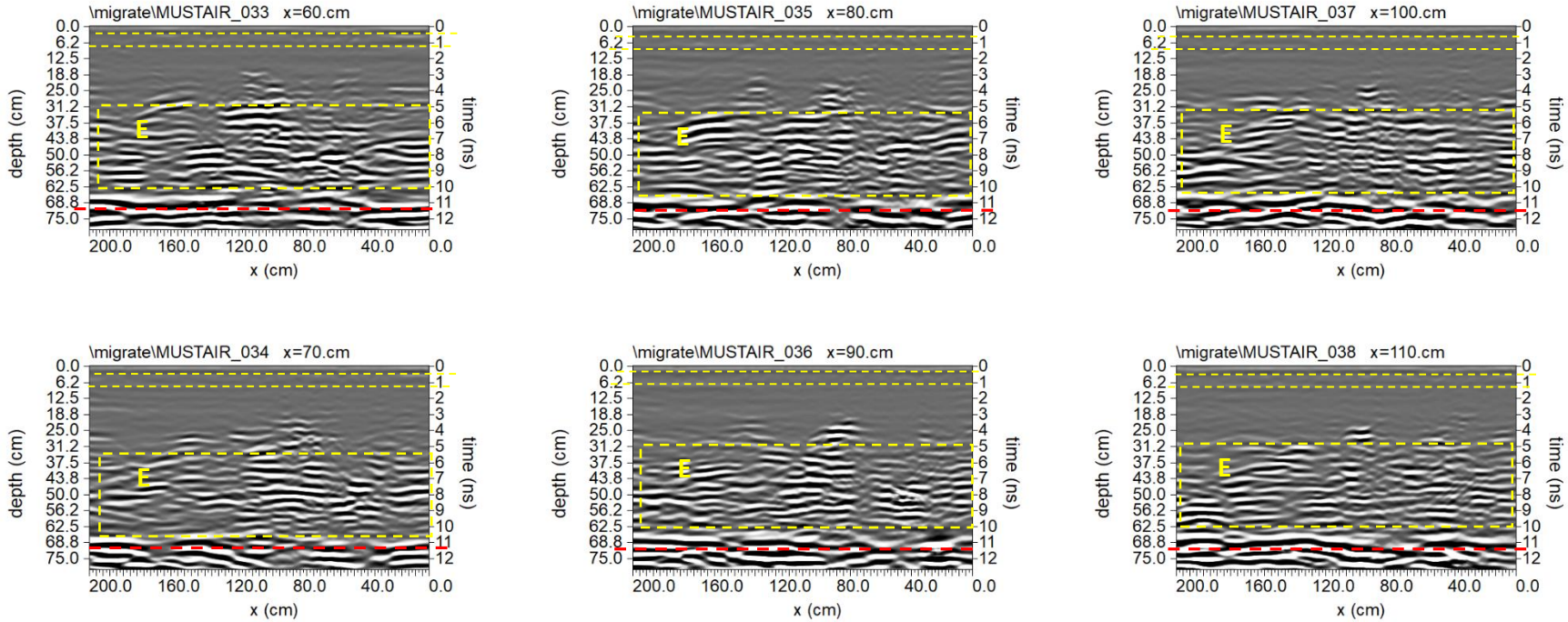

Fig. 32: 2GHz: middle pane: processed radar sections related to the profiles 33,…, 38; dashed red line indicates the end of the wall; dashed yellow lines indicates two layers of plaster; E: very deteriorated area;

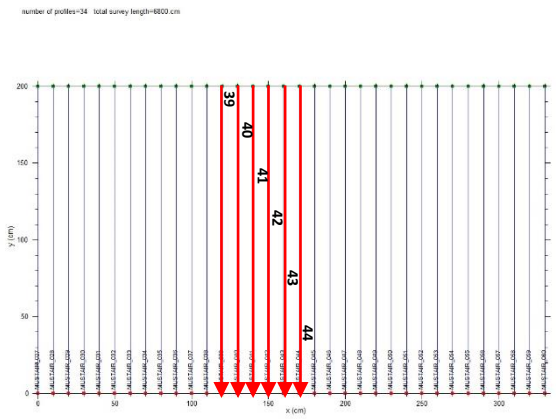

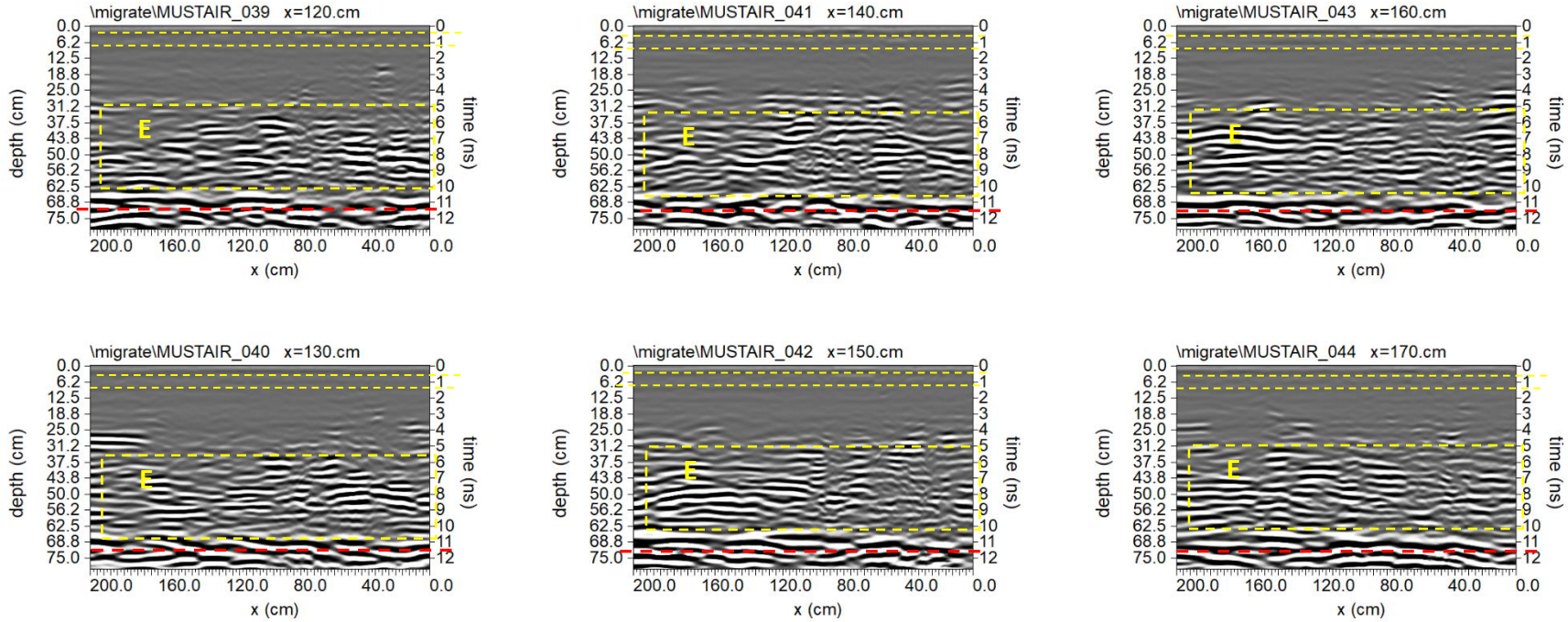

Fig. 33: 2GHz: middle pane: processed radar sections related to the profiles 39,…, 44; dashed red line indicates the end of the wall; dashed yellow lines indicates two layers of plaster; E: very deteriorated area;

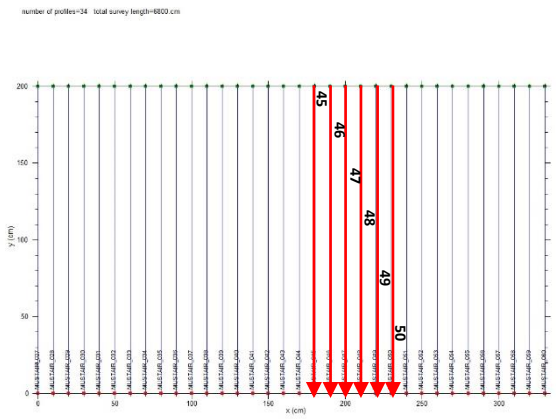

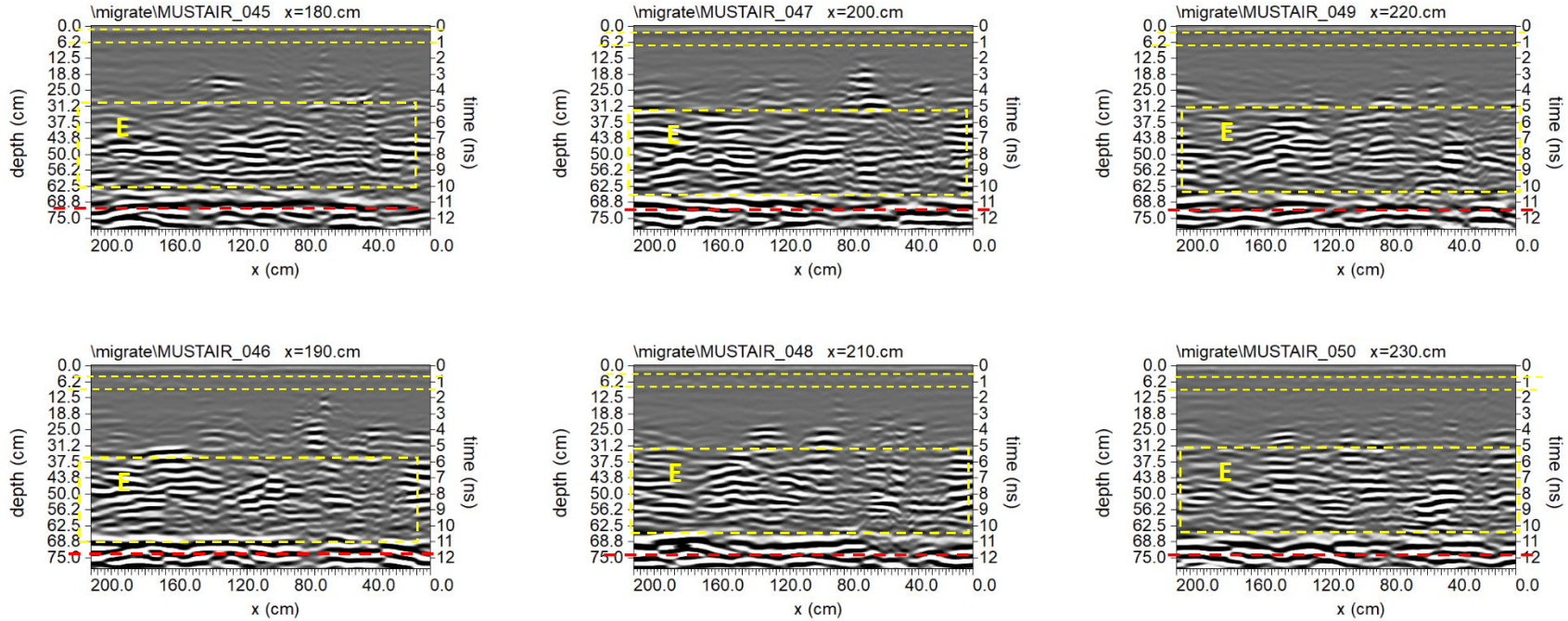

Fig. 34: 2GHz: middle pane: processed radar sections related to the profiles 45,…, 50; dashed red line indicates the end of the wall; dashed yellow lines indicates two layers of plaster; E: very deteriorated area;

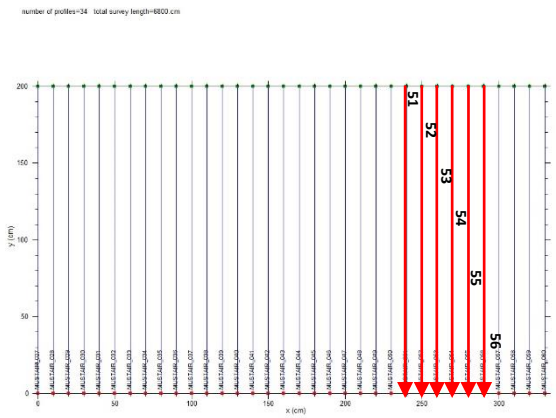

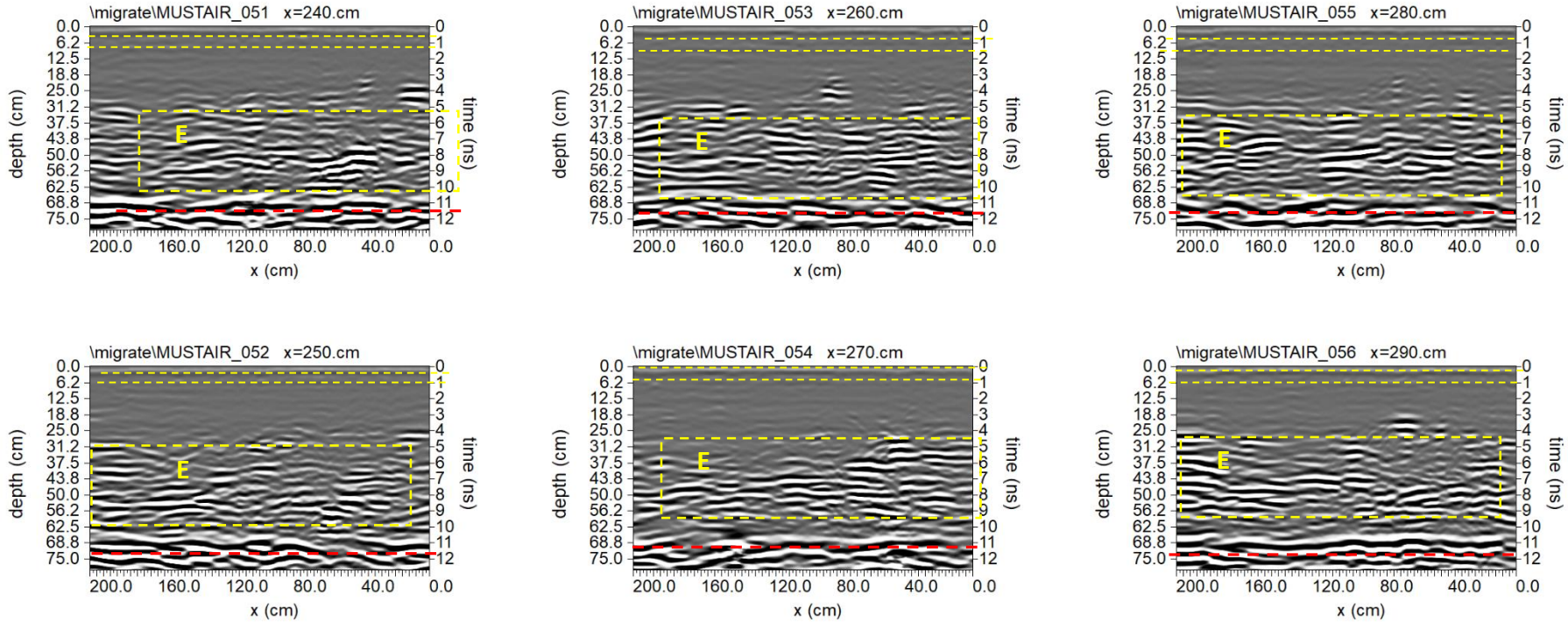

Fig. 35: 2GHz: middle pane: processed radar sections related to the profiles 51,…, 56; dashed red line indicates the end of the wall; dashed yellow lines indicates two layers of plaster; E: very deteriorated area;

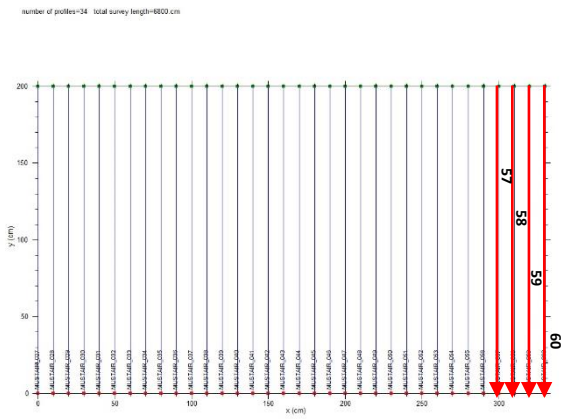

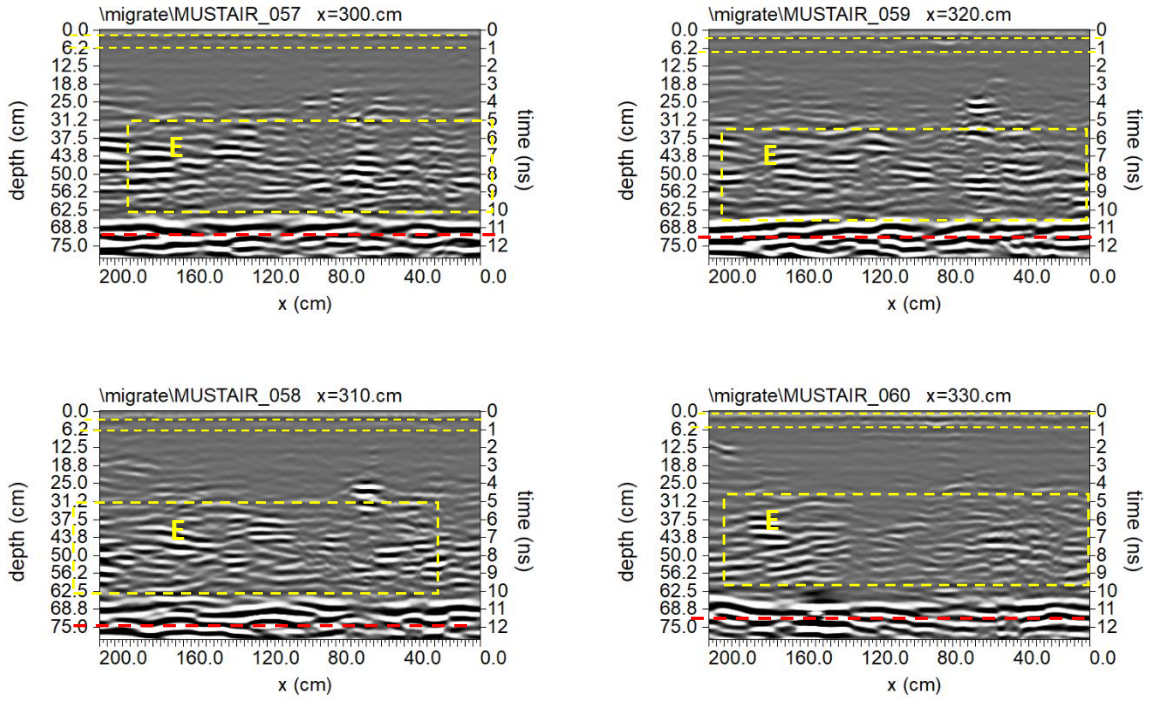

Fig. 36: 2GHz: middle pane: processed radar sections related to the profiles 57,…, 60; dashed red line indicates the end of the wall; dashed yellow lines indicates two layers of plaster; E: very deteriorated area;

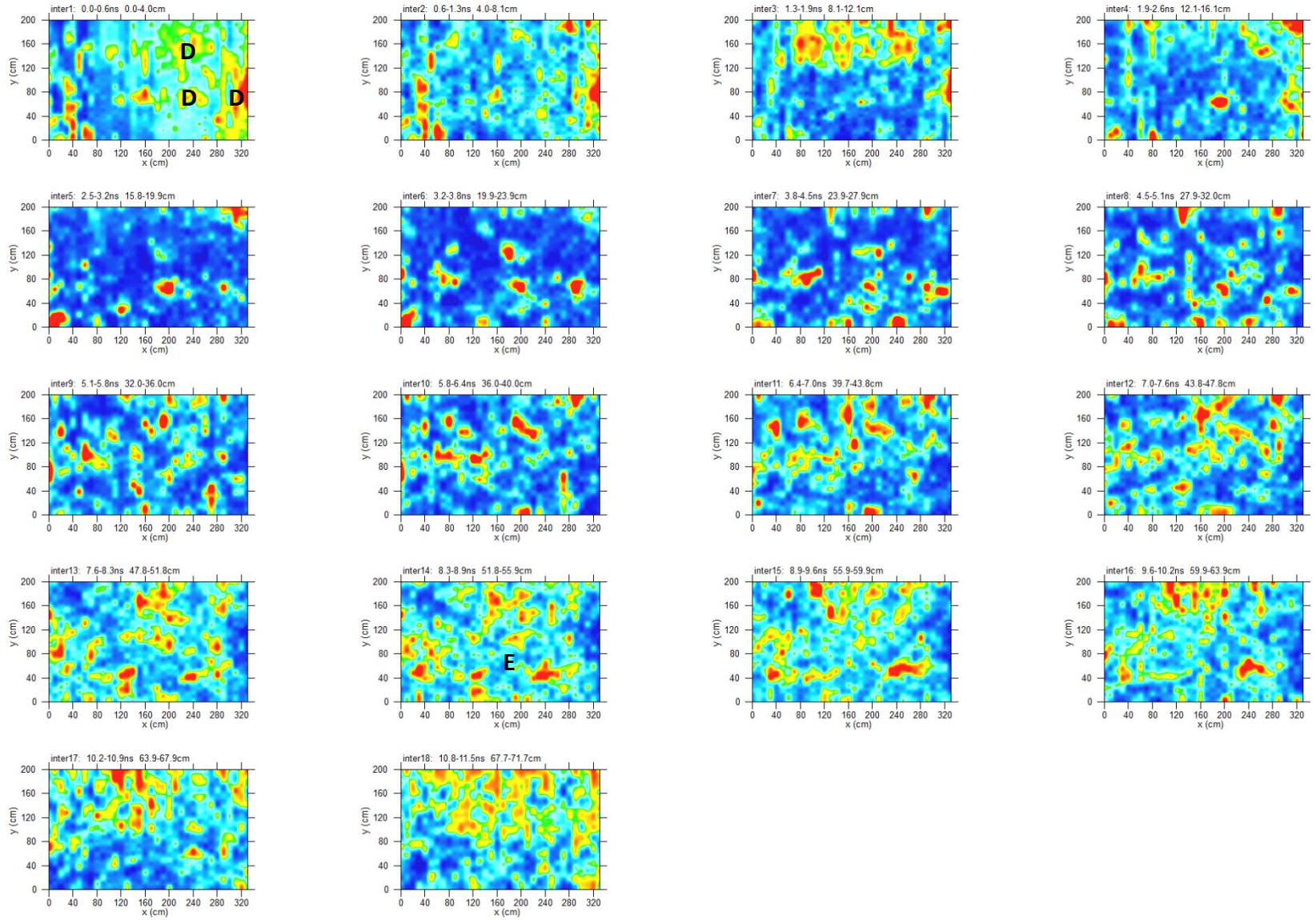

Fig. 37: 2GHz; middle pane: depth slices; D: probable severance; E: very deteriorated area.

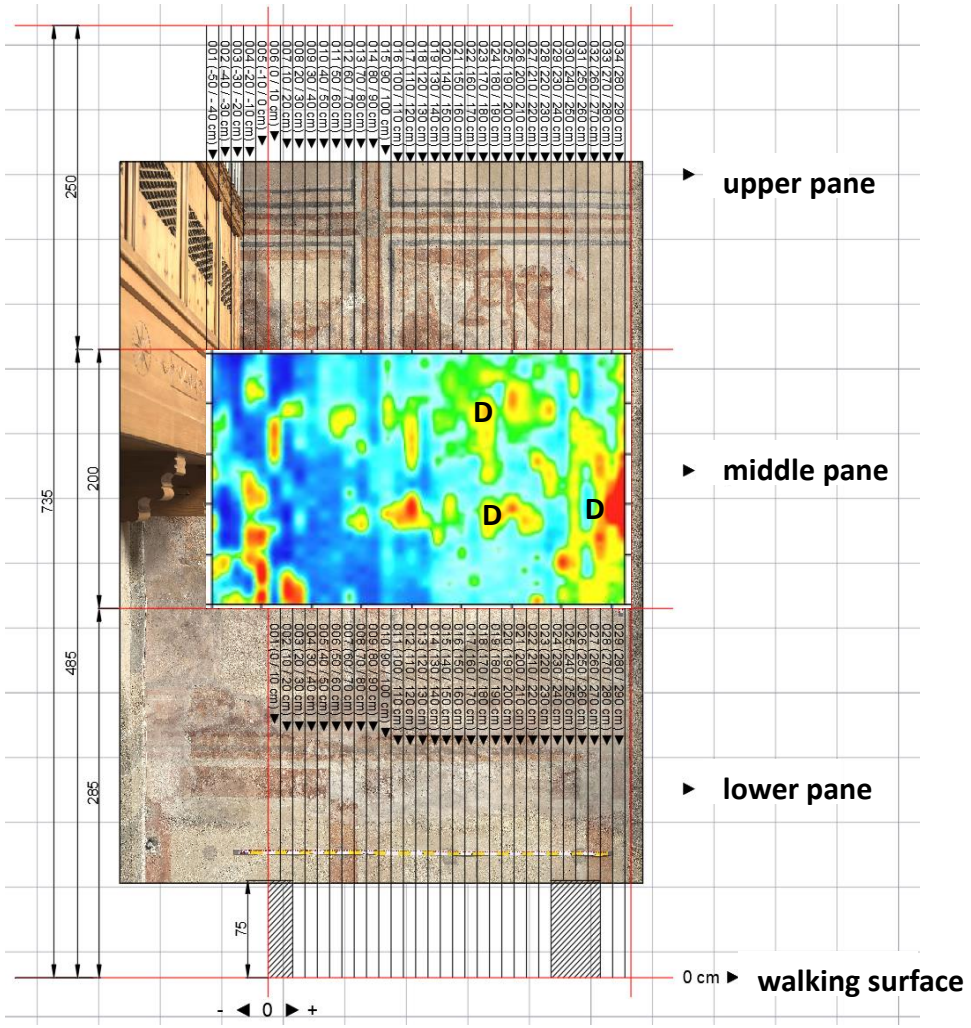

0-4cm

Fig. 38: 2GHz; middle pane: depth slices overlapped with the photo of the frescoes

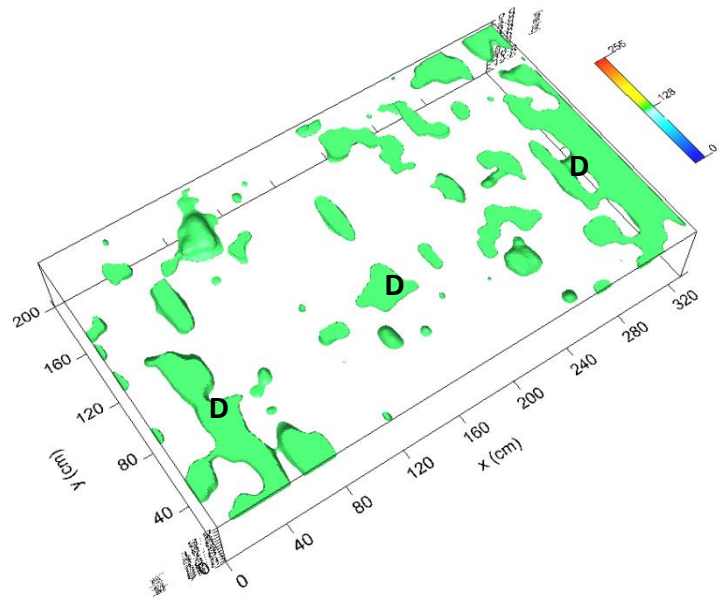

0-6cm

Fig. 39: 2GHz; middle pane: isosurfaces; D: probable severance

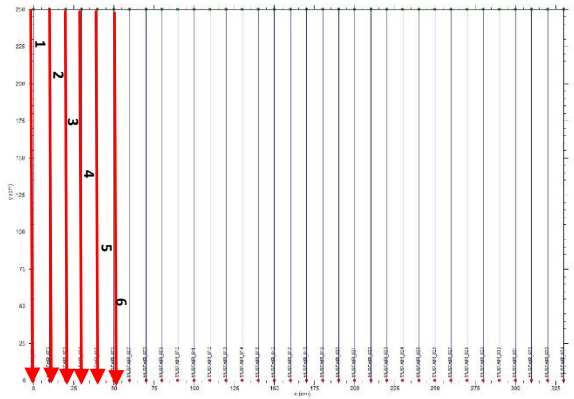

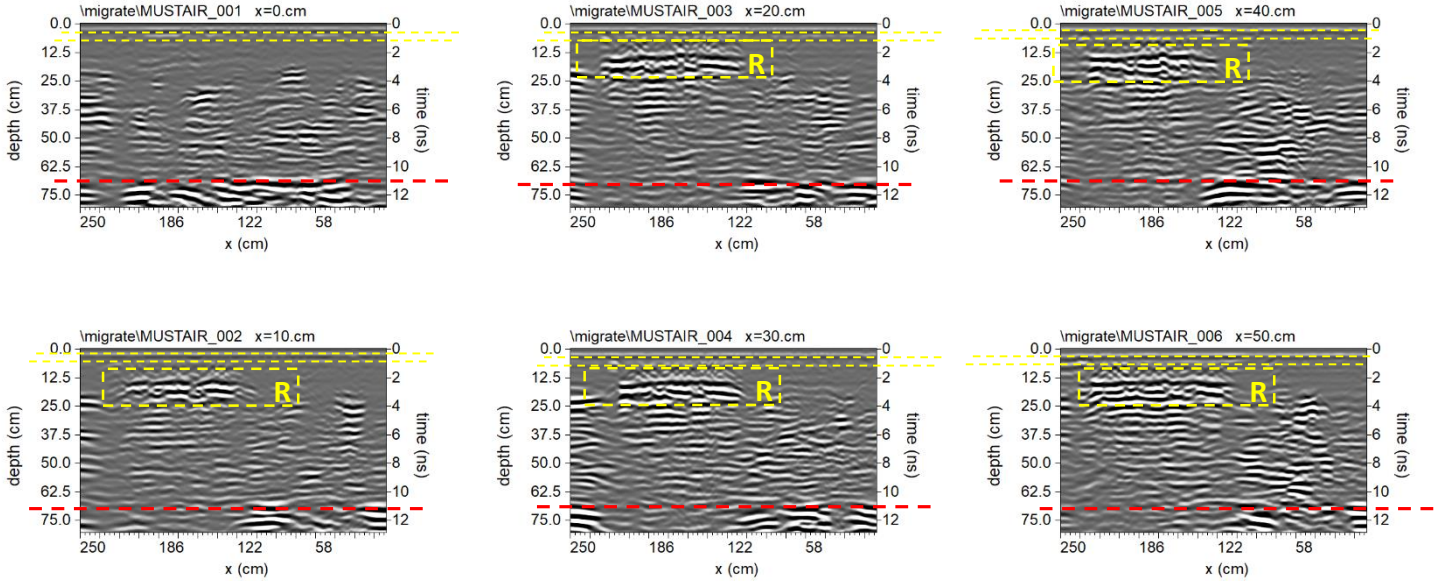

Fig. 40: 2GHz: upper pane: processed radar sections related to the profiles 1,…, 6; dashed red line indicates the end of the wall; dashed yellow lines indicates two layers of plaster; R: reinforcement;

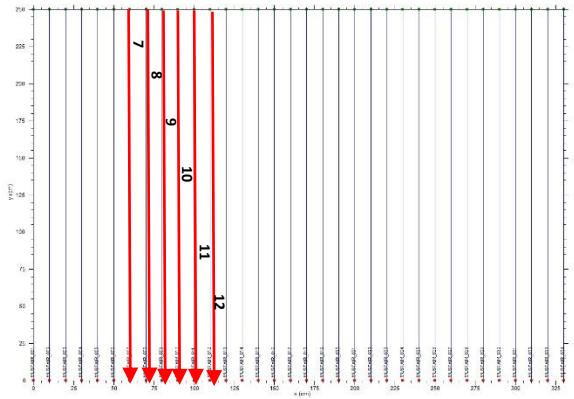

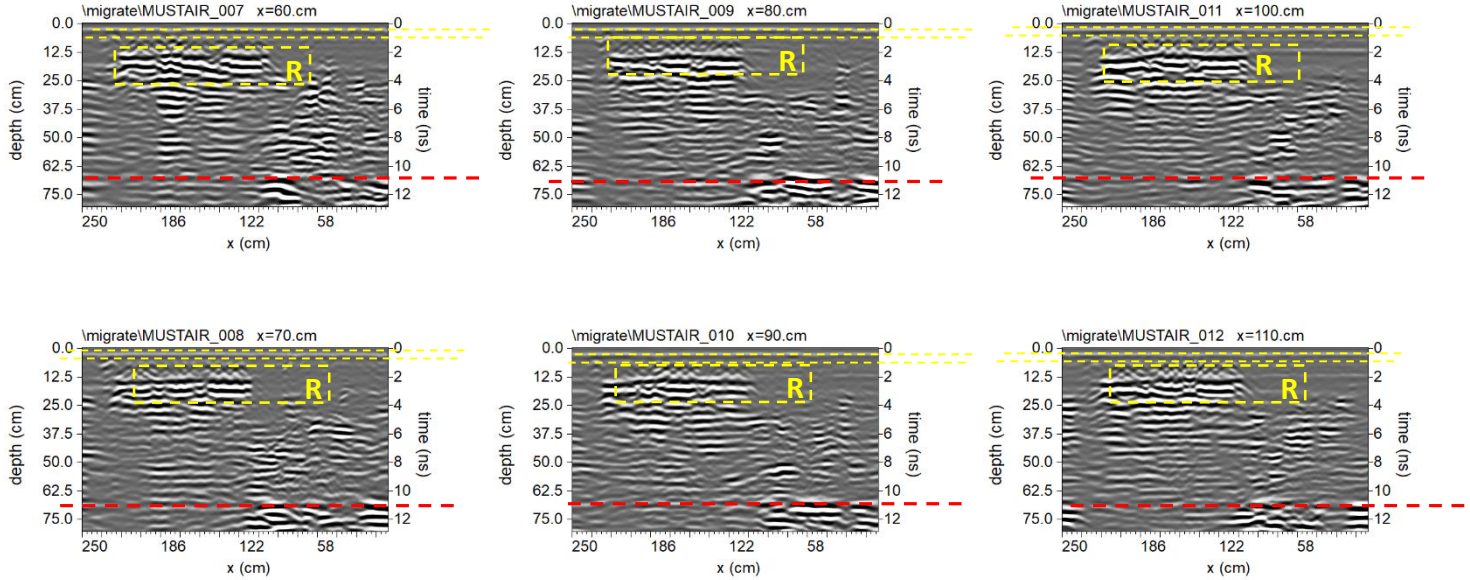

Fig. 41: 2GHz: upper pane: processed radar sections related to the profiles 7,…, 12; dashed red line indicates the end of the wall; dashed yellow lines indicates two layers of plaster; R: reinforcement;

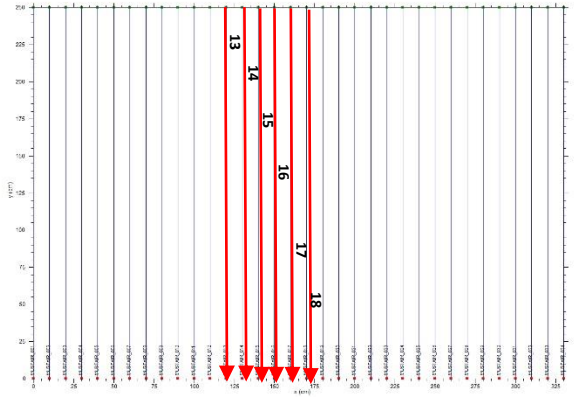

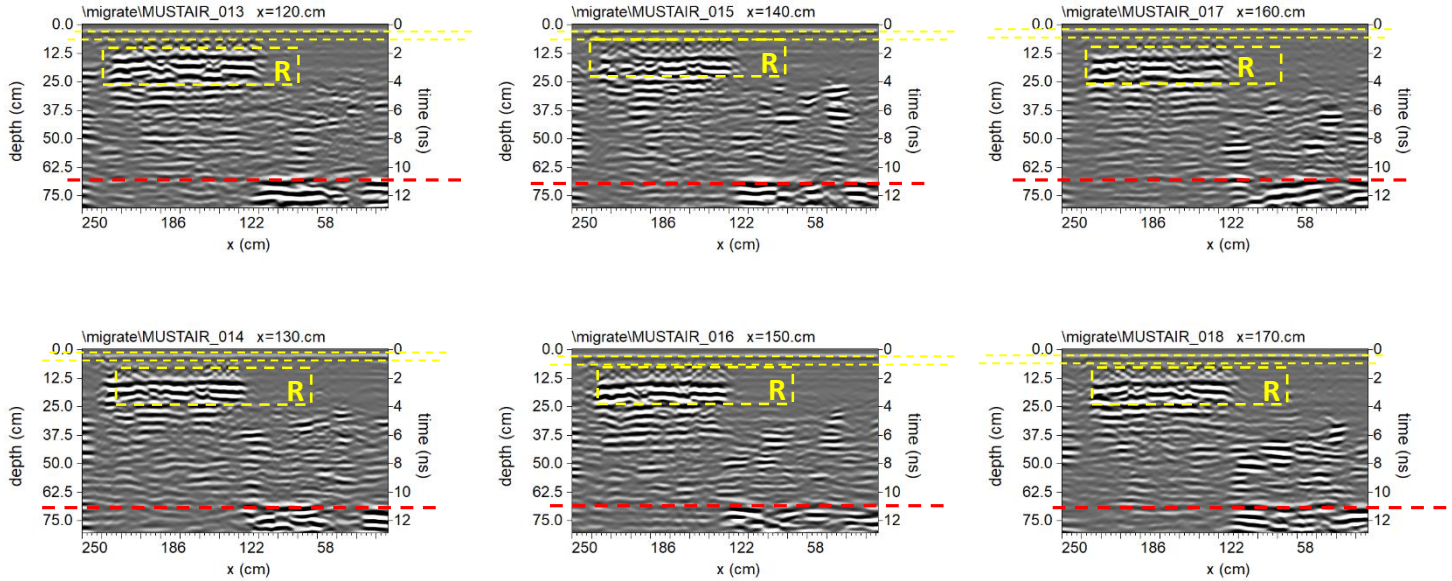

Fig. 42: 2GHz: upper pane: processed radar sections related to the profiles 13,…, 18; dashed red line indicates the end of the wall; dashed yellow lines indicates two layers of plaster; R: reinforcement;

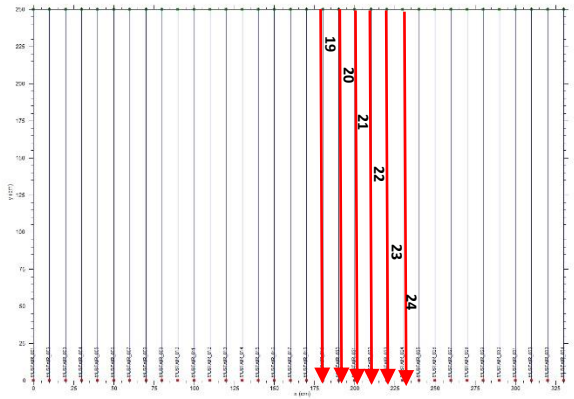

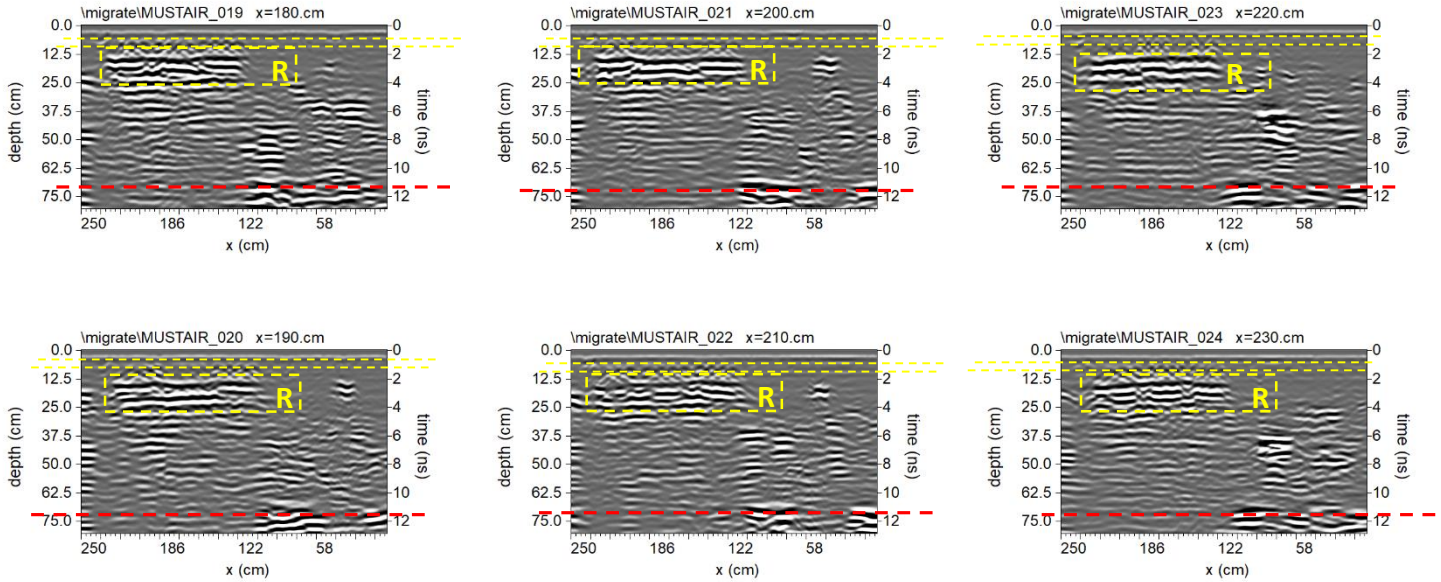

Fig. 43: 2GHz: upper pane: processed radar sections related to the profiles 19,…, 24; dashed red line indicates the end of the wall; dashed yellow lines indicates two layers of plaster; R: reinforcement;

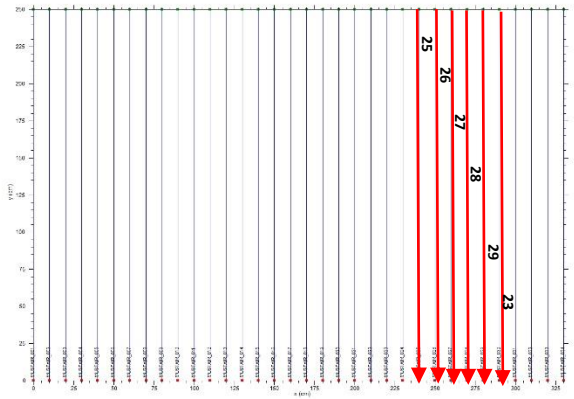

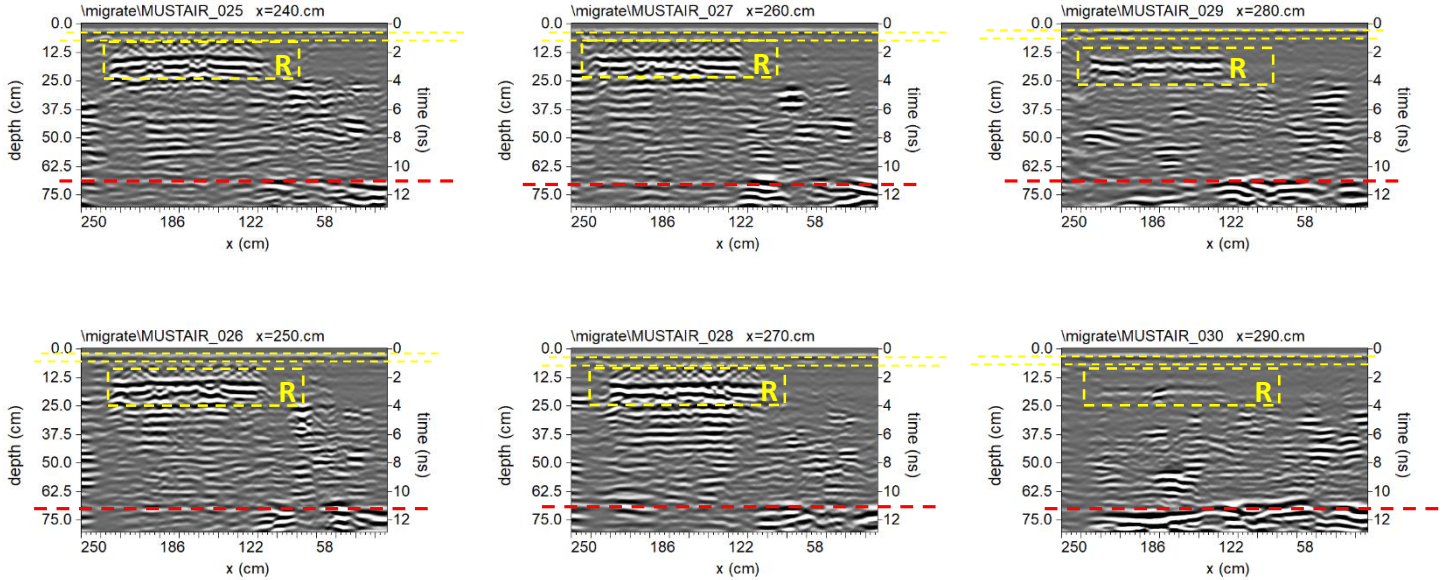

Fig. 44: 2GHz: upper pane: processed radar sections related to the profiles 25,…, 30; dashed red line indicates the end of the wall; dashed yellow lines indicates two layers of plaster; R: reinforcement;

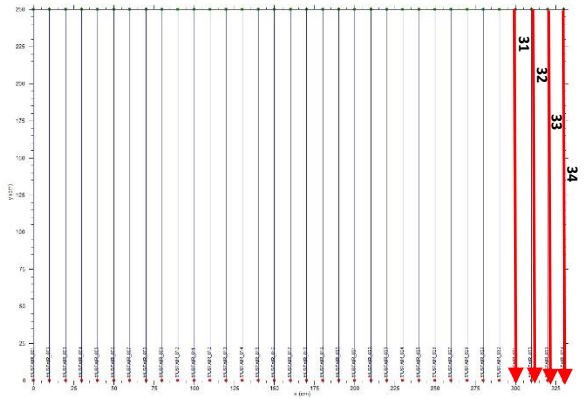

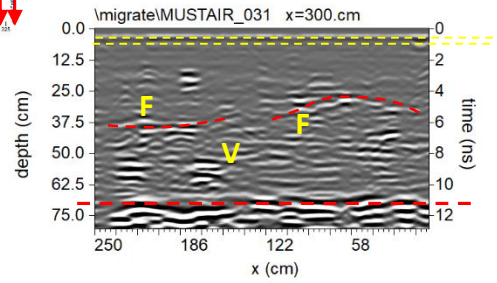

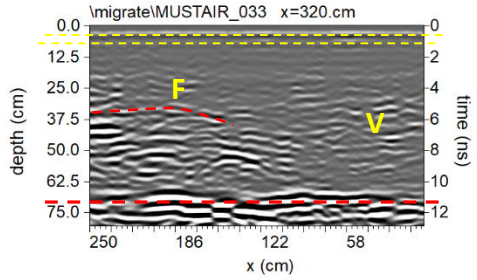

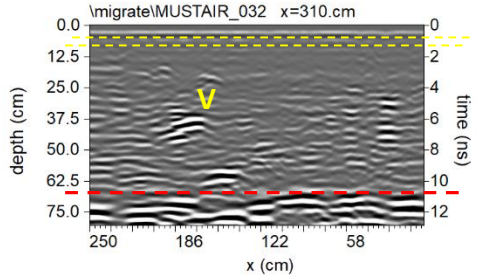

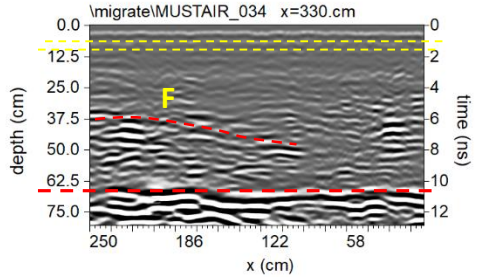

Fig. 45: 2GHz: upper pane: processed radar sections related to the profiles 31,…, 34; dashed red line indicates the end of the wall; dashed yellow lines indicates two layers of plaster; F: Fracture; V: voids

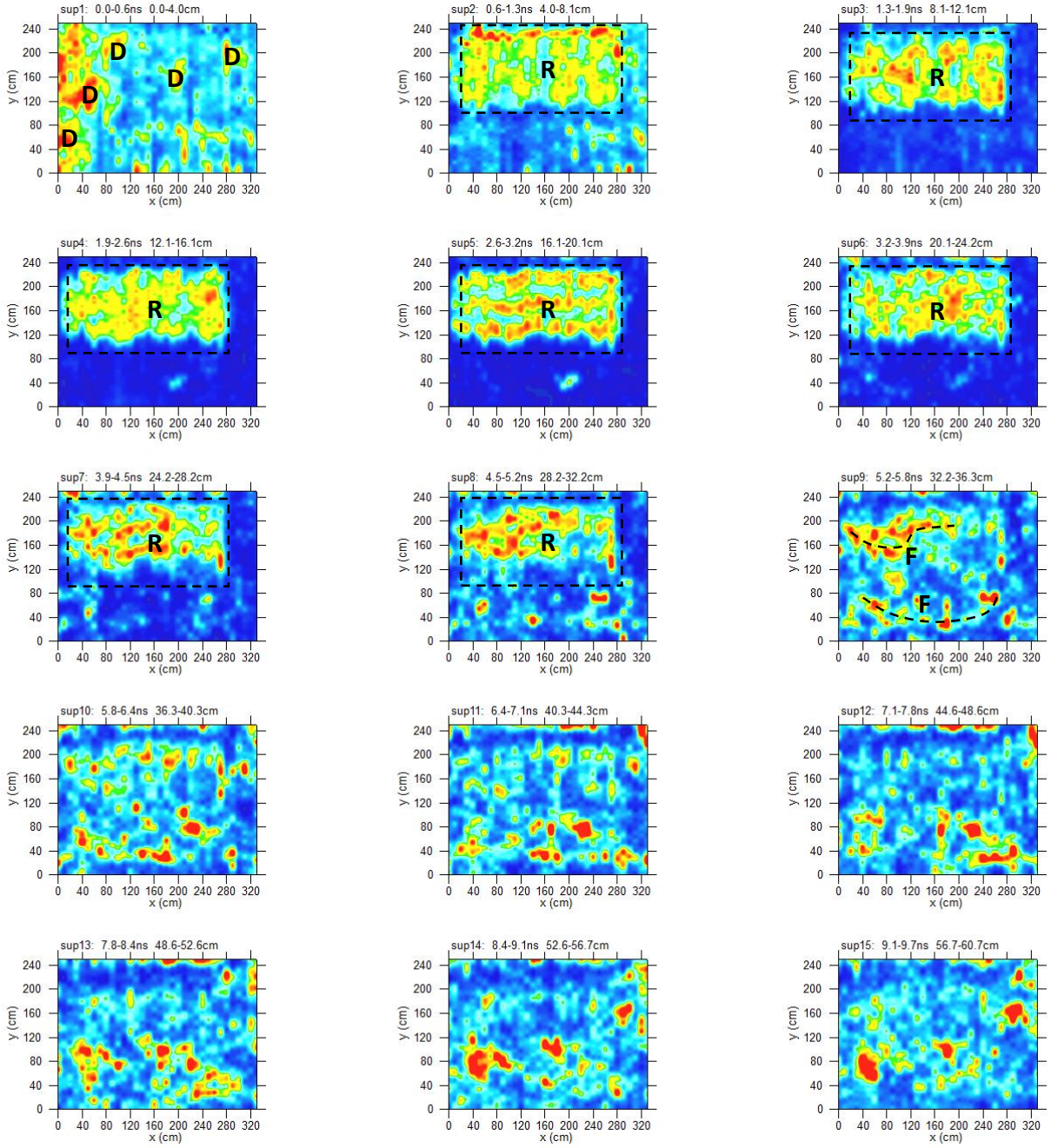

Fig. 46: 2GHz; upper pane: depth slices; D: probable severance; F: fractures; R: reinforcement.

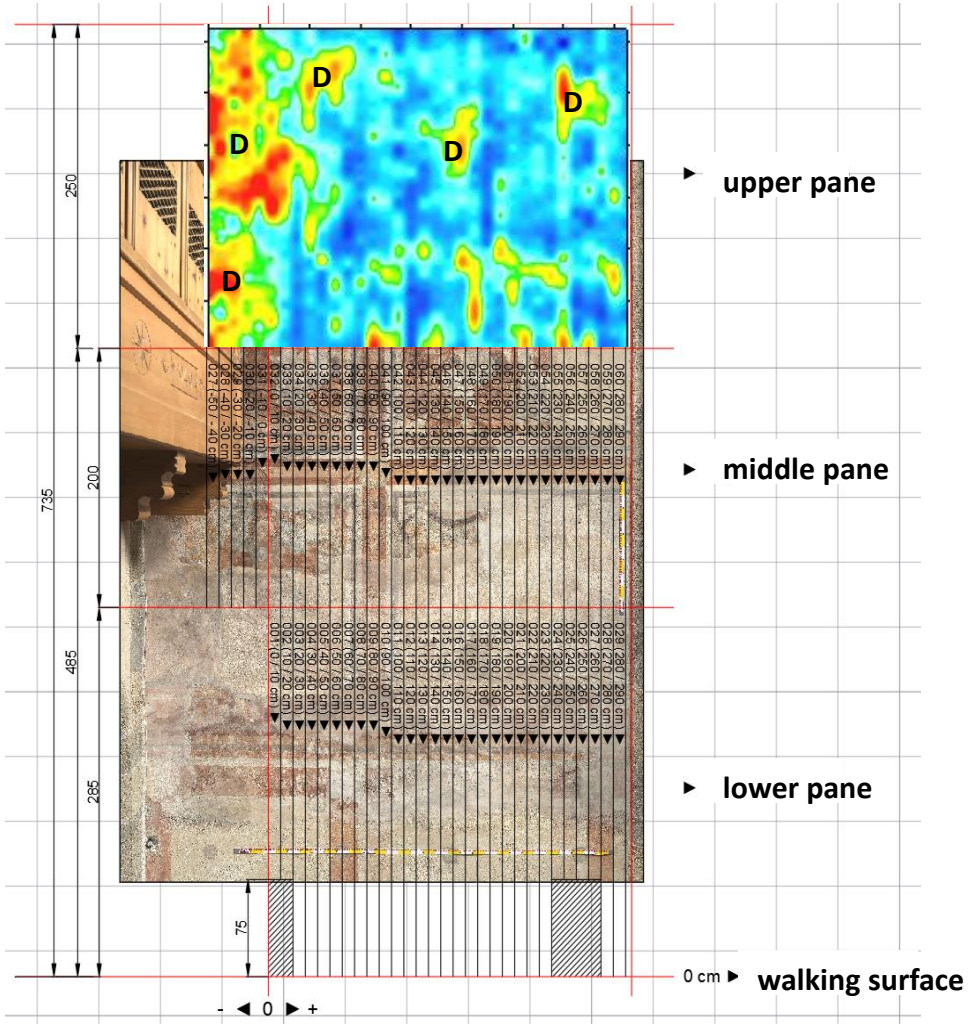

0-4cm

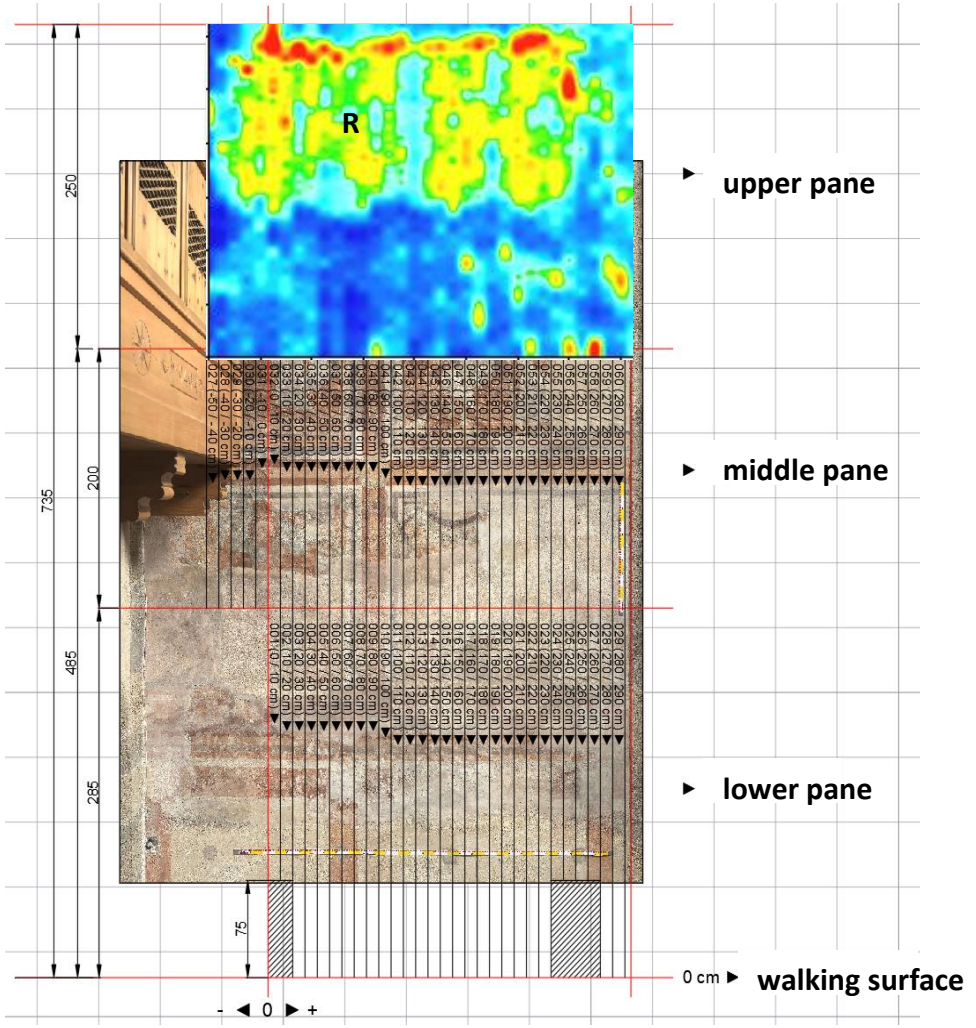

4-8cm

Fig. 47: 2GHz; upper pane: depth slices overlapped with the photo of the frescoes

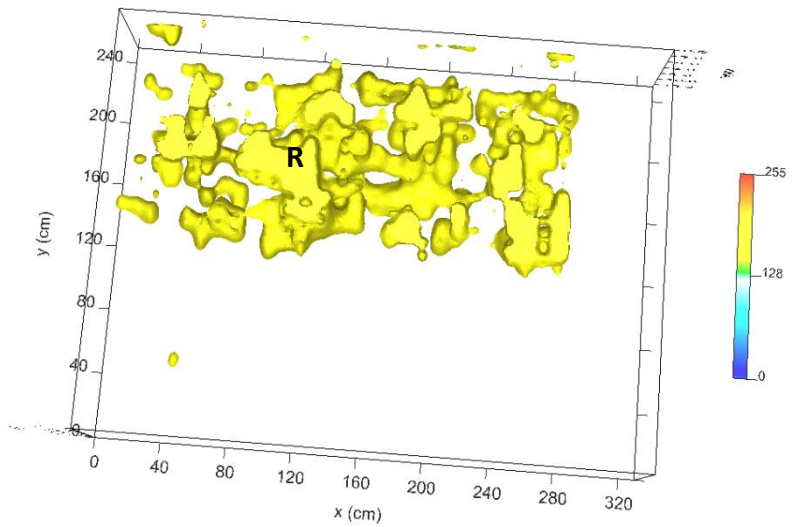

Fig. 48: 2GHz; upper pane: isosurfaces; R: reinforcement

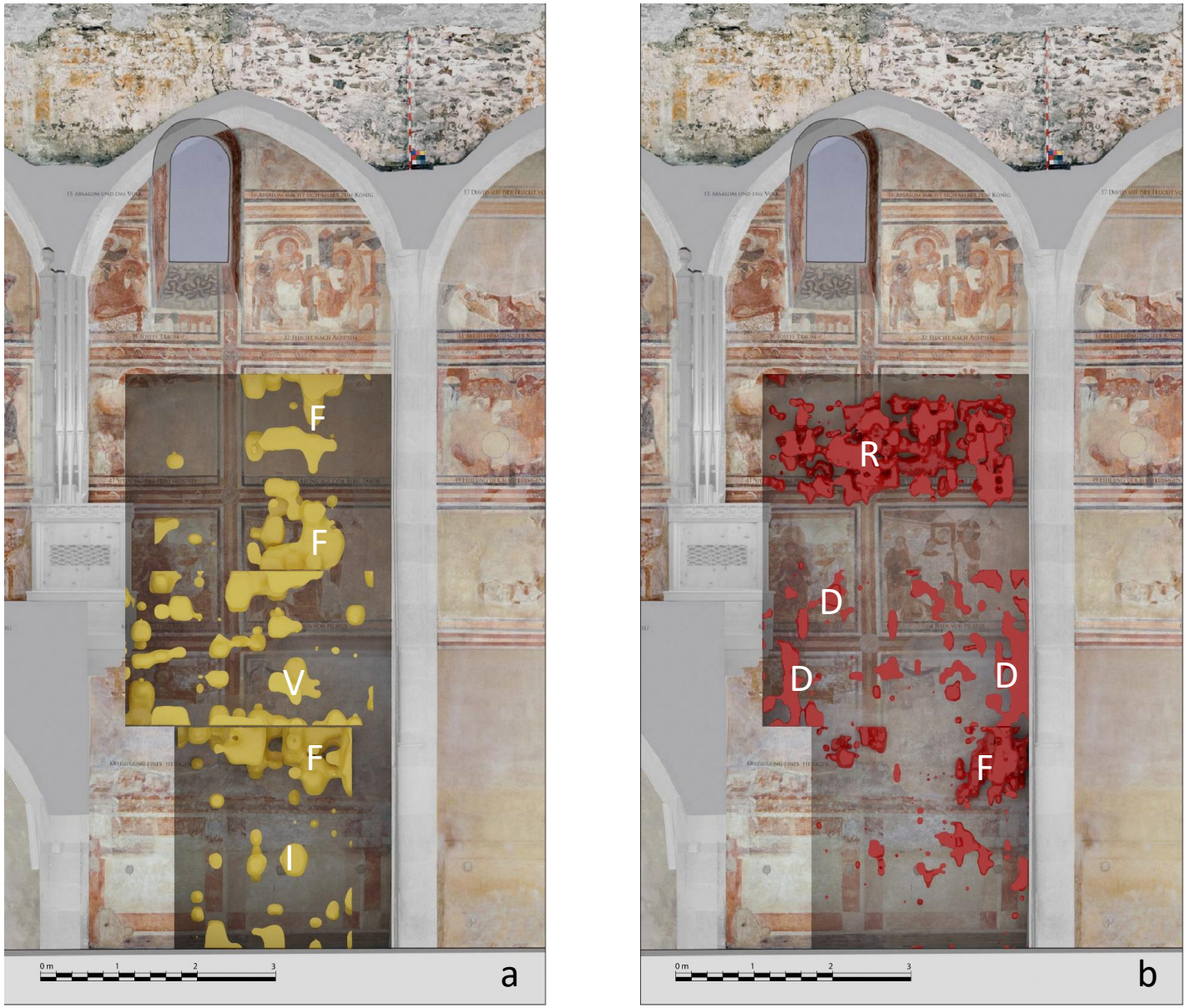

Fig. 49: The isosurfaces overlapped to the investigated area: a) 900MHz results, b) 2GHz results